DISS. ETH No 13089

Studies On Short-Range Air Pollution Modeling

A dissertation submitted to the
SWISS FEDERAL INSTITUTE OF TECHNOLOGY ZURICH

for the degree of

Doctor of Natural Sciences

presented by
Peter Jan de Haan
dipl. Phys. ETH
born November 16, 1969
citizen of the Netherlands

accepted on the recommendation of
Prof Dr A. Ohmura, examiner
Dr M. W. Rotach, co-examiner
Prof Dr S. R. Hanna, co-examiner

1999

Acknowledgements

First of all, my thanks go to my supervisor Dr Mathias Rotach. His encouragement and support during the last four years simply are the basis for the entire thesis. Occasional hour-long discussions with him over seemingly trivial concepts like pollutant puffs or dispersion marked my increasing understanding of a small, small part of science. Being a member of the research group of Prof Dr Atsumu Ohmura proved to be an inspiring mixture of freedom, and the obligation to do something useful with that freedom.

No matter which part of the field of atmospheric dispersion modeling I started working on, some of the fundamental papers always turned out to be written by Prof Dr Steven Hanna. It is a honor to me that he accepted to be co-examiner of this thesis.

The two-month research stay at Earth Tech, Inc. (formerly Sigma Research), working with Joseph Scire, David Strimaitis and, last but not least, Dr Robert Yamartino, initiated many different lines of work, of which only a part has already been finished and included in the present thesis.

Table Of Contents

Abstract

In this thesis a number of contributions on short-range dispersion modeling in the atmospheric boundary layer are collected. They include the development, validation and application of a model type called Puff-Particle Model (PPM), the investigation of a density kernel method to determine smooth concentration estimated for pure particle dispersion models, and the investigation of urban type surface structure on dispersion characteristics.

The PPM is a blend between a Lagrangian Gaussian puff model and a stochastic Lagrangian particle model. The pollutant puffs are advected by the mean wind; the dispersing effect of turbulent eddies smaller than the actual size of the puff is described by a relative dispersion parameterization. Additionally, the puffs exhibit artificial meandering on time scales shorter than the time interval between two consecutive updates of the mean wind field.

Commonly, puff models use either an absolute dispersion parameterization, which accounts for the dispersing effect of meandering as well. Such puff models provide predictions of the ensemble mean concentration. Alternatively, puff models may derive an estimate of the amount of meandering from the statistical properties of the ambient turbulence. This enables the specification of instantaneous ensemble mean concentration, together with its variance. In both cases, an instantaneous release is simulated by one puff. In contrast, in the PPM the puffs experience a stochastic but realistic meandering. To obtain ensemble statistics, an ensemble of puffs in the model has to be simulated for each released pollutant puff. Each simulated puff path is one possible realization of the release's dispersion. The main advantage is that all puffs are advected by the local wind at their current position. Concentration variances can be computed not only for instantaneous concentrations, but, due to the temporal correlation between subsequent positions of the meandering puffs, also for any other sampling time.

The puff meandering allows the PPM to compute the higher moments of concentration, along with the mean concentration, for any puff release. This provides a convenient way for risk assessment of hazardous releases, or for the computation of the frequency of exceedance of a given odor threshold. The particle model embodied within the PPM assumes that the evolution in time of particle velocity and position be a Markov process. This neglects the

spatial and temporal correlation between two neighboring particles. To extend the field of application of the PPM from puff to plume releases, a special puff-plume meandering scheme has been introduced. It constitutes a dependence of the individual puffs on their predecessors in the plume.

To ensure that the puff's meandering trajectory represents the correct amount of kinetic energy, the PPM computes a full three-dimensional particle trajectory, as supplied by a stochastic Lagrangian particle model. Such particle trajectories represent the entire spectrum of turbulent energy. A low-pass filter is thus applied which removes all eddies smaller than the actual puff size. The resulting time series of stochastic velocities is used as puff center trajectory. This avoids that an increasing part (as puff sizes grow) of the dispersion is double-counted both by the puff center trajectories and by the relative dispersion scheme.

The PPM can be used to compute ensemble-averaged concentrations by sampling over many individual puff trajectory realizations. For three tracer experiments, the PPM predictions are compared to those of other dispersion models. It is shown that, due to the built-in full-scale particle model, the PPM has approximately the same model prediction performance as pure stochastic particle models (which perform best). In the ensemble-average mode, the PPM is approximately one order of magnitude faster than pure particle models. This is due to the use of puffs, which lead to a smoother representation of the concentration density field. Particle models need to simulate more particles to allow for the same smoothness. A method is proposed for particle models to predict smoother concentration fields as well (and thus to speed them up accordingly), by assigning a density distribution to every particle. When concentrations are to be estimated, the size of these density distributions (called kernels) is chosen by optimizing between a smooth spatial concentration density and its oversmoothing.

Apart from the Puff-Particle Model, this thesis also focuses on the use of applied Gaussian plume models over urban environments. For single, high stack source configurations, Gaussian plume models give acceptable results. This is due to the fact that the condition of surface homogeneity is (more or less) fulfilled. Nowadays severe air pollution problems arise in the ever-growing cities. Built-up areas feature a different turbulence structure. It is shown for a specific example which adaptations in the use and computing code of an applied Gaussian plume model have to be undertaken in order to apply it to urban environments.

Zusammenfassung

Diese Dissertation besteht aus mehreren Beiträgen zur kurzreichweitigen Schadstoffausbreitung in der atmosphärischen Grenzschicht. Sie umfassen die Entwicklung, Validierung und Anwendung eines Modells namens Puff-Partikel Modell (PPM), die Untersuchung einer Methode zur Dichteschätzung für reine Partikel-Ausbreitungsmodelle mittels Dichtekerne, und die Behandlung der Auswirkungen von städtischen Oberflächen auf die Ausbreitungscharakteristiken.

Das PPM ist die Kombination eines Lagrange'schen Gauss'schen Puff-Modells und eines stochastischen Lagrange'schen Partikelmodells. Im PPM wird die Schadstoffemission simuliert durch anfänglich kleine Wölkchen (nachfolgend nach dem Englischen "Puff" genannt), welche durch den mittleren Wind fortbewegt werden Der dispersive Effekt von turbulenten Wirbeln, welche kleiner sind als das jeweilige Puff, wird durch eine Parametrisierung der relativen Dispersion beschrieben. Zusätzlich weisen die Puffs ein künstliches Mäandrieren auf mit Zeitskalen, welche kürzer sind als die Zeitspanne zwischen zwei aufeinanderfolgenden Aufdatierungen des mittleren Windfeldes.

Üblicherweise verwenden Puff-Modelle entweder eine Parametrisierung der absoluten Dispersion, welche auch die Dispersion aufgrund des Mäandrierens umfasst. Solche Modelle vermögen das Ensemblemittel der Schadstoffkonzentration vorherzusagen. Alternativ können Puff-Modelle den Beitrag des Mäandrierens separat aus den statistischen Eigenschaften der Turbulenz ableiten. Dies ermöglicht die Vorhersage der instantanen Konzentration zusammen mit ihrer Varianz. In beiden Fällen wird die Emission einer Schadstoffwolke durch ein 'Puff' simuliert. Im Gegensatz dazu weisen die Puffs im PPM ein stochastisches aber realistisches Mäandrieren auf. Um Ensemblemittel zu erhalten, muss für jede emittierte Schadstoffwolke eine Ensemble von Puffs simuliert werden. Jede simulierte Puff-Trajektorie stellt dabei einen möglichen Ablauf der Schadstoffausbreitung dar. Der Hauptvorteil dieses Ansatzes besteht darin, dass die Puffs immer mit dem mittleren Wind ihrer aktuellen Position transportiert werden können. Die Varianz kann nicht nur für die instantane Konzentration errechnet

werden, sondern wegen zeitlichen Korrelation zwischen aufeinanderfolgenden Positionen des mäandrierenden Puffs, auch für jene andere Mittelungsdauer.

Das Mäandrieren der Puffs erlaubt dem PPM, gleichzeitig mit dem Mittel der Konzentration auch die höheren Momente zu berechnen. Dies erlaubt die Risikoabschätzung für die Freisetzung von giftigen Gasen oder die Berechnung der Übertretenshäufigkeit einer bestimmten Geruchswahrnehmungsschranke. Das im PPM eingebaute Partikelmodell beschreibt die zeitliche Entwicklung von Partikelgeschwindigkeit und -ort als Markovprozess. Damit wird die räumliche und zeitliche Abhängigkeit zwischen zwei benachbarten Partikeln vernachlässigt. Um das PPM nicht nur für die Emission von Puffs, sondern auch für Rauchfahnen verwenden zu können, wurde ein spezieller Puff-Rauchfahne-Mäandrierungs-Algorithmus eingebaut. Es führt eine Abhängigkeit der einzelnen Puffs von ihren Vorgängern in der Rauchfahne ein.

Um sicherzustellen, dass diese Trajektorie die korrekte Menge an kinetischer Energie abbildet, berechnet das PPM für jedes Puff eine vollständige, drei-dimensionale Partikeltrajektorie. Diese Partikeltrajektorie wird mit Hilfe eines stochastischen Lagrangeschen Partikelmodells berechnet. Solche Partikeltrajektorien bilden das gesamte Turbulenzspektrum ab. Deshalb wird ein Tiefpassfilter verwendet, welches den Effekt aller turbulenten Wirbel entfernt, welche kleiner sind als das gegenwärtige Puff. Die resultierende Zeitreihe von stochastischen Geschwindigkeiten wird als Pufftrajektorie verwendet. Auf diese Weise wird vermieden, dass ein (mit wachsendem Puff) zunehmender Teil der Dispersion doppelt berücksichtigt wird, sowohl durch die Pufftrajektorie als auch durch die Parametrisierung der relativen Dispersion.

Das PPM kann verwendet werden, um herkömmliche mittlere Konzentrationen vorherzusagen. Dazu wird das Mittel über viele individuelle Pufftrajektorien gebildet. Für drei Tracerexperimente wird die Vorhersage des PPM mit jener anderer Modelle verglichen. Das PPM weist– wegen des eingebauten vollständigen Partikelmodells – etwa die gleiche Vorhersagefähigkeit auf wie vergleichbare reine Partikelmodelle (welche die besten Vorhersagen liefern), ist aber etwa eine Grössenordnung schneller. Dies ist auf die Verwendung der Puffs zurückzuführen, welche zu einer glatten Konzentrationsfeld-Vorhersage führen. Reine Partikelmodelle müssen dazu wesentlich mehr Partikel simulieren. Es wird eine Methode vorgeschlagen, wie auch Partikelmodelle glatte Konzentrationsfelder produzieren können,

was sie entsprechend beschleunigt. Dazu wird jedem Partikel eine Dichtefunktion zugeordnet. Zum Zeitpunkt der Konzentrationsberechnung wird dann die optimale Ausdehnung dieser Dichtefunktionen ermittelt, indem zwischen Glattheit und Überglättung des Konzentrationsfeldes optimiert wird.

Neben dem PPM bildet die Anwendung von Gauss'schen Rauchfahnen-Modellen über städtischem Gebiet ein weiterer Schwerpunkt der vorliegenden Arbeit. Für die Konzentrationsvorhersage alleinstehender Hochkaminen erzielen Gaussmodelle akzeptable Resultate, weil die Bedingung der Homogenität oft näherungsweise erfüllt ist. Heutzutage treten ernsthafte Luftreinhaltungsprobleme in den immer noch wachsenden Städten auf. Bebaute Gebiete weisen eine andere Turbulenzstruktur auf. Anhand eines konkreten Beispiels wird gezeigt, welche Änderungen in Einsatz und Programmcode notwendig sind, um einen Einsatz für städtische Gebiete zu ermöglichen.

Chapter 1

Introduction

1.1 OBJECTIVE OF THE THESIS

The main topic of this thesis is the modeling of the short-range atmospheric dispersion of puffs, a puff being an single instantaneous release of (pollutant, hazardous, or any other) material. The rate of growth of a puff depends on its size; as the puff grows, an increasing part of the spectrum of turbulent eddies will contribute to the puff's enlargement, instead of displacing it as a whole. For short-range applications, when puff sizes are small, this meandering caused by large turbulent eddies dominates the ensemble-averaged dispersion.

Thus the objective of the present thesis is the development of a short-range puff model simulating the instantaneous puff growth apart from the dispersing effect of meandering during the concentration sampling time. Puff growth is adequatly described by relative dispersion parameterizations. The main contribution of this thesis is the development of a scheme to simulate the meandering in three-dimensional space of pollutant puffs. The method adopted is to derive puff center meandering trajectories from stochastic particle paths, supplied by a Lagrangian particle model predicted ensemble-averaged dispersion. That part of the turbulent kinetic energy spectrum which is covered by the puff growth scheme has to be removed from the stochastic particle paths, in order to avoid the double-counting of dispersion. The resulting model approach is called Puff-Particle Model (PPM).

In contrast to relatively dispersing puff models intended for far-field applications like RIMPUFF (Mikkelsen *et al.* 1984) and, which use relative dispersion and aim at resolving the meandering movements by frequently updated flow fields, the artificial meandering of the PPM allows it to be applied in the near field where the small puff sizes would otherwise require flow field updates every few seconds. Several models have been developed based on Gifford's (1959) meandering plume concept to separate the dispersing effect of instantaneous plume (or puff) growth and of meandering (e.g. Hanna 1984, 1986; Savunen and Rantakrans 1997; Sykes 1988). They all have in common that a certain shape of the probability density function of concentration is assumed and that the variance of concentration fluctuations is

derived from the properties of turbulence. SCIPUFF (Sykes 1997) uses a second-order turbulence closure scheme predicting both the mean concentration and its variance. In contrast, the PPM aims at simulating a realistic three-dimensional meandering of the puffs, which allows for the direct determination of the higher moments of concentration, while enabling the individual puffs to account for inhomogeneous conditions.

1.2 ON POLLUTANT TRANSPORT MODELING IN THE PLANETARY BOUNDARY LAYER

1.2.1 Plume, puff and particle atmospheric dispersion models

In this thesis, a number of different studies on air pollution modeling is presented. Atmospheric dispersion is a direct result of atmospheric turbulence. In an Eulerian system, the conservation equation of a scalar quantity (e.g. concentration) contains turbulent fluxes which in general are not known directly. Using K-theory, parameterized eddy diffusivities can be used in order to obtain an analytical solution. When assuming homogeneity, stationarity, and uniform wind speeds regardless of height and eddy diffusivities, an analytical solution can be obtained which is commonly known as Gaussian plume model (e.g. Businger 1982).

Plume models describe the (continuously emitting) release with the use of a plume axis and standard deviations of the pollutant distribution in the lateral and vertical direction as a function of travel time (e.g. Hanna 1982; Sykes *et al.* 1986). The entire plume is always immediately affected by changes of the meteorological conditions at the point of measurement. This lack of causality limits the application of plume models to quasi-stationary conditions beforehand. The major disadvantage of plume models is that their inherent assumptions on homogeneity and stationarity are often not sufficiently fulfilled.

Using a Lagrangian framework, puff dispersion models and stochastic particle models can be distinguished. Puff models cluster the release into consecutively released pollutant puffs. Puffs have a center of mass, which is affected by the flow field, a mass assigned to the puff, and a density distribution (e.g. Mikkelsen *et al.* 1987). Usually, the density distribution is assumed to be Gaussian, so that the concentration can be computed when additionally specifying the lateral, longitudinal, and vertical standard deviations of the density distribution (i.e. puff).

Particle models split the pollutant emission up into discrete particles, which in most cases all have identical masses. The particles act like inertialess infinitely small parcels of air, thus exactly following the local flow field. The particles in these models are assumed to have an additional, stochastic velocity component. When applying 1-particle statistics (Thomson 1987), particle models will predict ensemble-averaged dispersion. This modeling approach allows for non-Gaussian turbulence, especially for the specification of a vertically skewed turbulence probability density function to describe day-time convective conditions (e.g. Luhar and Britter 1989). Using the more complicated 2-particle statistics (Thomson 1990; Borgas and Sawford 1994), relative dispersion is predicted. The major disadvantage of particle models is their need of computing time.

1.2.2 Absolute and relative dispersion

There are two different sampling times, one for the measured meteorological parameters, T_{sM}, and the other for the pollutant concentration prediction, T_{sC}. If the sampling time of an available meteorological information is longer than the desired sampling time of concentration, the dispersion parameterization has to predict the concentration for the concentration sampling time T_{sC}. Then, there is a "gap of dispersion" between T_{sC} and the sampling time of the meteorological input, T_{sM}.

The well-known "absolute" dispersion (so-called 1-particle statistics, or ensemble averaged dispersion), is the ensemble-averaged particle separation with respect to a fixed point in space (Taylor 1921). Richardson (1926) was the first to introduce the concept of relative dispersion, defined as the ensemble averaged separation between pollutant particles released together, i.e. the dispersion around the cluster's center. Gifford (1957a, 1957b) first pointed out that the instantaneous growth of puffs is governed by the concept of relative instead of absolute dispersion. Within the concept of relative dispersion (i.e. 2-particle statistics), turbulent eddies smaller than the actual puff size will contribute to its growth (increasing the ensemble 2-particle separation), while larger eddies move the puff as a whole (without changing the separation of the particles). Mikkelsen *et al.* (1987) derive a set of relative dispersion parameterizations for Gaussian puffs, based on the work of Batchelor (1952).

The missing link between relative and absolute dispersion is the dispersing effect of meandering over time-scales shorter than the averaging time for which the absolute dispersion parameterization applies. Here, "meandering" means movements of the center of the puff or

plume with respect to a fixed point in space. Most formulations of absolute dispersion correspond to an ensemble averaging time of roughly one hour, corresponding to the spectral gap between synoptic and turbulent frequencies. Hence, if $T_{sC} < 1$ hour, or if $T_{sM} > T_{sC}$, or if $T_{sM} < 1$ hour, relative rather than absolute dispersion should be used. For plume or puff models, this means that the meandering has to be treated separately.

1.2.3 Development of the Puff-Particle Model

In order to better understand puff dispersion, in chapter 5 an arbitrary definition of two categories of puff models is introduced. On the one hand, 'plume segment' models, which describe a segment of an ensemble averaged plume by using a puff; their absolute dispersion scheme accounts for the ensemble averaged dispersion (from cluster growth and cluster meandering) during the averaging time T between two consecutive updates of the mean flow field. On the other hand, 'cluster dispersion' models, which interpret a puff as being an instantaneous cluster of pollutants. The spectral gap between turbulent eddies covered by the flow field and those covered by the relative dispersion scheme is simulated with artificial meandering.

The main contribution of the present thesis is the development of the Puff-Particle Model (PPM). The PPM represents the second group of cluster dispersion models. It uses relative dispersion to describe the instantaneous growth of the cluster (puff); the range of turbulent eddies covered by the relative dispersion depends on the size of the cluster. Eddies larger than the cluster will displace the cluster as a whole without dispersing it. This meandering has to be simulated separately.

Within the PPM, the pollutant release is emitted as initially small clusters (puffs), which are advected by the mean wind. Additionally, the puffs exhibit artificial meandering on time scales shorter than the time interval between two consecutive updates of the mean wind field. The dispersing effect of turbulent eddies smaller than the actual size of the puff is described by a relative dispersion parameterization. The turbulent kinetic energy which is not covered by these small eddies is represented by the meandering of the puffs.

There are two ways of looking at the PPM: as a particle model which is speeded up by grouping particles into clusters. The total gain in computing speed is one order of magnitude. (Another factor of 10 can be gained by using an efficient way to estimate the concentration within particle models, see Section 1.2.5). Alternatively, the PPM may be considered as a puff

model with a meandering sub-model, thus allowing the use (and its benefits) of relative dispersion even when frequently updated meteorological information is not available. The basic principle of the PPM, the method to simulate meandering artificially, and a comparison of model results with predictions from other models, are given in Chapter 2

The PPM is a reseach model focussing on the treatment of relative dispersion and puff meandering. Operational puff models like CALPUFF (Scire *et. al.* 1997), U.S. EPA's INPUFF, RIMPUFF (Mikkelsen *et al.* 1984) or SCIPUFF (Sykes 1997), on the other hand, offer a wide range of different parameterizations which are missing in the PPM like, for example, CALPUFF's chemical reaction scheme, RIMPUFF's radiative dose integration capabilities, or SCIPUFF's advanced adaptive grid technique and puff splitting and merging procedures. Besides its main application as a puff meandering model, the PPM can also be driven in a 'plume segment' mode (using absolute dispersion without meandering) and in a 'pure particle' mode.

1.2.4 Avoiding the double-counting of dispersion

The puff-particle approach aims at simulating the dispersing effect of plume meandering by introducing puff center trajectories. These trajectories are determined by the low-frequency part of the turbulence spectrum, since relative dispersion only describes the effects of the high-frequency part. As the puff's size grows, the relative dispersion covers an increasing part of the spectrum (Batchelor 1952; Mikkelsen *et al.* 1987). Therefore, the trajectory of the puff's center of mass has to simulate the effect of a decreasing amount of turbulent eddies, and thus has to become 'smoother' as puff sizes grow.

In the PPM, the stochastic trajectories of the puff centers are derived from (but not identical to) paths of particles as simulated by a fully 3D Lagrangian particle model. The underlying assumption of the particle model employed is that turbulence is a Markov process. This means that the turbulent velocity of any particle at the next time step is fully explained by its current position and velocity. A very effective low-pass filter can be constructed by making use of the fact that the process is Markovian. The corresponding filter eliminates high-frequent stochastic movements and thus produces the required puff center meandering trajectories. These trajectories become smoother (only influenced by large eddies) as the puff grows. The scheme to avoid the double-counting of dispersion is discussed in some detail in Chapter 3.

1.2.5 Density kernels within particle models

In puff models, the computation of a predicted mean concentration at a certain location is done by superimposing the density distributions of all individual puffs at that location. Particle models use a different theory of diffusion than puff models. The Thomson (1987) family of particle models prescribes the (Eulerian) characteristics of turbulence at every point in space, and uses a (numerical) procedure to ensure that the (Lagrangian) motions of the inertialess particles complies with these characteristics. Puff models, on the other hand, aim at separating relative dispersion and dispersion originating from meandering (yielding absolute dispersion). Here, the boundary (a frequency in the spectrum of turbulent kinetic energy) between relative dispersion and dispersion originating from the larger eddies depends on the actual size of the puff in question.

For particle models, it is a common practice to calculate concentration averages over a grid cell in space by counting all particles in a box (a list of examples is given in section 4.2.1). The mass concentration is then obtained by multiplying the number of particles with their mass, and dividing this total mass by the size of the grid box. If the volume average over such a box is what the modeler wants, such box-counting methods are the most efficient.

Often, what is actually needed is the modeled concentration at a given *point* in space. Such point estimations are especially needed when comparing model predictions with measurements from tracer experiments. The “sampling volume” of the concentration measurement units commonly used in such field experiments are by far smaller than the volumes over which the concentration is averaged when employing the box-counting method.

For these reasons, another concentration estimation method is proposed in Chapter 4 of this thesis. It relies on the concept of density distributions of different shape which are ”added” to the particle’s position, i.e. the mass represented by the particle is spread out in space. Such a density distribution around the center of mass is called the density kernel. It has been used first by Lorimer (1986) and Yamada *et al.* (1987) and Yamada and Bunker (1988) within particle models. In the method proposed in Chapter 4, the size (bandwidth) of the kernel distribution is chosen such that the bias and variance of the concentration estimation are jointly minimized.

The kernel method has been widely applied in various fields of science. In atmospheric dispersion modeling, the box-counting method is still used despite its deficiencies. The kernel

method shows most pronounced improvements for concentration predictions in the near-source field, where changes in the particle density are sharp and large proportions of the total number of particles might still be within the volume of few sampling boxes, and for the estimation of surface concentrations, which are of interest for most air pollution simulations, but are likely to show gradients near the surface over distances similar to the vertical extent of box sampling volumes.

Within the PPM, a low-pass filter (which depends on the size of the relatively dispersed puff) removes dispersion from the particle trajectories (cf. previous Section, and Chapter 3). On the contrary, the ”dispersion” added to the model by the numerical kernel bandwidths should not be filtered out of the particle model. It is the smoothing necessary to interpolate between particle positions, and tends to zero as the number of particles approaches infinity, whereas the "overdispersion" (i.e. oversmoothing) caused by the physical sizes remains constant.

1.3 NATURAL VARIABILITY OF POLLUTANT CONCENTRATIONS

1.3.1 Modeling hazardous releases and odor problems

There are different classes of atmospheric pollutants (here, we restrict ourselves to boundary layer pollutants, leaving apart, e.g., gases with greenhouse warming potential). A first group is harmful to the environment (eco-systems, flora or fauna) on a long term basis. Fine particles belong to this first group. The total intake is the important parameter to human health. Whether this intake originates from a high background level or from episodes, is of lesser importance.

The second group can cause impacts on the human health during shorter episodes as well. The main matter of concern is their concentration level during periods of, say, one hour. A member of this group is, for example, ozone. For most species in this group (like NO_x, SO_2, etc.), but not, in general, for ozone, regulatory limits have been imposed both for yearly and (half-)hourly averages (or percentiles thereof). Ensemble-averaged concentration is suited for most applications concerning pollutants from these first two groups.

Atmospheric pollutants of a third group, however, are a health risk on even shorter time scales. Toxic gases can be lethal within minutes or seconds; in general, it is a certain dose (concentration intake integrated over time) which is considered lethal. Such toxic gases can be either emitted during chemical warfare, or as accidental release. Here, the term hazardous

release represents both. Although they do not represent a direct health risk, gases likely to cause odor impacts also belong to this group.

"Assessment of flammability or toxicity on the basis of ensemble-averaged concentrations can be seriously in error. These effects depend on short temporal- and spatial-scale fluctuations and thus the variance is essential for these predictions" (Sykes 1988, p. 354). Short temporal scale effects call for short (concentration) sampling times. This violates a basic assumption of many common air pollution models, since such averaging times are considerably shorter than the spectral gap (approximately one hour). Most models assume that the sampling time is "a time long enough to include most of the turbulent energy spectrum" (Hanna 1982, p. 278).

Often rather than estimating the ensemble-averaged concentration of hazardous material, predictions of a worst-case scenario is needed. This means that the higher moments of concentration have to be predicted as well as the type of distribution, i.e. the probability density function of concentration (which is specific for a given source-receptor configuration, and for a certain concentration sampling time). The need for probability density functions is characteristic for all *a priori* problems (where model outcomes are an input to decision making), in contrast to the more frequent *a posteriori* problems (where a concentration average suffices).

1.3.2 Plume and puff meandering models

„Surprisingly little work has been done in the proper application of statistical analysis techniques to the evaluation of models. Even fewer people recognize that an observed pollutant concentration, averaged over a time, T_a, is a turbulent variable" (Hanna 1986). Dispersion models, on the other hand, usually predict an ensemble-mean concentration, which cannot be expected to agree with a single observed concentration even if the model were „perfect".

Many researchers assume a two-scale system where the (turbulent) concentration fluctuations are due to (i) in-plume turbulence; and (ii) intermittency, i.e. meandering of the plume, leading to periods of zero concentration. This two-scale system is based on Gifford's (1959) fluctuating plume theory, which assumes that a narrow plume with an instantaneous standard deviation σ_{yI} meanders back and forth to give the total standard deviation σ_{yT}. The standard deviation of the meandering motions is σ_{yM}, and the three standard deviations are related by

$\sigma_{yT}^2 = \sigma_{yI}^2 + \sigma_{yM}^2$ (σ_{yI} and σ_{yM} are uncorrelated by definition). If the source aperture is very small, then σ_{yI} is small compared with σ_{yM} at travel times less than the Eulerian time scale, T_E, of the ambient turbulence.

Observations (Fackrell and Robins 1982) show that the most pronounced plume concentration fluctuations are produced very near to the source, and the form of the pdf (probability density function) changes from a near-source exponential to a intermediate-field normal distribution. Despite these forms, the ratio of peak to ensemble-averaged concentrations seems to remain constant. The relative amount of meandering (with respect to ensemble-averages dispersion) depends on atmospheric stability. For stable (night-time) conditions, for example, Hanna (1983) observed very high lateral plume meandering.

Savunen and Rantakrans (1999) present an odor model based on the assumption of a log-normal C-pdf, based on Gifford (1959) and Hanna (1986). Its second moment is estimated as the standard deviation of the meandering motion or, when the plume becomes well-mixed, as the standard deviation of turbulent velocity. Sykes *et al.* (1984) present a second-order turbulence closure scheme which accurately describes the near-field meandering and is able to predict the concentration variance along with the ensemble-mean concentration.

Borgas (1998) and Wilson and Hildermann (1999) focus on the prediction of the highest occurring concentration caused by internal fluctuations. Borgas (1998) uses theoretical relative dispersion considerations to derive the higher moments of the C-pdf, whereas Wilson and Hildermann (1999) use a stochastic Markov process to emulate the time series of internal concentration fluctuations, when the moments of the C-pdf are supplied by any plume meandering model.

1.3.3 Plume meandering during user-specified averaging times

Gifford's (1959) fluctuating plume dispersion model neglects dispersion in the direction of the mean wind, leading to a 'spreading disk' plume dispersion model. The mean concentration distribution as predicted by Gifford's (1959) model is identical with predictions from ensemble-averaged plume models. Additionaly, it predicts statistical properties like the variance of point concentrations. The 'split' between instantaneous plume growth and dispersion due to meandering is a function of down-wind distance, i.e. is different for each 'disk' of the fluctuating plume. These 'disks' do not actually move; it is the statistical property of their movement that is predicted. From this it follows that the statistical properties

of concentration as predicted by the Gifford (1959) approach apply to instantaneous (point) concentrations, i.e. with zero averaging time.

For a non-zero, arbitrary concentration averaging time, however, the correlation of the meandering movements between two neighboring 'disks', or puffs, has to be taken into account. Even though the statistical properties of concentration fluctuations for each point are correct, the statistical properties of concentration *averages* over time differ from non-correlated to correlated meandering. Sykes (1984) and Sykes and Gabruk (1997) present an extension to the Gifford (1959) model, introducing an autocorrelation function for concentration fluctuations. This allows for the computation of the influence of averaging time on the concentration variances.

By using two-particle statistics (Thomson 1990), Thomson (1996) theoretically derives expressions for the second-order moment structure (for different source configurations) of dispersing plumes and puffs in the near, intermediate and far field. This also ensures that the correlation of meandering motions of particles belonging to the same source is taken into account correctly when estimating concentration variances as a function of averaging time.

As has been outlined in Section 1.2, the PPM features stochastic trajectories for the centers of mass of the puffs. This is done to mimic the meandering caused by turbulent eddies larger than the puff itself. The PPM can thus be called a puff-meandering model, coupled with a puff growth parameterization. However, although the corresponding meandering of an individual puff is realistic (i.e. with the correct amount of turbulent kinetic energy), there is no correlation between individual puffs, neither in space nor time. Neighboring puffs will act totally independent of one another. Their trajectories may even cross.

This is a direct consequence of the use of Lagrangian stochastic particle model based on the Markov assumption (thus yielding absolute dispersion, or 1-particle statistics). The Markov assumption implies that the current position, velocity and acceleration of a particle only depend on the corresponding values of the same particle one timestep ago. However, the (spatial and temporal) correlation between parcels of air (represented by puffs) is crucial to the correct estimation of concentration fluctuations. If this correlation (that is, the turbulent eddies themselves) is ignored, the frequency spectrum of simulated concentration is shifted towards higher frequencies. This means that the worst-case episodes are underestimated,

which makes the prediction useless. Thus, by its basic concept, the PPM suffers from the same short-coming as the Gifford (1959) approach.

Therefore, a special plume-puff meandering scheme has been introduced into the PPM (Section 5). It uses “threads of puffs” to represent a plume, or a plume segment. Within such a thread, the puff “knows” the turbulent velocities of its predecessor. Depending on the spatial and temporal separation between the two puffs, the stochastic movements are correlated. This scheme still has some limitations, for example there will be no correlation between two sources which are situated close to each other. However, for a single, continously emitting source, where the average wind speed does not drop below a certain threshold, this scheme is considered to give a realistic (meaning: with the correct spectrum) picture of meandering.

This plume-puff meandering scheme fully models the second of the two time scales of concentration fluctuations (Hanna 1984, 1986): intermittency, i.e. plume meandering. The internal (in-puff, i.e. in-cluster) concentrations fluctuations, however, cannot be modeled with this approach. For this, an additional internal fluctuation model should be used as a postprocessor.

1.4 ADAPTING CONTINOUS PLUME MODELS TO URBAN ENVIRONMENTS

1.4.1 On air pollution modeling within cities

Particle or puff models exhibit advantages over Gaussian plume models as discussed in the previous sections. Their application becomes virtually impossible, however, when it comes to the simulation of an entire year for all sources from e.g. a city. Gaussian plume models are still the method-of-choice for such applications. They have been successfully used for rural single stack configurations. Extensive data sets from corresponding tracer experiments are available and have been used to validate Gaussian plume models (e.g. Hanna and Chang 1993; Olesen 1995; Carruthers *et al.* 1992).

An increasing percentage of the population lives in agglomerations. Cities with their generally high pollutant emission densities affect an increasing population. Technical measures undertaken to reduce air pollution levels addressed heavily polluting industrial activities first. Nowadays, the air pollution level often originates from a countless number of small, not well determined emission sources, especially within cities. Air pollution modeling faces the challenge to shift from the classical single source (with a high stack) dispersion problem, in a

rural surrounding, towards multi-source, multi-receptor situations, in inhomogeneous urban environments.

Although crucial to micro-scale dispersion modeling, very little is known concerning the flow and turbulence structure over built-up areas with irregularly spaced buildings and trees. The latter induce a roughness sublayer (RS), which ranges from ground-level to several times the average obstacle height (Raupach *et al*. 1991). Over urban areas, the vertical extension of the roughness sublayer cannot be neglected. Within this roughness sublayer, the flow and turbulence fields are different from that of the surface layer above (Högström *et al.* 1982; Roth and Oke 1993; Roth 1993; Oikawa and Meng 1995). For example, the Reynolds Stress increases with height (Rotach 1993a). This leads to a smaller gradient of mean wind speed as compared to the 'logarithmic profile' of the surface layer (Rotach 1993a) and the necessity to revise the scaling concept for the turbulence statistics such as velocity variances (Rotach 1993b). Based on these observations, Rotach (1997) proposes a method to introduce the roughness sublayer into existing dispersion models.

1.4.2 Adaptation of a Gaussian plume model

In principle, dispersion modeling over cities could be done with particle models or with puff models like the PPM. Due to limited computational resources, however, Gaussian plume models are still used to handle multi-source / multi-receptor problems. The validity of the Rotach (1997) approach has first been testes with an advanced particle model for a tracer experiment. In this thesis, it then is introduced into a Gaussian plume model which is first validated with two tracer experiments conducted over suburban environments (Section 6). Then, it is applied to the emission inventory of a city for a whole year of meteorological data (Section 7). The method of Rotach (1997) requires changes in the meteorological pre-processor. If the dispersion model uses similarity theory instead of stability classes, the concept of local scaling (the friction velocity being a function of height in the RS) needs to be implemented in the dispersion model itself.

Apart from the RS, the presence of roughness elements also leads to a higher amount of mechanically induced turbulence, as compared to rural environments for the same synoptic conditions. This leads to a tendency of the stability over urban surfaces towards neutral conditions, as compared to the rural areas surrounding the city. One of the more pronounced effects is that there seems to be a minimum value to the Obukhov length, L, such that really

stable as well as free convection conditions hardly ever occur within the center of a city (Hanna and Chang 1992, 1993).

Another characteristic to urban turbulence is the urban energy balance, which differs from the energy balance as it could be observed in the rural environment surrounding the city. The very high fraction of built-up areas leads to a lower albedo, and to a fast run-off of precipitation together with a reduced water storage capacity. Moreover, after the event of snowfall, the over-all albedo changes rapidly away from that of fresh snow, because snow is removed from large parts of the road surfaces, and the remainder of the snow gets dirty.

1.4.3 Limitations to applied modeling

Plume models represent a valid (analytical) solution to the diffusion equation only for idealized circumstances. Stationarity and homogeneity of the turbulence characteristics are requested. In practice, none of these conditions is fully satisfied, but Gaussian plume models have proved to be successful for a variety of applications. As for any other modeling approach, useful results can be obtained as long as the modeler does not interpret the model results in a direction for which no physical parameterizations have been implemented. For example, the homogeneity condition limits the spatial resolution: only concentration predictions averaged over an area of a certain size (for which the city's different areas start looking homogeneous) are reliable.

When adapting continuous plume models to urban environments, in general there is no such thing as an averaged mean wind speed in the lowest few tens of meters, i.e. between the building structures themselves. Plume models can thus not be used in the layer between the buildings. But the majority (in number) of the emission sources, and of the (human) receptors, is situated there. The lowest height which can safely be chosen as the model boundary is the zero plane displacement height (Rotach 1994). Predicted concentrations, too, can only be computed for this minimum height.

An additional source of uncertainty when using plume models within cities is the fact that almost all emissions originate from combustion processes (road traffic, domestic heating, waste incineration, etc.) and thus have a buoyancy induced plume rise. On the aggregated level of gridded emission inventories, the individual characteristics of stacks (like diameter, temperature excess, and vertical exit velocity) are of no importance. An attempt has been made to parameterize the over-all effect of plume rise, and to include this in the model.

1.4.4 Using dispersion models togehter with gridded emission inventories

When applied to an emission inventory, dispersion models will only predict area averaged concentrations, but the measurements will essentially be point concentrations. The latter may be influenced by local emission sources (like major roads), or they may not (giving the urban background concentration). If local influences are present, they may either be resolved by the emission inventory, or they may not.

The representativeness of measurement stations depends on the local influence from roads or near-by buildings. This calls for a detailed investigation of all measurement sites. For any validation of model results, the available point receptor measurements should be classified to at least these three groups (urban background, influenced by major roads with or without local influences). A dispersion model is expected to perform best in predicting the urban background, second-best in predicting concentrations where roads are adequately resolved in the emission inventory, and will show considerable error when local non-resolved effects influence the concentration measurement.

When a concentration measuring unit is positioned such that strong local influences exist (for example in a street canyon), the measured concentration may strongly depend on the mean wind direction. Then, the stationarity condition, and the ensemble-average approach, only allow for concentration sampling times of 24 hours and longer to be compared with the corresponding model predictions. They also do not allow for the comparison of the distribution of hourly concentration, i.e. of quantile-quantile plots of predicted vs. observed concentration, as a model validation tool for such sites with local influences.

REFERENCES

Batchelor, G. K. (1952): Diffusion in a field of homogeneous turbulence–Part II: The relative motion of particles. *Proc. Camb. Philos. Soc.*, **48**, 345–362

Borgas, M. S., and Sawford, B. L. (1994): A family of stochastic models for two-particle dispersion in isotropic homogeneous stationary turbulence. *J. Fluid. Mech.*, **279**, 69–99

Borgas, M. S. (1998): The variability of pollutant doses in atmospheric plumes. Presented at 14th Clean Air & Environment Conf., Oct. 18–22, 1998, Melbourne, Australia

Businger, J. A. (1982). In: Atmospheric turbulence and air pollution modelling, F. T. M. Nieuwstadt and H. van Dop (eds.), Reidel, Dordrecht, pp. 1–36

Carruthers, D. J., Holroyd, R. J., Hunt, J. C. R., Weng, W.-S., Robins, A. G., Apsley, D. D., Smith, F. B., Thomson, D. J. and Hudson, B. (1992): UK Atmospheric Dispersion Modelling System. In van Dop, H. and Kallos, G. (eds.), *Air Pollution Modelling and its Applications IX*, Plenum Press, New York

Fackrell, J. E., and Robins, A. G. (1982): Concentration fluctuations and fluxes in plumes from point sources in a turbulent boundary layer. *J. Fluid. Mech.*, **117**, 1–26

Gifford, F. A. (1957a): Relative atmospheric diffusion of smoke puffs. *J. Meteorol.*, **14**, 410–414

Gifford, F. A. (1957b): Further data on relative atmospheric diffusion. *J. Meteorol.*, **14**, 475–476

Gifford, F. A. (1959): Statistical properties of a fluctuating plume dispersion model. *Adv. Geophys.*, **6**, 117–138

Hanna, S. R. (1982): Applications in air pollution modeling. In: Atmospheric turbulence and air pollution modelling, Nieuwstadt, F. T. M, and van Dop, H. (eds.). Kluwer Academic Publishers, Dordrecht, Netherlands, 275–310

Hanna, S. R. (1983): Lateral turbulence intensity and plume meandering during stable conditions. *J. Clim. Appl. Meteorol.*, **22**, 1424–1430

Hanna, S. R. (1984): Concentration fluctuations in a smoke plume. *Atm. Environ.*, **18**, 1091–1106

Hanna, S. R. (1986): Spectra of concentration fluctuations: The two time scales of a meandering plume. *Atmos. Environ.*, **20**, 1131–1137

Hanna, S. R., and Chang, J. C. (1992): Boundary-layer parameterizations for applied dispersion modeling over urban areas. *Boundary-Layer Meteorol.*, **58**, 229–259

Hanna, S. R., and Chang, J. C. (1993): Hybrid Plume Dispersion Model (HPDM) – improvements and testing at three field sites. *Atm. Environment*, **27A**, 1491–1508

Högström, U., Bergström, H., and Alexandersson, H. (1982): Turbulence characteristics in a near-neutrally stratified urban atmosphere. *Boundary-Layer Meteorol*., **23**, 449–472

Lorimer, G. S. (1986): A kernel method for air quality modelling – I: Mathematical foundation. *Atmospheric Env.*, **20**, 1447–1452

Luhar, A. K. and Britter, R. E. (1989): A random walk model for dispersion in inhomogeneous turbulence in a convective boundary layer. *Atmospheric Env.*, **23**, 1911–1924

Mikkelsen, T. and Larsen, S. E. (1984): Description of the Risø puff diffusion model. *Nuclear Technology*, **67**, 56–65

Mikkelsen, T., Larsen, S. E. and Pécseli, H. L. (1987): Diffusion of Gaussian puffs. *Quart. J. Roy. Met. Soc*., **113**, 81–105

Oikawa, S., and Meng, Y. (1995): Turbulence characteristics and organized motion in a suburban roughness sublayer. *Boundary-Layer Meteorol*., **74**, 289–312

Olesen, H. R. (1995): The model validation exercise at Mol: Overview of results. *Int. J. Environment Pollution*, **5**, 761–784

Raupach, M. R., Antonia R. A. and Rajagopalan S. (1991): Rough-wall turbulent boundary layers. *Appl. Mech. Rev*., **44**, 1–25

Richardson, L. F. (1926): Atmospheric diffusion shown on a distance-neighbour graph. *Proc. Royal Soc*., Series A, **110**, 709–737

Rotach, M. W. (1993a): Turbulence close to a rough urban surface. Part I: Reynolds stress. *Boundary-Layer Meteorol*., **65**, 1–28

Rotach, M. W. (1993b): Turbulence Close to a Rough Urban Surface Part II: Variances and Gradients. *Boundary-Layer Meteorol*., **66**, 75–92

Rotach, M. W. (1994). Determination of the zero plane displacement in an urban environment. *Boundary-Layer Meteorol*., **67**, 187–193

Rotach, M. W. (1997): Towards meteorological preprocessing for dispersion models in an Urban Environment. *Inter. J. Environment Pollution*, **8**, 548–556

Roth, M., and Oke, T. R. (1993): Turbulent transfer relationships over an urban surface. I: Spectral characteristics. *Quart. J. Roy. Meteorol. Soc*., **119**, 1071–1104

Roth, M. (1993): Turbulent transfer relationships over an urban surface. II: Integral statistics. *Quart. J. Roy. Meteorol. Soc*., **119**, 1105–1120

Savunen, T., and Rantakrans, E. (1999): Description and application of an odour dispersion model. Presented at 23rd NATO/CCMS ITM, Bulgarian, 1998. To be published in: Air Pollution Modeling and Its Application XIII, S.-E. Gryning and E. Batchvarova (eds.), Plenum Press, New York.

Scire, J. S., Strimaitis, D. G., Yamartino, R. J., and Insley, E. M. (1997): A user's guide for the CALPUFF dispersion model (Version 5.0). Earth Tech, Inc., Concord, MA 01742, USA.

Sykes, R. I., Lewellen, W. S., and Parker, S. F. (1984): A turbulent-transport model for concentration fluctuations and fluxes. *J. Fluid. Mech.*, **139**, 193–218

Sykes, R. I. (1984): The variance in time-averaged samples from an intermittent plume. *Atmos. Env.*, **18**, 121–123

Sykes, R. I., Lewellen, W. S., and Parker, S. F. (1986): A Gaussian plume model of atmospheric dispersion based on second-order closure. *J. Clim. Appl. Met.*, **25**, 322–331

Sykes, R. I. (1988): Concentration fluctuations in dispersing plumes. In: Lectures in air pollution modeling, A. Venkatram and J. C. Wyngaard (eds.), American Meteorological Society, Boston, USA

Sykes, R. I., and Gabruk, R. S. (1997): A second-order closure model for the effect of averaging time on turbulent plume dispersion. *J. Appl. Met.*, **36**, 1038–1045

Sykes, R. I. (1997). PC-SCIPUFF version 1.0 technical documentation. Technical report, Titan Corp., Princeton NJ, USA

Taylor, G. I. (1921): Diffusion by continuous movements. *Proc. London Math. Soc.*, Ser. 2, **20**, 196–211

Thomson, D. J. (1987): Criteria for the selection of stochastic models of particle trajectories in turbulent flows. *J. Fluid Mech*., **180**, 529–556

Thomson, D. J. (1990): A stochastic model for the motion of particle pairs in isotropic high-Reynolds-number turbulence, and its application to the problem of concentration variances. *J. Fluid. Mech.*, **210**, 113–153

Thomson, D. J. (1996): The second-order moment structure of dispersing plumes and puffs. *J. Fluid. Mech.*, **320**, 305–329

Wilson, D. J., and Hilderman, T. L. (1999): Stochastic reconstruction of intermittent zero concentration periods in plumes for accidental toxic and flammable releases. Presented at 23rd NATO/CCMS ITM, Bulgaria, 1998. To be published in: Air Pollution Modeling and Its Application XIII, S.-E. Gryning and E. Batchvarova (eds.), Plenum Press, New York

Yamada, T., Bunker, S., and Niccum, E. (1987): Simulations of the ASCOT Brush Creek data by a Nested-Grid, Second-Moment Turbulence Closure Model and a Kernel Concentration Estimator. AMS 4th Conference on Mountain Meteorology, 25–28 Aug. 1987, Seattle, WA

Yamada, T. and Bunker, S. (1988): Development of a Nested Grid, Second Moment Turbulence Closure Model and Application to the 1982 ASCOT Brush Creek Data Simulation. *J. Appl. Meteorol.*, **27**, 562–578

Chapter 2

A Novel Approach to Atmospheric Dispersion Modelling: The Puff-Particle Model (PPM)*

Abstract—The Puff-Particle Model (PPM) uses a new approach to problems of three-dimensional atmospheric dispersion from micro- to meso-scale. The pollutant particles are grouped in clusters treated as Gaussian puffs, which are dispersed making use of the concept of relative diffusion. The centre of mass of each puff is moved along a stochastic trajectory. This trajectory is derived from particle trajectories given by a Lagrangian stochastic-dispersion model. In this way, the PPM retains the advantages of traditional puff models and those of particle models, and is able to take into account the correct probability density function of the stochastic velocity components. The effect of meandering (caused by turbulent eddies larger than the puff but not resolved by the flow field) is simulated by the puff centre trajectories, yielding a complete description of dispersion. The PPM is validated using measurements from three tracer experiments in Copenhagen, Lillestrøm and Kincaid.

Key words: Lagrangian dispersion, model validation, particle model, puff model, relative diffusion.

2.1 INTRODUCTION

Particle models (or random flight models) are generally accepted to be most appropriate to describe dispersion from passive non-buoyant releases in inhomogeneous turbulence (Wilson and Sawford 1996). In particular, dispersion in the convective boundary layer is successfully modelled using this approach (e.g. Luhar and Britter 1989; Hurley and Physick 1993; Rotach *et al.* 1996). According to the underlying theory they yield ensemble plume statistics, i.e. absolute dispersion. The major disadvantage of this model type is its excessive consumption of computing time. Puff models are much faster (and thus less computing time demanding) than particle models, but still allow for simulating dispersion in inhomogeneous turbulence. When using relative dispersion to grow the puffs, this approach is furthermore suited to model instantaneous releases (one single realisation of

---

* this chapter has been published as:
de Haan, P., and Rotach, M. W. (1998): A novel approach to atmospheric dispersion modelling: The Puff-Particle Model. *Quart. J. Roy. Meteorol. Soc.*, **124**, 2771–2792

a plume). This quality makes them useful for predicting concentration fields for cases of hazardous releases of toxic material (Mikkelsen and Larsen 1984). On the other hand, when being used in conjunction with absolute dispersion, puff models yield ensemble plume statistics. Since the shape of the puffs often is assumed to be Gaussian, these predictions might be less accurate than those of particle models, especially for non-Gaussian turbulence (convective conditions), but again, they are 'cheaper' in terms of computing time. As additional advantages over particle models, puff models allow for a reasonable description of the effects of buoyant emissions (plume rise) and might even allow for treating chemical reactions within the puffs.

The Puff-Particle Model (PPM) attempts to combine the advantages of both these model types. As a 'generic puff model' it is able to predict instantaneous statistics but it uses the information of its 'particle part' to describe the trajectories of the puffs, thus assuring an optimal representation of the dispersion process even under convective conditions.

Hurley (1994) has proposed a model 'Partpuff' which goes in the same direction as the PPM, but is based on a different concept. Essentially, he uses a one-dimensional particle model to describe the vertical dispersion while assuming a horizontal dispersion of Gaussian shape. Another model, the RAPTAD (Random Particle Transport and Diffusion) model of Yamada and Bunker (1988), combines a particle model with absolutely dispersed Gaussian puffs. This approach is compared to the PPM in more detail in section 2.3.

The principles of the PPM were first described in de Haan and Rotach (1995). Here, a full description will be provided (section 2.2), several improvements of the original concept are presented (section 2.3) and the model is extensively validated against tracer data (section 2.4).

2.2 PRINCIPLES OF THE PPM

2.2.1 The concept

In short, puff models simulate the dispersion of a 'cluster of pollutant particles', which is released as an entity, by following it on a trajectory and continuously increasing the puff's dimensions. Basically, it can be distinguished between two different approaches:

- If the puff model aims at identifying the puff with an individual, physically realistic cluster of particles, the concept of relative dispersion (i.e. 2-particle statistics, Borgas and Sawford 1994) has to be used. This concept takes into account that eddies smaller than the actual puff size will contribute to its growth while larger eddies move the puff as a whole (Fig. 1). Relative

dispersion accounts for the dispersion of a cluster with respect to the centre of mass of the cluster. This way, the dispersion of a single plume is described correctly.

- If the puff model has the goal to predict the dispersion of an ensemble of plumes rather than a single plume, absolute dispersion should be used to describe the growth of the puffs. These puffs are not corresponding to any cluster in nature. They are an average over many realisations of individual clusters. Most formulations in the literature of absolute dispersion correspond to an plume averaging time of roughly one hour, corresponding to the spectral gap between synoptic and turbulent frequencies. Absolute dispersion then gives an estimate of the mean dispersion of a plume averaged over one hour, which is the combined effect of relative diffusion and of the meandering of the puff respective to a fixed point, caused by eddies larger than the puff.

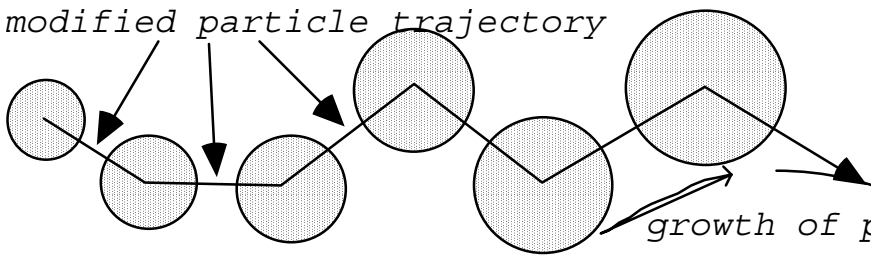

Figure 1 The puff-particle model groups together pollutant particles in puffs, whose centres of mass are moved along particle trajectories calculated by a stochastic particle model.

This means that puff models using *absolute dispersion* are able to predict ensemble plume concentrations. They are not suited to give correct concentration predictions for instantaneous releases (systematically overpredicting dispersion and hence underpredicting concentrations). For the latter case, relative diffusion should be used. When using *relative diffusion* in puff models, the predicted spread of a puff resembles the spread of one single pollutant cluster, but no prediction can be made about the amount of meandering of the trajectory of such a single cluster. However, for near-field predictions, the dispersing effect of meandering should be taken into account since otherwise, concentrations might be overpredicted.

When modelling instantaneous releases, flow fields may often be available for several times during one hour. However, the use of absolute dispersion can only be justified if the time, T, between the succeeding flow fields available to the dispersion model is at least roughly 30 min. If T becomes smaller, an increasing range of turbulent eddies will be resolved by the flow fields. Their dispersing effect is also included in absolute dispersion, leading to overestimated total dispersion. One way to

circumvent this problem would be to adjust the turbulence parameters σ_u, σ_v, and σ_w that are used to determine the rate of growth of the puffs so they correspond to T.

If, on the other hand, relative diffusion together with frequently updated flow fields are used, there generally will be a 'gap of dispersion' not covered by the flow fields nor by the relative dispersion. This gap will be largest in the beginning when the puff is small and vanishes later on, when the size of the puff reaches the order of $\overline{u}T$, where $\overline{u}$ is a representative mean wind speed.

In practice it is difficult (or at least computationally very expensive) to provide the flow field at a sufficiently high temporal rate. For example, Thykier-Nielsen *et al.* (1994) use three ten-minute intervals to simulate the low frequency contribution to the puff movement over a period of half an hour.

In the PPM the concept of relative diffusion is used to describe the spread of individual puffs as in other puff models (Mikkelsen and Larsen 1984; Thykier-Nielsen *et al.* 1989). The 'gap' in the description of dispersion is 'filled in' by artificially generating the meandering of the puffs' centres of mass. These meandering trajectories aim at simulating the meandering effect of all those eddies not resolved by the flow field but still larger than the puff. These trajectories of the puffs' centres of mass are determined from 'particle trajectories' as obtained from a stochastic particle dispersion model (Fig. 1). This concept has several advantages:

- The puff-particle approach gives a realistic picture of the transport (caused by the mean wind, and provided by the flow field updates), the amount of meandering (covered by the stochastic puff centre trajectories) and the diffusion of the release itself (caused by eddies smaller than the size of the puff, and taken into account by relative diffusion). The amount of meandering which has to be simulated by the puff centre trajectories depends on T.
- For the computation of ensemble plume statistics (absolute dispersion), an average is taken over many of such single meandering plume realisations. The 'particle-part' of the PPM thus fills the 'gap' (if there is one) in dispersion caused by the spectral gap between the range of eddies resolved by the flow field and those covered by relative diffusion.
- It is possible to have only one single flow field computation which may even be determined from parametrized flow and turbulence profiles in horizontally homogeneous conditions. In this case, T is set equal to the total averaging time for the concentration measurements, normally equal to the total duration of the experiment to be simulated.
- Dispersion in convective boundary layers can be simulated realistically with the PPM. With conventional puff models reasonable results are difficult to obtain unless a highly sophisticated

model (e.g. Large-Eddy Simulation) is used to produce the meteorological information (which, in turn, makes it unnecessary to use any dispersion model).

The 'particle part' of the PPM accounts for the effects of eddies larger than the actual puff size, which move the puff as a whole (meandering). In consequence, the cycling frequencies represented by this meandering must correspond to the turbulent eddies to be simulated, i.e. the low-frequency part of the energy spectrum. This is done by defining a threshold frequency, n^*, changing with puff size, i.e. travel time. With increasing puff size, large parts of the turbulent fluctuations will have to be eliminated from the particle trajectories when using them as puff centre trajectories in the particle part of the PPM (low-pass filter). Eventually, this allows for 'turning off' the particle part when the puff size has reached a certain extent (see section 2.3). Since absolute dispersion as simulated by stochastic particle models is not an explicit function of T, but only assumes that T is in the so-called 'spectral gap', no high-pass filter is used in the PPM. This would be necessary for T smaller than approximately 15 min.

Two possible interpretations can be given for the concept of the PPM. Firstly, it can be viewed as a modified puff model, in which the dispersion is described correctly, since the effect of all eddies not resolved by the flow field is simulated using the particle part of the PPM. On the other hand, the PPM may be considered a method to speed up a true particle model by combining each, say, 100 particles into one puff, thereby saving considerable computing time. Due to the additional calculation of the dispersion of the puffs, puff splitting schemes etc., the PPM is approximately twenty times faster than a comparable particle model.

2.2.2 The puff part of the PPM

In the PPM, all pollutants are described as clusters of particles and are approximated by three-dimensional Gaussian puffs. With the puff-particle approach, the dispersing effect of the turbulent eddies smaller than the puff itself are taken into account by the puff part of the model, whereas the effect of the larger eddies is simulated by the particle part. Within the statistical approach to describe dispersion of passive scalars, a distinction must be made between the dispersion of particles relative to a fixed co-ordinate system (absolute dispersion) and the spread of a cluster of particles (relative diffusion). One of the first to point out this fundamental difference was Richardson (1926). The first approach treats every particle as being independent (1-particle statistics) and thus can only describe absolute dispersion of the plume. To describe the effects of relative diffusion, 2-particle statistics must be used (see, e.g., Borgas and Sawford 1994, for a

review). During its growth, a cluster of particles is affected by an increasing range of turbulent eddies, since larger and larger eddies will be capable of separating two particles from each other as puff sizes grow. On the other hand, within the framework of absolute dispersion, turbulent eddies of all sizes are capable of influencing the distance of a single particle from its point of release, thus enhancing the plume dimensions.

To identify the cluster, marked passive particles with an absolute velocity u within the fluid are followed, released at a time $t = 0$. The spread, σ, of such a cluster at subsequent times is defined as:

$$\sigma^2(t) = \overline{\left\langle \left\{ \int_0^t v(\tau) \mathrm{d}\tau \right\}^2 \right\rangle}, \tag{1}$$

where the integration runs along a Lagrangian orbit $v = u - V_{\mathrm{cm}}$, and the absolute velocity of the centre of mass of the cluster is denoted by V_{cm}. The overbar in Eq. (1) and subsequently up to section 2.2.4 denotes the average over all the particles within the puff, and the angular brackets throughout refer to an ensemble average. Mikkelsen *et al.* (1987) use a kinematic-statistical model in which the rate of growth (Batchelor 1952; Smith and Hay 1961) of the puff:

$$\frac{\mathrm{d}\sigma^2}{\mathrm{d}t} = 2\int_0^t \overline{\langle v(t) v(t-\tau) \rangle} \mathrm{d}\tau \tag{2}$$

is related to one-dimensional velocity spectra. They assume that the stochastic displacements of the particles obey independent and identical Gaussian statistics, thus leading to clusters of particles (i.e. puffs) being of Gaussian shape.

Batchelor (1952) distinguishes 'near-field', 'intermediate range' and 'far-field' approximate solutions to Eq. (2). In the initial phase of spread of the puff, the initial size of the puff, σ_0, is an important parameter. For travel times $t < \left\{ \sigma_0^2 \Big/ \overline{\langle v^2(0) \rangle} \right\}^{1/2}$, he gives as the near-field approximation:

$$\sigma_{\mathrm{nf}}^2(t) = \sigma_0^2 + \overline{\langle v^2(0) \rangle} t^2 . \tag{3}$$

For the 'intermediate' time interval, when viscosity and the initial puff size are no longer dominant parameters, but before the Lagrangian integral time scale T_{L} becomes an important scaling parameter (i.e. for times corresponding to a frequency in the inertial subrange), the intermediate-field approximation is:

$$\sigma_{\mathrm{if}}^2(t) = C\varepsilon t^3 , \tag{4}$$

where ε denotes the dissipation rate of turbulent kinetic energy. Mikkelsen *et al.* (1987) relate Eq. (4) to the universal constant of the Lagrangian structure function, C_0, as $\sigma^2(t) = \left(C_0 \varepsilon t^3 \right) \Big/ 3$. Recent

estimates for C_0 indicate that $C_0 = 3.0 \pm 0.5$ (Du *et al.* 1995; Rotach 1995), so that the corresponding value of C in Eq. (4) has been chosen equal to unity in the present work.

For $t > T_L$, Eq. (2) reduces to the description of single-particle dispersion in the far-field limit (Taylor 1921), thus leading to the far-field formulation:

$$\sigma_{ff}^2(t) = 2\langle u^2 \rangle T_L t \,. \tag{5}$$

Evaluating $\overline{\langle v^2(0) \rangle}$ from Eq. (3) is not trivial. If the initial fluctuating velocity components of the particles within the puff originate from a three-dimensional Gaussian distribution (leading to $\vec{V}_{cm}(0) = \vec{0}$ for the cluster):

$$\overline{\langle v^2(0) \rangle} = r_1^E \langle u'^2(0) \rangle + r_2^E \langle v'^2(0) \rangle + r_3^E \langle w'^2(0) \rangle \,, \tag{6}$$

with the velocity variances being evaluated at $t = 0$. Here, $\langle u'^2(0) \rangle$, $\langle v'^2(0) \rangle$ and $\langle w'^2(0) \rangle$ denote the variances corresponding to this Gaussian distribution, and are equal to the variances of the longitudinal, lateral and vertical turbulent velocities, respectively, at the point of release. Equation (6) does not depend on the correlation coefficient $\rho = \langle u'w' \rangle / \left(\langle u'^2 \rangle \langle w'^2 \rangle \right)$ of the distribution. Recall that v denotes the absolute velocity relative to the puff's centre, whereas the u_i' refer to the fixed coordinate system with the u-axis parallel to the direction of the mean wind.

The three terms r_i^E $(i = 1, 2, 3)$ in Eq. (6) range from zero for point releases to unity for very large source sizes. They indicate what amount of the total kinetic energy is represented by eddies smaller than the initial source size. The superscript E denotes that they depend on the Eulerian turbulent velocity spectra at the point of release. The definition of these ratios is given in section 2.3, where ratios depending on Lagrangian spectra are also investigated.

In atmospheric dispersion modelling with Gaussian puffs, which are characterised by the values of the three standard deviations, s_i $(i = 1, 2, 3)$ for the longitudinal, lateral and vertical direction, respectively, σ^2 in Eqs. (1) to (5) can be replaced by s_i^2 if $\overline{\langle v^2(0) \rangle}$ is replaced by $\langle u_i^2(0) \rangle$ and $\langle u^2 \rangle$ by $\langle u_i^2 \rangle$ (Eq. 5), where $(u_1, u_2, u_3) = (u', v', w')$.

In the PPM, Eqs. (3), (4) and (5) are used to describe the growth of puffs for small, intermediate and large travel times, respectively. These equations give puff standard deviations as a function of t. In Lagrangian particle models, t is not normally known (and causes problems after furcation of puffs where the puff dimensions become smaller, see below). Therefore, the pseudo-time method, which is frequently used in Lagrangian puff models (e.g. Scire *et al.* 1995), is applied to Eqs. (3) to (5). At the beginning of time step $t' = t + \Delta t$, with the spread σ_t of the puff at time t, we calculate a pseudo-time $\tau = f(\sigma_t)$ using Eqs. (3), (4) or (5). Then, we evaluate $\sigma_{t+1} = \sigma(t + \Delta t)$. This scheme

allows for inhomogeneous and nonstationary turbulence conditions. When a puff travels from a region with a low turbulence level into a region with high turbulence, its pseudo-time will change. This change in pseudo-time reflects the fact that the turbulence spectrum at the new location has changed, i.e. the rate of growth, depending on the turbulent kinetic energy of those eddies being small enough to disperse the puff, has increased. For T_L, the estimates of Gryning *et al.* (1987) are adopted.

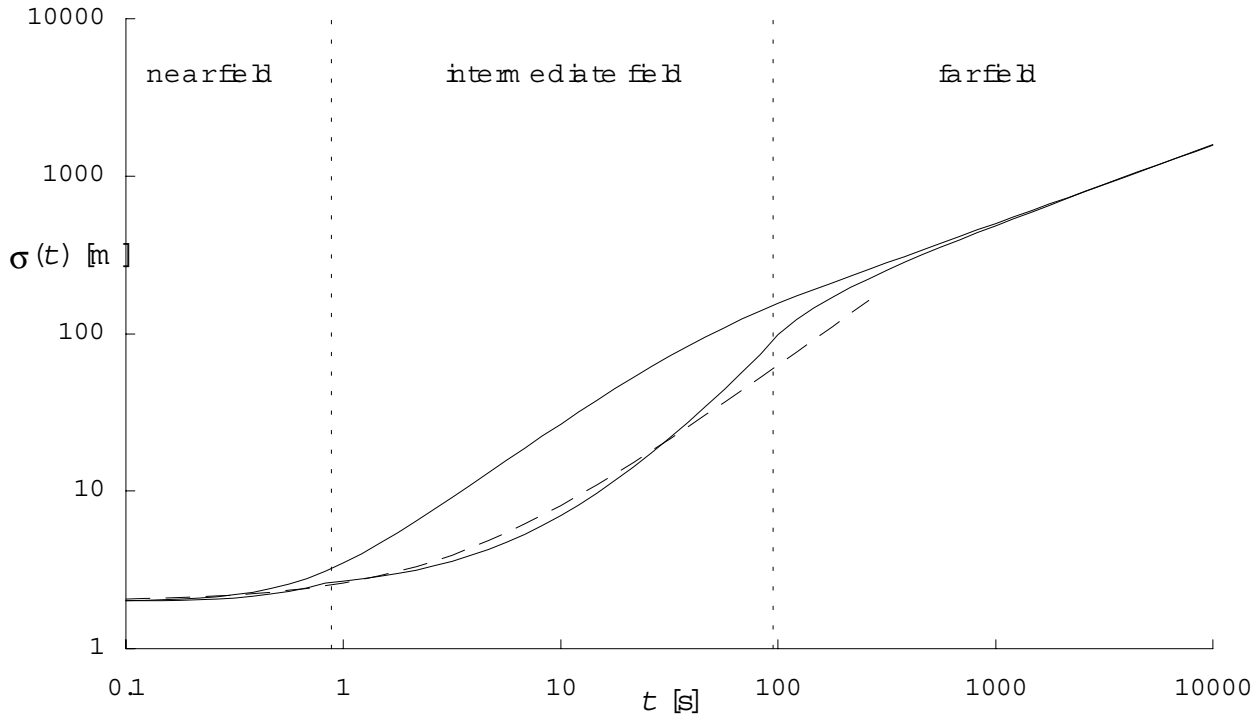

Figure 2 Puff spread σ (as defined by Eq. 1) as a function of travel time t. The upper solid line is calculated from Taylor's (1921) single particle diffusion theory, $0.5\,\mathrm{d}\sigma^2/\mathrm{d}t = \overline{\langle u^2 \rangle} t_a(t)$, where $t_a(t) = \int_0^t \exp(-\xi/T_L)\,d\xi$ is assumed and an initial source size $\sigma_0 = 2$ m was adopted. The lower solid line shows the integration of Eqs. (3), (4) and (5), where the vertical dotted lines mark the change between them. Also shown (dashed line) is the puff formula of Pasquill and Smith (1983), $\sigma_{\max} = \sigma_0 + \alpha \overline{\langle u^2 \rangle}^{1/2} t$, with the re-evaluated value $\alpha = 0.30$.

Figure 2 shows the resulting puff size under modestly convective conditions. Since Eq. (3) is valid for $t < \left\{\sigma_0^2 / \overline{\langle v^2(0) \rangle}\right\}^{1/2}$, the transition from the near-field to the intermediate field approximation is assumed at a threshold time $t_1 = c_1 \left\{\sigma_0^2 / \overline{\langle v^2(0) \rangle}\right\}^{1/2}$, with $c_1 = 0.5$. The transition from the intermediate to the far-field formulation is assumed to take place as soon as $\mathrm{d}\sigma/\mathrm{d}t$ from Eqs. (4) and (5) become equal, i.e. at $t_2 = (1/3)\sqrt{\left(2\langle u^2 \rangle T_L\right)/\varepsilon}$. Figure 2 shows that the difference in puff dimensions from absolute and relative diffusion is largest in the intermediate field. The

approximation of Pasquill and Smith (1983, pp. 230–232, dashed line in our Fig. 2) is valid for near-field and intermediate-field travel times only, since it does not approach the Taylor (1921) limit (Eq. (5)).

The initial standard deviations of the puff's normal distribution equal the radius of the source. All emitted puffs carry an initial mass such that the sum of the puffs which are emitted per unit time equals the emission rate of the source. During a simulation time step of, say, 1 second, the centres of mass of the puffs are moved along a trajectory derived from particle trajectories (see section 2.3). Based on the new position and the travel distance, new puff dimensions σ_1 are calculated. Furthermore, an option allows for the puffs to be split up into several new puffs, for example after exceeding the grid size of the wind field in either direction. This mass-consistent procedure is called furcation and its implementation in the PPM is a modified version of the procedure of Thykier-Nielsen *et al.* (1989). In the PPM, a trifurcation is applied in the vertical direction and a pentafurcation (the original puff is replaced by five new puffs) in the horizontal plane. The new puffs have half the size and are placed half a standard deviation apart from the original puff, and one new puff is placed at the original location itself. The masses of the new puffs are chosen such that the new total density distribution (of the three or five furcated puffs) is as similar as possible to the distribution of the original puff.

Any location within the three-dimensional domain can be specified as a 'receptor'. This procedure based on time steps of 1 second is repeated until the pollutant concentrations have reached a quasi-steady state at the receptor point most distant from the source. Typically, the trajectories of about 1000 puffs are followed to model three-dimensional concentration patterns.

2.2.3 The stochastic dispersion model

To move the centres of mass of the puffs, any particle model can be used in principle. In the PPM, a three-dimensional Lagrangian stochastic-dispersion model is used that fulfills the well-mixed condition for neutral to convective conditions. It is based on a model described in Rotach *et al.* (1996) but is expanded to three dimensions. This model allows for a continuous transition between correlated Gaussian turbulence on the one hand, and uncorrelated skewed turbulence on the other, of which the latter is characteristic for the convective boundary layer. The evolution of velocity $\vec{u}$ and position $\vec{x}$ of tracer particles is described by the stochastic differential equations $\mathrm{d}u_i = a_i(\vec{x}, \vec{u}, t)\mathrm{d}t + b_{ij}\mathrm{d}\xi_j$ so that $\mathrm{d}\vec{x} = \vec{u}\mathrm{d}t$. The $\mathrm{d}\xi_i$ must be a Wiener process with zero mean and

variance dt. The well-mixed criterion (Thomson 1987) requires that the probability density function (pdf) of the particle velocities, P_{2d}, fulfils the Fokker-Planck equation:

$$\frac{\partial}{\partial t}P_{2d} = -\frac{\partial}{\partial x_i}\left(u_i P_{2d}\right) - \frac{\partial}{\partial u_i}\left(a_i P_{2d}\right) + \frac{\partial^2}{\partial u_i \partial u_j}\left(B_{ij} P_{2d}\right) \tag{7}$$

where $2B_{ij} = b_{ij}b_{jk}$. Equation (7) is used to derive the functions a_i and b_i (see Rotach *et al.* 1996 for details). For stationary turbulence it can be written:

$$a_i P_{2d} = \frac{\partial}{\partial u_j}\left(B_{ij} P_{2d}\right) + \Phi_i, \tag{8}$$

where Φ_i obeys:

$$\frac{\partial}{\partial u_i}\Phi_i = -\frac{\partial}{\partial x_i}\left(u_i P_{2d}\right), \tag{9}$$

with the restriction on Φ_i that $\Phi_i \to 0$ for $|\vec{u}| \to \infty$.

The particle model of Rotach *et al.* (1996) is constructed from a two-dimensional pdf P_{2d}:

$$P_{2d} = fP_u P_c + (1-f)P_g \tag{10}$$

where P_c is a one-dimensional skewed pdf for the vertical velocity (Luhar and Britter 1989). P_u is a one-dimensional Gaussian distribution of the horizontal longitudinal velocity component, P_g is a two-dimensional jointly Gaussian distribution for u' and w' and f is a transition function. If $f = 1$, the total pdf becomes equal to $P_u \cdot P_c$ (i.e. the velocity components are uncorrelated, w is skewed). On the other hand, if $f = 0$, u' and w' are jointly Gaussian distributed. From this pdf the model for the velocity increments is constructed in the usual manner (see e.g. Thomson 1987).

The transition function f is formulated in such a way that for large w_* (the convective velocity scale) f becomes unity throughout most of the boundary layer and equals zero over large parts of a neutral or stable boundary layer $(w_* = 0)$. Thus, it is assumed that the transitions from a Gaussian to a skewed distribution in w' on the one hand and from correlated to uncorrelated velocity fluctuations (u', w') are occurring at the same rate, governed by the transition function f, as stability changes. For more details about the transition function f, see Rotach *et al.* (1996).

To extend the above model to three dimensions, the lateral velocity fluctuations, v', are assumed to be fully independent of the other fluctuations, with a Gaussian pdf. Thus, the three dimensional total pdf is constructed through $P_{tot} = P_{2d}P_v$, where P_v is the Gaussian distribution of the lateral velocity component. The three-dimensional model is again constructed according to the constraints outlined by Thomson (1987). This requires for horizontally homogeneous conditions:

$$\frac{\partial}{\partial u_i}\Phi_i = -\frac{\partial}{\partial z}\left(w' P_{2\mathrm{d}} \cdot P_v\right). \tag{11}$$

In order to retain the formulations of the two-dimensional model, we take $\Phi_u^{2\mathrm{d}}$ and $\Phi_w^{2\mathrm{d}}$, which fulfill:

$$\frac{\partial}{\partial u}\Phi_u^{2\mathrm{d}} + \frac{\partial}{\partial w}\Phi_w^{2\mathrm{d}} = -\frac{\partial}{\partial z}\left(w' P_{2\mathrm{d}}\right). \tag{12}$$

On defining $\Phi_u = \Phi_u^{2\mathrm{d}} \cdot P_v$ and $\Phi_w = \Phi_w^{2\mathrm{d}} \cdot P_v$, this leads to:

$$\frac{\partial}{\partial v}\Phi_v = -w' P_{2\mathrm{d}} \frac{\partial}{\partial z}\left(P_v\right), \tag{13}$$

so that:

$$\Phi_v\left(v'\right) - \Phi_{v'=-\infty} = -w' P_{2\mathrm{d}} \int_{-\infty}^{v'} \left(\frac{\partial}{\partial z} P_v\right) \mathrm{d}v, \tag{14}$$

where the second term on the left hand side of Eq. (14) equals zero. The solution of this integral is straight forward and the final result is:

$$\Phi_v = w' \cdot P_{2\mathrm{d}} v' P_v \frac{1}{\sigma_v} \frac{\partial \sigma_v}{\partial z}, \tag{15}$$

where σ_v is the standard deviation of the lateral velocity component in P_v.

2.2.4 Parametrisation of turbulence statistics

In principle, the PPM can be driven with any kind of meteorological input. If no measurements or output from a flow simulation is available, similarity formulations are used. Essentially, the formulations employed are those from Rotach *et al.* (1996). However a revised formulation is used for the profile of Reynolds stress. In a near-neutral boundary layer, the Reynolds stress profile has been parametrized by Brost *et al.* (1982) as:

$$\overline{u'w'}(z) = -u_*^2\left(1 - \frac{z}{z_i}\right), \tag{16}$$

where from now on the overbar stands for an average over time; u_* is the friction velocity. For stable conditions it has been parametrized by Nieuwstadt (1984) as:

$$\overline{u'w'}(z) = -u_*^2\left(1 - \frac{z}{z_i}\right)^{3/2}, \tag{17}$$

where z_i is used for the mixing layer height of the convective boundary layer as well as for the depth of the stable boundary layer. Rotach *et al.* (1996) have slightly modified Eq. (16) in order to

obtain an approximately constant Reynolds stress within the surface layer. (This can be desirable when focusing on dispersion problems within the surface layer or close to the surface. In such cases the 'constant-flux assumption' is then consistent with the more general Reynolds stress parametrization.) Here, a minor modification to their formulation is proposed, which allows it to cover both the unstable (Eq. 16) and stable (Eq. 17) boundary layer:

$$\overline{u'w'}(z) = -u_*^2 \left(1 - \frac{z}{z_i}\right)^a \Psi , \tag{18}$$

where:

$$\Psi^{-1} = \text{logit}(\xi) + \{1 - \text{logit}(\xi)\} \left(1 - \frac{z}{z_i}\right)^a , \tag{19}$$

with $a = 1$ for near-neutral conditions, $a = 3/2$ in a stable boundary layer, $0.1\xi = \sqrt{z/z_i} - 0.5$ and

$$\text{logit}(\xi) = \frac{\exp(\xi)}{1 + \exp(\xi)} . \tag{20}$$

The function Ψ alters the original parametrizations, Eqs. (16) and (17), only slightly in the region of the surface layer, where the value of $\overline{u'w'}(z)$ becomes approximately constant and asymptotically approaches $-u_*^2$ near the ground.

2.3 REDUCTION OF THE LARGE-SCALE CONTRIBUTION AS PUFF SIZES GROW

The particle-part of the PPM represents the contributions for the whole turbulence energy spectrum. However, the relative diffusion in the puff-part of the PPM already accounts for the effects of all eddies smaller than, or equal to, the puff size. With this, the total dispersion is overestimated more and more as the travel time increases, leading to underestimated ground-level concentrations far away from the source.

The procedure to circumvent this problem in the PPM is very simple: the turbulent velocities of the individual particles as calculated by the particle part of the model are smoothed, so that they only take into account the low-frequency part of the spectrum. The stochastic movement of the puff's centre is then based on these smoothed turbulent velocities. This approach is more accurate than smoothing the particle trajectories directly. This would prevent puff trajectories from closely approaching either the ground or the upper model-boundary, since particles are reflected there, and a smoothed trajectory will thus never reach these reflecting boundaries. When smoothing the

turbulent velocities instead, the puff centres will still be well mixed all over the boundary layer as soon as the particles positions are well mixed.

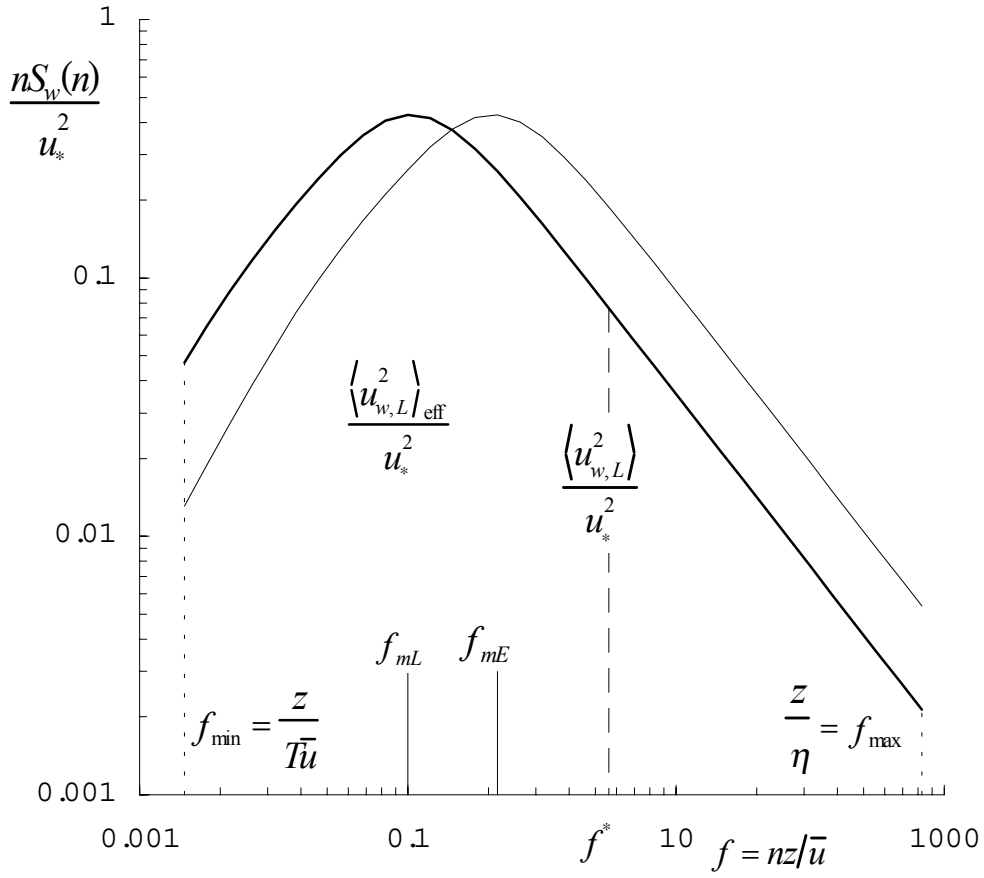

Fig. 3. Determination of the ratio of turbulent eddies smaller and larger than the puff size, example for the vertical velocity component. The spectral density corresponds to a surface layer formulation of Højstrup (1981), with $L = -10$ m and $z_i = 1000$ m. The thin line shows the Eulerian spectrum, and the thick line the derived Lagrangian spectrum. The frequencies where their peaks occur are denoted as f_{mE} and f_{mL}, respectively. See text for further definitions and explanation.

To calculate the amount of dispersion which has to be 'smoothed away', the proportion of relative to absolute dispersion is calculated by means of the energy spectra. This proportion depends on the Lagrangian properties along the trajectory of the centre of the puff. Using Taylor's frozen-turbulence hypothesis, a frequency $n^*_{x,y,z} = \bar{u}(t)/(2\sigma_{x,y,z})$ for each direction is defined from the actual puff sizes σ_x, σ_y, σ_z (i.e. the standard deviations). We denote the integral over the low-frequency part of the Lagrangian energy spectrum as $\langle u_i^2 \rangle_{\text{eff}}$ $(i = u, v, w)$, where $\langle u_i^2 \rangle_{\text{eff}} = \int_{n_{\min}}^{n_i} S_i \mathrm{d}n$, where S_i is the Lagrangian spectral density. Then, the ratio $r_i = \langle u_i^2 \rangle_{\text{eff}} / \langle u_i^2 \rangle$ is determined (Fig. 3). The integration of the whole spectrum runs from $n_{\max} = \bar{u}/\eta$, where $\eta = (\nu^3/\varepsilon)^{1/4}$ is the Kolmogorov micro-scale, ν is the kinematic molecular viscosity and ε as before

is the dissipation rate, to $n_{\min} = 1/T$, where T is the averaging time for the measurements of the properties of the flow field, i.e. $\langle u_i^2 \rangle = \int_{n_{\min}}^{n_{\max}} S_i \mathrm{d}n$. This ratio r_i denotes the amount of dispersion which is not covered by relative dispersion.

To filter out the effect of the high-frequency part of the energy spectrum (i.e. the small eddies), a smoothing procedure over time is applied. The time series of stochastic turbulent velocity components of each particle is smoothed by use of a procedure with the effect of a low-pass filter. The trajectory of the centre of mass of the puffs is then calculated based on the time series of these smoothed turbulent velocities.

As the smoothing procedure, a Kalman filter is applied (see de Haan and Rotach 1997 for more details on Kalman filtering). This filtering technique is normally used to filter a 'true' value out of a noisy signal. It is especially suited, however, to smooth time series from stochastic processes. A traditional running mean, smoother for any instant of the time series, would rely on both past and future values (which are not yet known within stochastic processes), and requires all these values to be stored in the model (necessitating a huge storage capacity, as many values for thousands of three-dimensional trajectories are to be smoothed). The Kalman filter makes use of the fact that the order and the basic parameter of the underlying stochastic process of the particle model are known (an AR(1)-process, see Section 2.2.3), and for any time step it depends only on the smoothed value at the previous time step.

The amount of smoothing depends on the so-called 'window width', τ. It is chosen to be zero as $r_i = 1$ (i.e. for a very small puff the particle velocities are not smoothed at all). For large puffs $r_i \to 0$, and accordingly $\tau \to \infty$ is used in the PPM; thus the smoothing increases as the puffs grow. The ratios r_i are evaluated for each puff individually. As long as the puff sizes are small, the r_i will remain close to unity. Thus the turbulent velocities of the centres of the puffs within the PPM will closely resemble those of the particles (Fig. 4). As puff size grows, the values of the r_i decrease and eventually approach zero, leading to only minor turbulent movements of the puff centres. This allows the particle model within the PPM to be switched off as soon as r_i equals zero, then moving the puff centres with the average flow field only. For far-field concentration predictions, this causes considerable computational savings. Even when averaged over T, the velocity fluctuation of a stochastic process will not give exactly zero. Therefore, to ensure that the smoothed turbulent velocities approach zero as $r_i \to 0$, the smoothed values are multiplied by the factor $[0.5 \sin\{\pi(r_i - 0.5)\} + 0.5]$. Figure 4 depicts this procedure of smoothing the time series of the particle turbulent velocities, as calculated by the particle part of the model. More details about the

application of a Kalman filter to remove the relative dispersion from particle velocities which account for absolute dispersion can be found in de Haan and Rotach (1997).

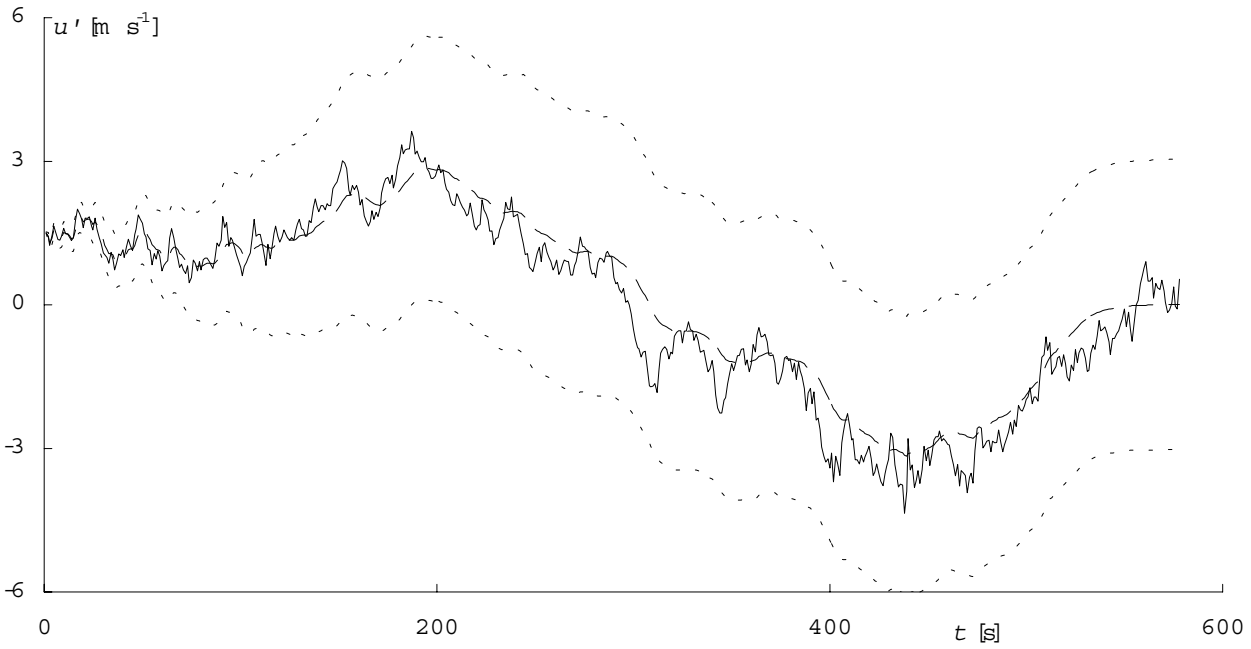

Figure 4 Example of smoothing of the time series of the turbulent velocity (u') as calculated by the particle model (solid line) with a Kalman filter (dashed line). The envelope (dotted lines) marks the interval $u'(t) \pm \tau(\sigma_x)$. Conditions of forced convection ($u_* = 0.4\,\mathrm{m\,s^{-1}}$, $L = -50$ m, $z_i = 2000$ m, $\overline{u} = 3.4\,\mathrm{m\,s^{-1}}$) are used for this example. See text for definitions and further explanation.

The literature about the form of Lagrangian velocity spectra is very sparse. Generally, it is assumed that the spectra show the same form as measured Eulerian fixed-point spectra, but are shifted towards lower frequencies by a factor $\beta = f_{\mathrm{mE}} / f_{\mathrm{mL}}$, where the non-dimensional frequency $\left(f = nz/\overline{u}\right)$ where the maximum of the spectrum occurs is denoted by f_{mE} and f_{mL} for the Eulerian and Lagrangian spectra, respectively (see Fig. 3). Pasquill and Smith (1983; pp. 80–87) give as the best estimate from several different measurements $\beta i \approx 0.6$, where $i = \sigma_u / \overline{u}$ is the turbulence intensity. In the PPM, an additional upper limit of 4 is assumed for β under weak turbulence conditions, which is supported by the measurements reported by Pasquill and Smith (1983; their Fig. 2.19).

Models of Eulerian velocity spectra are then taken from Højstrup (1981) for the unstable surface layer and Højstrup (1982) for the unstable planetary boundary layer. The model of Kaimal *et al.* (1972) is used for the neutrally stratified surface layer. For the stable surface layer, the model of Olesen *et al.* (1984) is adopted. For the upper part of the neutral and of the stable boundary layer, no parametrizations for the velocity spectra can be found in the literature. In the present work, the

same formulations as for the surface layer are used. Each of the above models is either given as an expression of the form $C\left(1+Df^{5/3}\right)^{-1}$ or as $A_1\left(1+B_1 f\right)^{-5/3}$, or as a sum of both forms. To allow for an analytical integration between the boundaries $f_{\min}$, f^* and $f_{\max}$, the models of the form $C\left(1+Df^{5/3}\right)^{-1}$ are transformed into the form $A_2\left(1+B_2 f\right)^{-5/3}$ by use of the transformations $B_2 = 1.5^{2/5} D^{3/5}$ and $A_2 = \left(3.1/1.5\right)^{3/5} C$. This ensures that the position of the maximum and the total integral are conserved. These transformations modify the shape of the spectrum from a 'pointed' to a more 'blunted' shape. $nS_i(n)$ becomes larger at small and large n, and smaller around the position of the maximum. In the present work, $nS_i(n)$ is only used to calculate r_i. The change in r_i caused by the above transformations depends on the spectral model used. The maximum decrease in r_i occurs for $f \approx 0.1$ (and is about –12% in the most extreme case, where the original spectrum only consists of an expression of the form $C\left(1+Df^{5/3}\right)^{-1}$), and the maximum increase occurs at $f \approx 10$ (+14%).

The approach outlined in this section aims at letting the dispersion in the 'puff-part' and in the 'particle-part' of the model sum up to 100%. Yamada and Bunker (1988) report that their RAPTAD model yields best results when their full particle model is used together with Gaussian shaped density estimators (e.g. puffs). These puffs are applied to each particle position, and enable the model to produce much smoother concentration fields as compared to the box-counting of particles. To determine the standard deviations of the puffs, absolute diffusion is used (Eq. (5)). Yamada and Bunker (1988) investigated the effect of reducing the amount of dispersion in the particle and puff parts of their model. They found that using the full particle model and absolute diffusion for the puffs yields better results as compared to enforcing the diffusion of the particle and puff parts of the model to sum up to 100%. It appears that they reduced the dispersion of both model parts with constant factors, not depending on the size of the puff. It is clear that the combination of a full particle model with absolutely dispersed puffs theoretically leads to an overestimation of dispersion. The good results reported by Yamada and Bunker might be explained by the fact that they apply their combined model to distances of 10 to 20 km from the source, i.e. clearly in the far-field limit. In this limit, relative and absolute dispersion differ from one another only marginally (see Fig. 2). Thus it becomes evident from the above considerations that the puff part of the model is expected to account for almost 100% of the total dispersion, and in the far-field limit the question whether actually relative or absolute dispersion is used is of no importance. As soon as puff dispersion is the larger effect than particle dispersion, the latter will hardly influence the resulting concentration distribution. This is illustrated by the fact that Yamada and Bunker mention that the

amount of dispersion covered by the particle model is rather insensitive, and that correct concentration distributions are yielded as long as the puffs use full absolute dispersion (which equals relative diffusion in the far-field limit), and are not reduced by multiplication with a constant factor. Hence, for mesoscale applications as in Yamada and Bunker (1988), the particle part could actually be switched off (only regarding the dispersion; an advanced particle model with skewed pdf still would be needed to scope with convective conditions). For mesoscale applications, the additional dispersion caused by the particle model is unlikely to influence the results. For the intermediate field (as defined in section 2.2.2), however, this approach will yield better results if the dispersion covered by the puff- and particle-part of any combined model sums up to 100%, where the relation between the two parts depends on the puff size.

2.4 VALIDATION

2.4.1 Model validation experiments

Due to the very limited amount of suitable experimental data on spatially inhomogeneous dispersion events, for which the PPM has been designed, this first validation is performed using tracer data from simpler flow configurations. The data sets used to validate the PPM are all from tracer experiments over flat terrain with a roughness length which is assumed to be constant, and without any information provided concerning the variation of the wind during the individual hours of measurement.

In a series of workshops that aimed at harmonising short-range dispersion models in Europe (Olesen and Mikkelsen 1992; Cuvelier 1993; Kretzschmar *et al.* 1994; Kretzschmar and Cosemans 1996) three 'reference data sets' were defined for model comparison (Olesen 1995a).

From the Copenhagen tracer experiment, data from 9 hours of measurements under conditions of forced convection are available. The tracer was released at a height of 115 m, over a suburban surface. For the experiments in Lillestrøm, strongly stable winter conditions prevailed during the 8 observational periods of 15 minutes each. The experiment took place in a suburban environment, with a release height of 36 m. In the Kincaid tracer experiment, convective conditions were observed during most of the 171 hours of measurements within the present data set. The tracer was injected into the exhaust gases of a power plant situated in a rural environment at a height of 187 m. This short overview over the tracer experiments shows that these data sets represent a wide range of atmospheric stability conditions, and are suited for model validation. More details about the tracer

experiments can be found in Gryning and Lyck (1984) for Copenhagen, Haugsbakk and Tønnesen (1989) for Lillestrøm and Bowne and Londergan (1983) for Kincaid. For the present validation, all runs of these three experiments have been simulated, except for the Lillestrøm data set where u_* was recorded as zero during one of the runs, a condition which the PPM cannot handle.

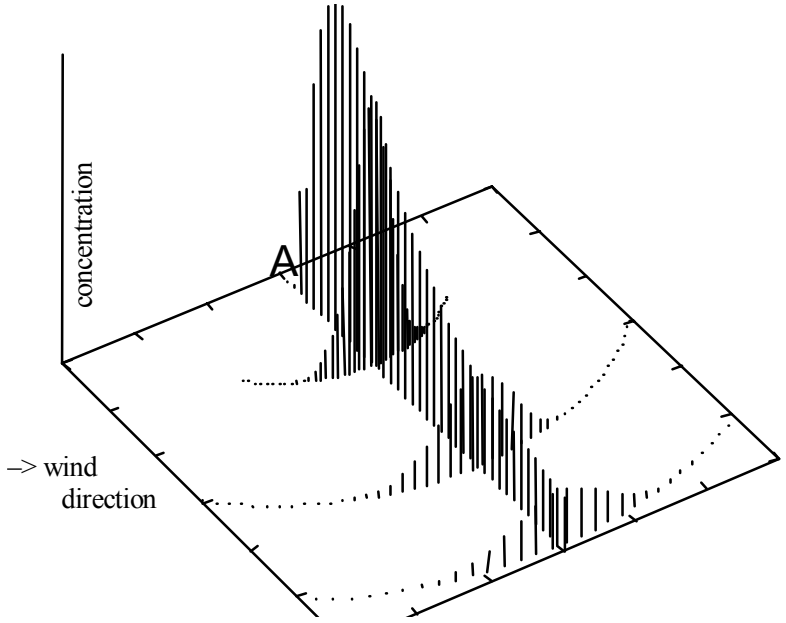

Figure 5 Simulated ground level concentrations for the Copenhagen tracer experiment (run from 30 April, 1979). The source location is indicated by 'A'. The concentration values are displayed at three virtual receptor arcs at 2, 4.2 and 5.9 km distance down wind from the source and in the plume centre line.

In all three tracer experiments, the receptors were placed on several arcs downwind of the source, and hourly (Lillestrøm: quarter-hourly) average measurements of the tracer concentrations were made at 2 m above ground. The mean wind speed was measured at different levels. For Kincaid, values for u_* and Obukhov length, L, are based on the meteorological pre-processor of Hanna and Paine (1989). Mixing-depth estimates come from several daily radiosonde soundings. For Copenhagen u_* and L were determined using a method identical to the one given in Hanna and Paine (1989). The mixing height is based on a daily radio sounding. In Lillestrøm, u_* and L were determined from sonic anemometer measurements at 10 m height. No mixing-depth information is available.

Additionally, for the Copenhagen and Lillestrøm data sets, measurements of the velocity statistics, $\langle u_2^2 \rangle$ and $\langle u_3^2 \rangle$, are available (those for the Kincaid experiment are generally considered to be unreliable). The releases in Copenhagen and Lillestrøm were non-buoyant, whereas at Kincaid a

very strong plume rise (with vertical exit velocities in the range of 10–30 m s^{-1} and a temperature excess of over 100 deg C) has to be taken into account.

In general, in Copenhagen and Lillestrøm the measured concentration patterns on the arcs (i.e. the cross-wind contribution) exhibit more or less Gaussian shapes. Therefore, even Gaussian plume models can be expected to yield realistic results, although some meandering in Lillestrøm seems to have occurred. On the other hand, the concentration patterns observed on the receptor positions in Kincaid indicate that, owing to the convective conditions and possibly wind shear, the continuous plume release is torn into pieces. The lateral concentration pattern is very irregular in almost all the experiments.

2.4.2 Validation set-up

The scaling parameters provided with the data sets (u_*, L, z_i) are used as model input. Where measurements of $\langle u_2^2 \rangle$ and $\langle u_3^2 \rangle$ were available (Copenhagen and Lillestrøm), the parametrized profiles were scaled (i.e. multiplied with the same constant for all heights) in order to match the measured values. The simulations are performed essentially by rebuilding the experimental set-up. Figure 5 depicts an example of the placement of the simulated receptors on 3 arcs and in the plume centre line. At the mixing height as well as at the ground, perfect reflection without any deposition of pollutants is assumed. For the Gaussian concentration distribution belonging to each puff, six image sources are assumed at $z = -h_s$, $2z_i - h_s$, $-2z_i - h_s$, $4z_i - h_s$ etc., where h_s is the actual height of the puff's centre. In the case of the Lillestrøm experiments, the height of the stable boundary layer, which had not been measured, is determined according to $z_i = d\sqrt{u_* L / f_c}$, with $d = 0.28$ (Stull 1988). To ensure that the inverse of the time steps for the simulation lies in the inertial subrange for the particle part of the model, the criteria after Rotach *et al.* (1996) are applied.

The mean wind profile was determined based on an approach from Sorbjan (see Rotach *et al.* (1996) for details) and has been scaled to minimise the sum of squared differences from the measurements. From the predicted concentrations at the individual receptors, the arcwise maximum concentration, the standard deviation of the concentration distribution on the arc and the cross-wind integrated concentration (on the arc) are determined.

2.4.3 Results

As statistical measures to describe the model performance, the fractional bias, $FB = \left(\overline{C}'_{\text{obs.}} - \overline{C}'_{\text{pred.}}\right) / \left\{0.5\left(\overline{C}'_{\text{obs.}} + \overline{C}'_{\text{pred.}}\right)\right\}$, the normalised mean square error, $NMSE = \overline{\left(C'_{\text{obs.}} - C'_{\text{pred.}}\right)^2} / \left(\overline{C}'_{\text{obs.}} \overline{C}'_{\text{pred.}}\right)$ and the correlation coefficient, $COR =$

$\overline{(C'_{\text{obs.}} - \overline{C}'_{\text{obs.}})(C'_{\text{pred.}} - \overline{C}'_{\text{pred.}})}/(\sigma_{\text{obs.}}\sigma_{\text{pred.}})$ are determined; $C'_{\text{obs.}}$ is the normalised observed concentration, $C'_{\text{obs.}} = C_{\text{obs.}}/Q$ where Q denotes the source strength; $C'_{\text{pred.}}$ is the simulated one, and $\sigma_{\text{obs.}}$ and $\sigma_{\text{pred.}}$ are the respective standard deviations. Confidence limits have been calculated using the seductive blockwise bootstrap resampling method proposed by Hanna (1989). 1000 samples from $C'_{\text{obs.}} - C'_{\text{pred.}}$ pairs are taken, and 95% confidence limits are based on the 2.5% and 97.5% quantiles of the distribution of statistics for the 1000 samples (so-called bootstrap-percentile confidence intervals).

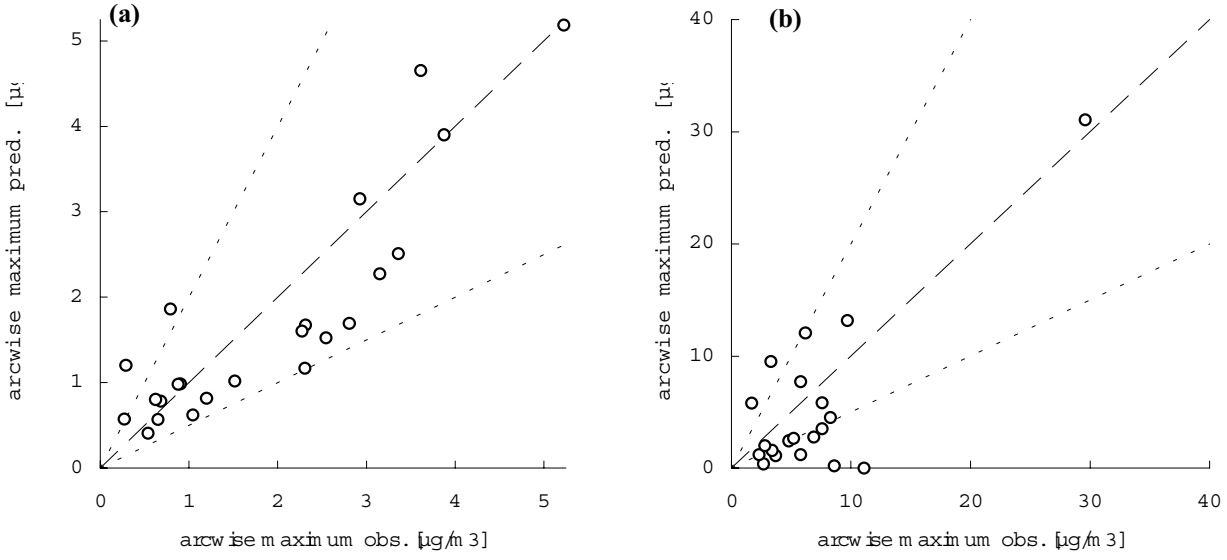

Figure 6 Scatter plots of the observed and predicted (PPM) arcwise maximum concentrations for (a) the Copenhagen and (b) the Lillestrøm tracer experiment. The dashed lines limit the area with a predicted value within a factor of 2 of the observed value.

(a) Copenhagen

The simulated results for the Copenhagen experiment show, in general, a good correspondence to the observations (Fig. 6(a)). Since the receptors during the Copenhagen experiment seem to have missed the concentration maximum, which occurred closer to the source than the closest receptor, no conclusion can be drawn concerning the ability of the PPM to predict the maximum surface concentration. Figure 6(a) shows the comparison of the observed and predicted arcwise maximum concentrations. Only two predicted values differ from the observation by more than a factor of 2. These data points belongs to the only experimental run for which the parametrized profile of wind fluctuation standard deviations had to be multiplied by a high factor, in order to let the profile match the measured value (see section 2.4.2). On average, a small underprediction of the arcwise

maximum (*ArcMax*) and a more pronounced underprediction of the cross-wind integrated concentration (*CIC*) can be observed (positive *FB* in Fig. 8). The underprediction is significantly different from zero, on a 95% level for *CIC* (i.e. the confidence limits do not include zero). The correlation is remarkably high for *ArcMax* and somewhat lower for *CIC*. The scatter (i.e. the *NMSE*) is rather low for the predicted *ArcMax* and, as for the *FB*, higher for the *CIC*, and differs from zero on a 95% level in both cases.

The results of using the Lagrangian particle dispersion model (LPDM) of Rotach *et al.* (1996) alone (which constitutes the particle part of the PPM) are also shown in Fig. 8 for *CIC*. For the Copenhagen data set the PPM performs only slightly worse than the full particle model, indicating that the approximation of a number of particles as a puff (according to the second interpretation of the PPM concept in section 2.2.1) does not lead to a much worse performance, while additionally providing information on the lateral concentration distribution.

(b) Lillestrøm

For the Lillestrøm experiment, the statistical measures for the *ArcMax* are encouraging (Fig. 6(b)). Regarding the difficult dispersion regime, the *NMSE* of below unity (see Fig, 9) can be regarded as satisfying. Note however, that a single data point (see Fig. 6(b)) has a very strong influence on these statistical measures. This leads to very large confidence limits. For two succeeding observational periods with a very small Obukhov length (12 January 1987), the PPM predicts the maximum concentration far away from the source, while the measurements indicate a well-defined maximum close to the source as for the other episodes (not shown). Therefore, the *CIC* is underpredicted by roughly 30% on average, with the most severe underpredictions for the arc closest to the source. The underprediction of the *ArcMax* is lower and not significantly different from zero on a 95% level. Compared to the LPDM, the PPM even performs slightly better in *NMSE* and *COR*.

(c) Kincaid

The release during the Kincaid experiment was highly buoyant. The effective plume height has been parametrized using the formulae of Briggs (1984) (for all models compared in section 2.4.4). Figure 7(a) depicts a scatter plot of the results for the Kincaid experiment. For the present validation, those hours of measurements tagged as ‘quality 3’ (Olesen 1995a) have been selected. This highest-quality tag indicates that a clearly defined maximum concentration could be identified on the receptor arcs. The quality-3 subset contains a total of 338 receptor arc measurements. Considering the patchy concentration patterns observed during the Kincaid campaign, plume

models not suited for convective conditions will tend to fail. Advanced particle models based on a skewed probability function are expected to yield better results. The same holds true for the PPM since it uses a particle model allowing for a convective pdf (section 2.2.3). Because of the stochastic nature of the experimental data, no model can be expected to be able to predict to a good correspondence the spatial and time-dependent concentration distribution. But the distribution of predictions should resemble the distribution of the measurements. Therefore, and since the number of observations is much larger than for the two other experiments, a quantile-quantile plot is shown in Fig. 7(b). The agreement between the distribution of predicted and observed *ArcMax* appears to be very good, with a slight tendency of overprediction towards high concentration values.

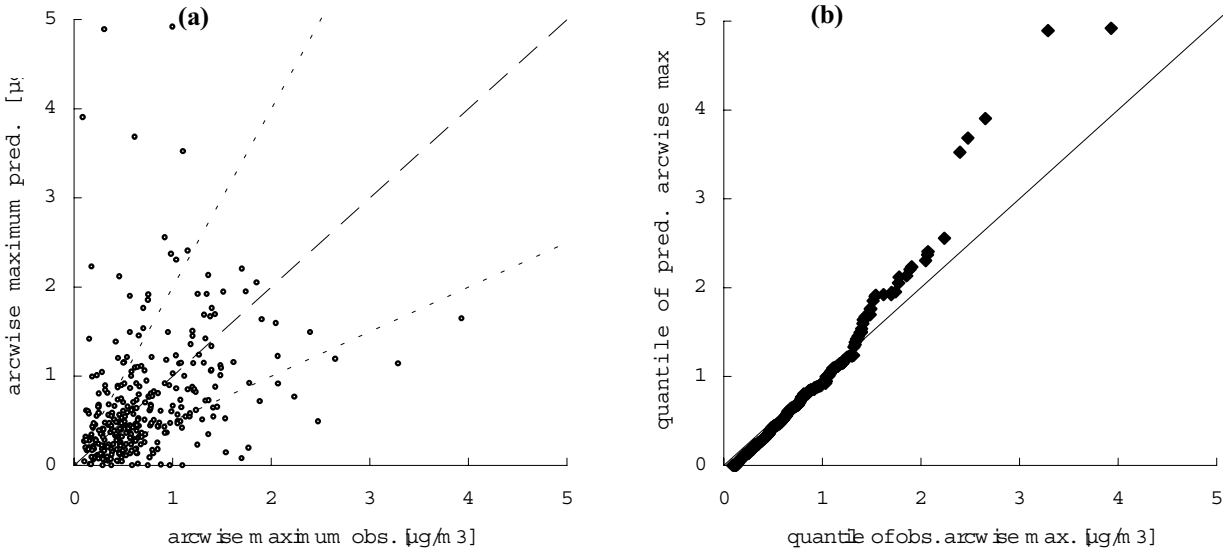

Figure 7 (a) Scatter plot and (b) quantile-quantile plot of observed (obs.) and predicted (pred.) arcwise maximum concentrations for the Kincaid tracer experiment.

No reliable measurements of the *CIC* are available for the Kincaid data set. The underprediction of the PPM on the *ArcMax* is modest and not significantly different from zero (Fig. 10). The correlation of approx. 0.4 is also considered to be a very good result with respect to very irregular concentration patterns. The latter, of course, is responsible for the value of the *NMSE* close to unity. In general, the fact that this data set consists of 338 data points leads to more precise estimates of the model performance than depicted by the other statistical measures discussed in this section. This becomes evident in the confidence limits which are generally smaller than those shown in Figs. 8 and 9 (see Fig. 10).

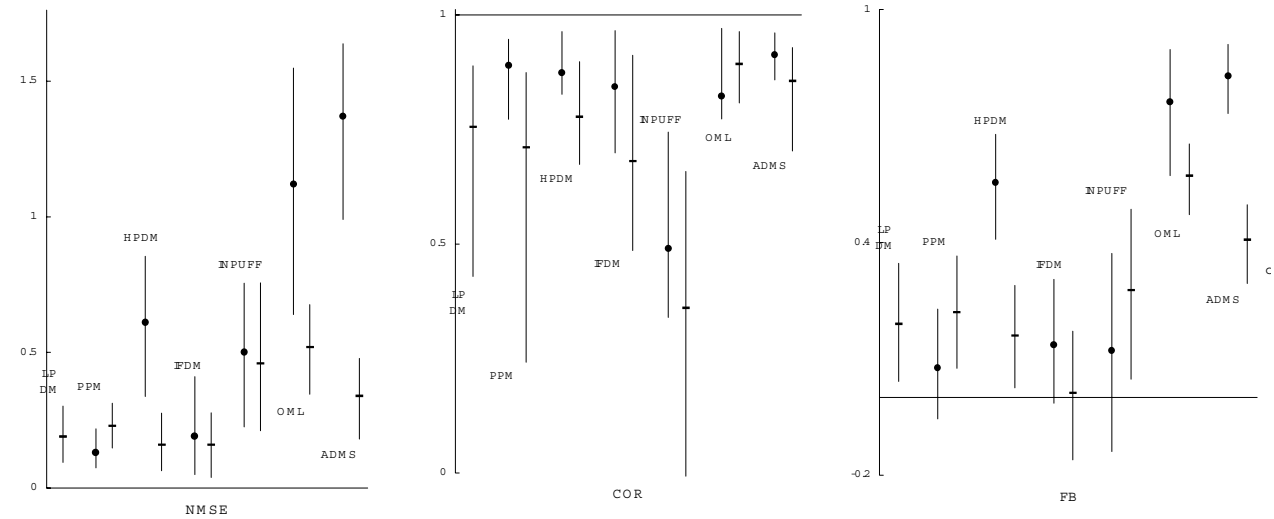

Figure 8 Copenhagen. NMSE, COR and FB for arc-wise maximum, ArcMax (shown with dots, ¥), and cross-wind integrated concentration, CIC (minus sign, –). 23 observations. The vertical lines show the 95% confidence limits calculated with bootstrap resampling. The horizontal lines depict the values for a perfect model (NMSE and FB: 0, COR: 1) (data of the other models from Olesen, 1995b). For the acronyms of the other models see text. LPDM refers to the Lagrangian Particle Dispersion Model of Rotach et al. (1996).

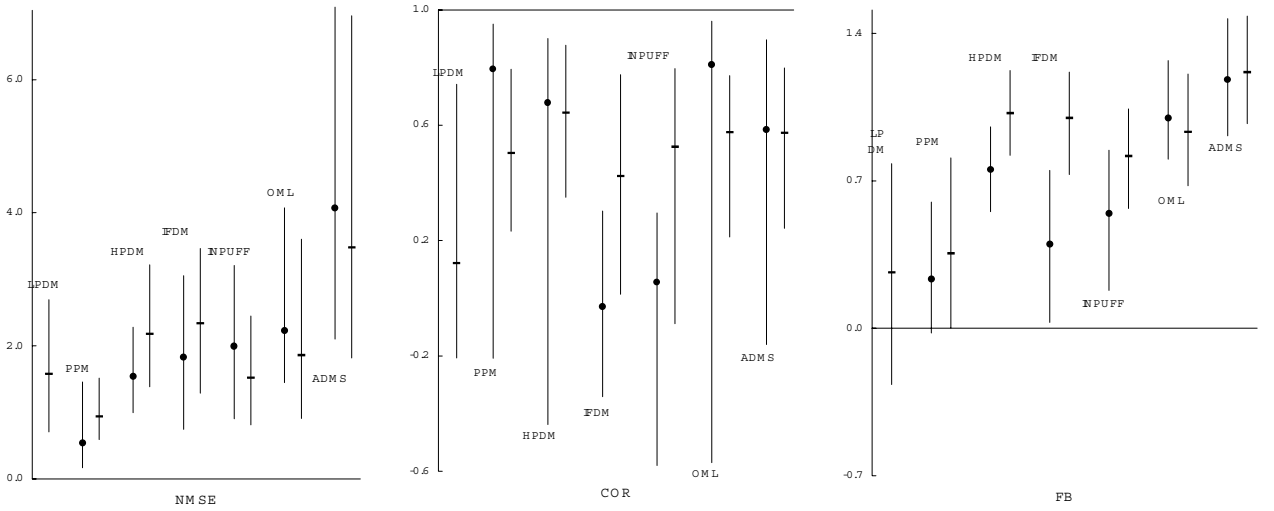

Figure 9 As Fig. 8 but for the Lillestrøm experiment and 20 observations.

2.4.4 Comparison to other models

The results for the simulations with the PPM and the LPDM are also compared to those of five other dispersion models. These are the HPDM-4 (Hybrid Plume Dispersion Model; Hanna and Chang 1993), the Danish OML (Operationalske Modeller om Luftforureninger; Olesen *et al.* 1992), the IFDM (Immission and Frequency Distribution Model; Cosemans *et al.* 1992), INPUFF (Integrated Puff dispersion model; Sandu 1995), and UK-ADMS (Atmospheric Dispersion Modelling System; Carruthers *et al.* 1992). The OML and UK-ADMS are new-generation Gaussian

plume models, whereas IFDM and INPUFF are a Gaussian plume and puff model, respectively, depending on stability classes, and the HPDM is a new-generation hybrid model consisting of four sub-models for different atmospheric stability regimes. For the Copenhagen and the Lillestrøm data set, all models but the OML used the measured values of $\langle u_2^2 \rangle$ and $\langle u_3^2 \rangle$. For the model intercomparison, 95% confidence intervals are estimated on the differences in *FB* and *NMSE* between each pair of models, using the bootstrap resampling (Hanna 1989). Models are considered as having different performance only if their *FB* and/or *NMSE* are different on a 95% level. While comparing the performance of the PPM and the LPDM with the other models, it should be kept in mind that the PPM requires much larger (roughly 2 orders of magnitude) computational time than models solving plume equations analytically, and the LPDM even needs another factor of ten times more CPU time than the PPM.

All models, including the PPM and the LPDM, underpredict the surface concentrations for the Copenhagen data set (positive *FB*, Fig. 8). This has been attributed by Rotach and de Haan (1997) to the influence of the rough urban character of the underlying surface, which leads to the formation of an urban roughness sublayer. Using the LPDM, Rotach and de Haan (1997) have shown, that this underprediction can be resolved when the turbulence and flow structure of an urban roughness sublayer is explicitly taken into account. The performance of the IFDM model, which relies on stability classes, is remarkable. Most models perform better on predicting the *CIC* than the *ArcMax* (this is most pronounced for the ADMS and OML models, which have severe difficulties predicting the *ArcMax* but perform clearly better on the *CIC*). The correlation coefficient is generally very high, with the values of the INPUFF model being lowest. Comparing the models, the performance of the PPM is significantly better than that of the HPDM, OML and ADMS, regarding the *FB* and *NMSE*. Concerning *COR*, the PPM differs significantly only from the INPUFF model. For *CIC*, the PPM can only be said to be significantly better than the OML (regarding *NMSE* and *FB*) and the ADMS and IFDM (*FB*).

For Lillestrøm, all models perform worse in terms of the given statistical measures than for the Copenhagen data set. Generally, large differences can be detected between the individual models (Fig. 9). For all the experiments in Lillestrøm, the sun was at a very low angle (they were started only 15 minutes after sun rise on average). Furthermore, no stable boundary layer heights were observed (a ground-based inversion was present). The INPUFF and IFDM model do not require a mixing depth as input; the LPDM, HPDM, PPM and ADMS use the parametrisation given in section 2.4.2, where the ADMS assumes a minimum value of 50 m (Carruthers 1997, personal

communication). The OML assumed the mixing depth to have a constant value of 200 m. These different parametrizations are likely to have a strong impact on the simulation results. Nevertheless, the results from the PPM seem to be encouraging as compared to the other models (Fig. 9). The PPM has a smaller bias and scatter (*NMSE*) than all other models, and the smaller confidence limits (though still very large) also show up in a high *COR* value. Because of the very large confidence limits, differences between the PPM and other models for *ArcMax* are significant compared to HPDM, OML and ADMS (regarding *NMSE* and *FB*). For *CIC* predictions, differences are significant for the HPDM and ADMS (*NMSE*) and to all models regarding *FB*.

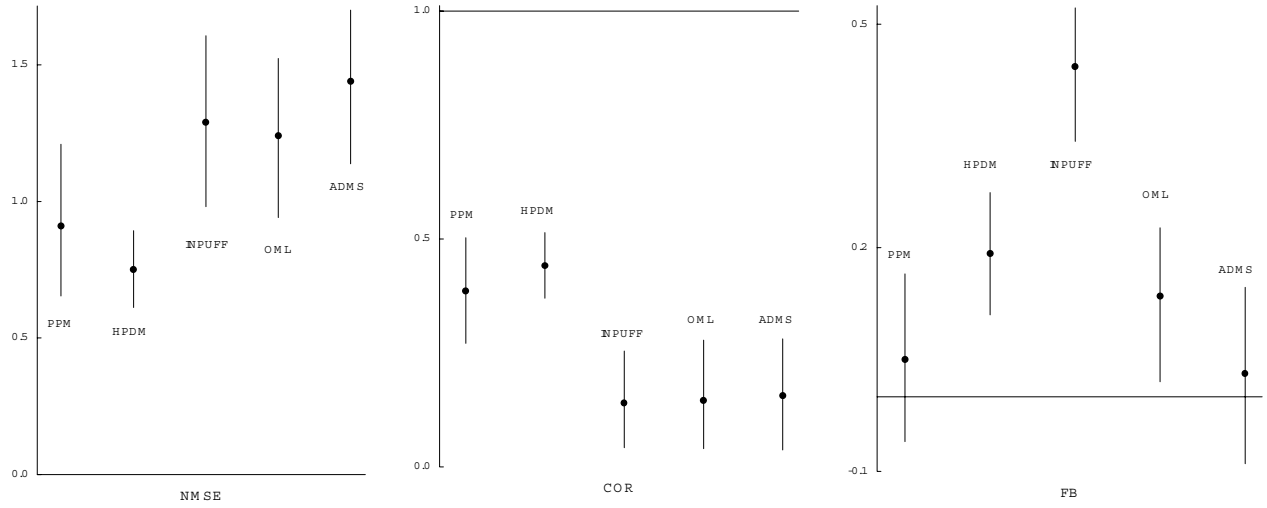

Figure 10 As Fig. 8 but for the Kincaid tracer experiment and for 338 observations.

For the Kincaid experiment, the large differences in model performance, even between the three Gaussian plume models (Fig. 10) is partly due to the fact that some modellers used the observed mixing height as input parameter, whereas others used the results from a meteorological pre-processor. For the present simulations with the PPM, the predicted mixing heights after Hanna and Paine (1989) are used. The HPDM also used these predicted values, whereas the other models (i.e. OML and ADMS) used the observed values. For several non-zero observations, most of them measured after sun set, the PPM gives a prediction of zero. The PPM has a very low bias, not significantly different from zero, and a modest scatter (*NMSE*) and correlation. Overall, the PPM performs best, with similar *NMSE* and *COR* as the HPDM (the second-best model), but with a significantly smaller *FB*. This probably is caused by the fact that the PPM is the only model using a convective pdf. The results for the Kincaid data set might be regarded more valuable, because of the high number of observations allowing for a better model intercomparison.

2.5 SUMMARY AND CONCLUSIONS

In the present paper, an approach to model dispersion is presented which aims at combining the advantages of puff models and particle models. The resulting model type is called Puff-Particle Model (PPM). In the PPM, a few hundred puffs are simulated in three-dimensional space, as compared to many thousand particles usually required in pure particle models. The concept of the PPM is very simple: while puff growth is described by the concept of relative dispersion (thus accounting for eddies smaller than the puff), the effect of meandering (i.e. the variation between the trajectories of different puffs) due to larger eddies (larger than the actual puff size) is simulated by introducing puff centre trajectories derived from particle trajectories from a particle model. Thus, the PPM can be interpreted in two ways: first, compared to conventional Lagrangian particle models the PPM requires less computing time, not accompanied by a significant loss in accuracy; second, it can be regarded as a puff model for applications in which no frequently updated meteorological fields are available to resolve all eddies larger than the puffs. Thus, in the absence of frequently updated meteorological information, the PPM is able to give better predictions in the near-field compared to traditional puff models. If one puff trajectory is followed, this gives a single realisation of an instantaneous release, with the correct dispersion (relative diffusion). Averaging over, say, one thousand such realisations gives an appropriate picture of the additional effect caused by meandering, since the meandering effect of all those eddies larger than the puff, but not resolved by the flow field, is simulated using stochastic puff-centre trajectories, yielding the correct ensemble plume statistics.

The validation with the data from three different tracer experiments covering all atmospheric stability conditions, shows a good model performance for the prediction of both the maximum concentration on an arc of receptors (*ArcMax*) and the cross wind integrated concentration (*CIC*). In general, the predictions of the PPM have statistical measures which are better than those of other models.

The PPM allows for a correct description of dispersion, regardless of the updating frequency of flow field information, i.e. regardless of the fact whether all large eddies are resolved by the flow field. This way, the modeller is not forced to choose between absolute dispersion (and only allowing for one flow field per, say, 60 minutes in order not to overestimate dispersion) on the one hand, and the use of relative diffusion on the other hand, with the effect of missing part of the dispersion, which will be most important for near- and intermediate-field concentration predictions. Instead, the modeller might use just as many flow field information updates as there are available.

The main fields of possible application of the PPM are those of conventional puff models, where the turbulence statistics of the flow field are sparse or infrequently provided. Additionally, the PPM has advantages for situations in which particle models have their strength (e.g. convective boundary layers, or in and above canopies), since it requires less computing time than the latter and at the same time offers the advantages of puff models, especially concerning the treatment of buoyant plume rise.

Acknowledgements—The present work was financed by the Swiss Federal Department of Education and Sciences (BBW) and the Swiss Agency of Environment, Forest and Landscape (BUWAL) through a project in the framework of COST 615 (citair). Thanks go to both reviewers for their many instrumental suggestions and for drawing our attention to the work of Hanna (1989).

REFERENCES

Batchelor, G. K. (1952): Diffusion in a field of homogeneous turbulence–Part II: The relative motion of particles. *Proc. Camb. Philos. Soc*., **48**, 345–362

Borgas, M. S. and Sawford, B. L. (1994): A family of stochastic 0odels for two-particle dispersion in isotropic homogeneous stationary turbulence. *J. Fluid. Mech*., **279**, 69–99

Bowne, N. E. and Londergan, R. J. (1983): Overview, results, and conclusions for the EPRI plume model validation and development project: Plains site. EPRI report EA-3074, Electrical Power Research Institute, Palo Alto, USA

Briggs, G. A. (1984): Plume rise and buoyancy effects. In *Atmospheric Science and Power Production.* Ed. D. Randerson, DOE/TIC 27601. Department of Commerce, Springfield, USA

Brost, R. A., Wyngaard, J. C. and Lenschow, D. H. (1982): Marine stratocumulus layers. Part II: Turbulence budgets., *J. Atmos. Sci*., **39**, 818–836

Carruthers, D. J., Holroyd, R. J., Hunt, J. C. R., Weng, W.-S., Robins, A. G., Apsley, D. D., Smith, F. B., Thomson, D. J. and Hudson, B. (1992): UK atmospheric dispersion modelling system. In *Air Pollution Modelling and its Applications IX.* Eds. H. van Dop and G. Kallos. Plenum Press, New York, USA

Cosemans, G., Kretzschmar, J. and Maes, G. (1992): The Belgian Immission Frequency Distribution Model. Pp. 149–150 in Olesen, H. R. and Mikkelsen, T. q.v.

Cuvelier, C. (Ed.) (1994): Proceedings of the 2nd Workshop on intercomparison of advanced practical short-range atmospheric dispersion models, 30 Aug.–3 Sept. 1993, Manno, Switzerland. Available from C. Cuvelier, JRC Ispra, TP 690, I-21020 Ispra (VA), Italy

Du, S., Sawford, B. L., Wilson, J. D. and Wilson, D. J. (1995): A Determination of the Kolmogorov constant (C_0) for the Lagrangian velocity structure function, using a second-order Lagrangian stochastic model for decaying homogeneous, isotropic turbulence. *Phys. Fluids*, **1**, 3083–3090

Gryning, S.-E., Holtslag, A. A. M., Irwin, J. S. and Sivertsen, B. (1987): Applied dispersion modelling based on meteorological scaling parameters. *Atmospheric Env*., **21**, 79–89

Gryning, S.-E. and Lyck, E. (1984): Atmospheric dispersion from elevated sources in an urban area: Comparison between tracer experiments and model calculations'. *J. Clim. Appl. Met*., **23**, 651–660

de Haan, P., and Rotach, M. W. (1995): A puff-particle dispersion model. *Int. J. Environment and Pollution*, **5**, Nos. 4–6, 350–359

de Haan, P., and Rotach, M. W. (1998): The treatment of relative dispersion within a combined Puff-Particle Model (PPM). In: Air Pollution Modeling and Its Application XII, S.-E. Gryning and N. Chaumerliac (eds.), Plenum Press, New York, 389–396

Hanna, S. R. (1989): Confidence limits for air quality model evaluations, as estimated by bootstrap and jackknife resampling methods. *Atmospheric Env*., **23**, 1385–1398

Hanna, S. R. and Paine, R. J. (1989): Hybrid Plume Dispersion Model (HPDM) development and evaluation. *J. Appl. Meteorol*., **28**, 206–224

Hanna, S. R. and Chang, J. C. (1993): Hybrid Plume Dispersion Model (HPDM) improvements and testing at three field sites. *Atmospheric Env*., **27A**, 1491–1508

Haugsbakk, I and Tønnesen, D. A. (1989): Atmospheric dispersion experiments at Lillestrøm 1986–1987. Data Report NILU OR 41/89. Available from Norwegian Inst. for Air Research, PO Box 100, N-2007 Kjeller, Norway

Højstrup, J. (1981): A simple model for the adjustment of velocity spectra in unstable conditions downstream of an abrupt change in roughness and heat flux. *Boundary-Layer Meteorol*., **21**, 341–356

Højstrup, J. (1982): Velocity spectra in the unstable planetary boundary layer. *J. Atmos. Sci*., **39**, 2239–2248

Hurley, P. and Physick, W. (1993): A skewed homogeneous Lagrangian particle model for convective conditions. *Atmospheric Env*., **27A**, 619–624

Hurley, P. J. (1994): Partpuff – A Lagrangian Particle-Puff approach for plume dispersion modelling applications. *J. Appl. Meteorol*., **33**, 285–294

Luhar, A. K. and Britter, R. E. (1989): A random walk model for dispersion in inhomogeneous turbulence in a convective boundary layer. *Atmospheric Env*., **23**, 1911–1924

Kaimal, J. C., Wyngaard, J. C., Coté, O. R. and Izumi, Y. (1972): Spectral characteristics of surface layer turbulence. *Quart. J. Roy. Met. Soc*., **98**, 563–589

Kretzschmar, J. G., Maes, G. and Cosemans, C. (eds.) (1994): Pre-prints of the 3rd Workshop on Operational Short-Range Atmospheric Dispersion Models for Environmental Impact Assessment, Nov. 21–24, 1994, Mol, Belgium. Available from J. Kretzschmar, VITO, Boeretang 200, B-2400 Mol, Belgium

Kretzschmar, J. G. and Cosemans, C. (eds.) (1996): Pre-prints of the 4th Workshop on Harmonisation within Atmospheric Dispersion Modelling for Regulatory Purposes, May 6–9, 1996, Oostende, Belgium. Available from J. Kretzschmar, VITO, Boeretang 200, B-2400 Mol, Belgium

Mikkelsen, T. and Larsen, S. E. (1984): Description of the Risø puff diffusion model. *Nuclear Technology*, **67**, 56–65

Mikkelsen, T., Larsen, S. E. and Pécseli, H. L. (1987): Diffusion of Gaussian puffs. *Quart. J. Roy. Met. Soc*., **113**, 81–105

Nieuwstadt, F. T. M. (1984): The turbulent structure of the stable, nocturnal boundary layer. *J. Atmos. Sci*., **41**, 2202–2216

Olesen, H. R., Larsen, S. E. and Højstrup, J. (1984): Modelling velocity spectra in the lower part of the planetary boundary layer. *Boundary-Layer Meteorol*., **29**, 285–312

Olesen, H. R., Løfstrøm, P., Berkowicz, R. and Jensen, A. B. (1992): An improved dispersion model for regulatory use: the OML model.In van Dop, H. and Kallos, G. (eds.), Air Pollution Modelling and its Applications IX, Plenum Press, New York, USA

Olesen, H. R. and Mikkelsen, T. (eds.) (1992): Proceedings of the 1st Workshop on Objectives for Next Generation of Practical Short-Range Atmospheric Dispersion Models, May 6–8, 1992, Risø, Denmark. Available from H. Olesen, NERI, PO Box 358, DK-4000 Roskilde, Denmark

Olesen, H. R. (1995a): Data sets and protocol for model evaluation. *Int. J. Environment and Pollution*, **5**, 693–701

Olesen, H. R. (1995b): The model validation exercise at Mol: overview of results. *Int. J. Environment and Pollution*, **5**, 761–784

Pasquill, F. and Smith, F. B. (1983): Atmospheric Diffusion. 3rd edition, John Wiley & Sons, New York

Richardson, L. F. (1926): Atmospheric diffusion shown on a distance-neighbour graph. *Proc. Royal Soc*., Series A, **110**, 709–737

Rotach, M. W. (1995): The universal constant of the Lagrangian structure function: its effect on dispersion characteristics under varying stability. Pp. 289–292 in Pre-prints 11th Symposium on Boundary Layers and Turbulence, Charlotte, NC. American Meteorological Society, Boston, USA

Rotach, M. W., Gryning, S.-E. and Tassone, C. (1996): A two-dimensional stochastic Lagrangian dispersion model for daytime conditions. *Quart. J. Roy. Met. Soc*., **122**, 367–389

Rotach, M. W., de Haan, P. (1997): On the urban aspect of the Copenhagen data set. *Int. J. Environment Pollution*, **8**, 279–286

Sandu, I. (1995): Evaluation of the Gaussian puff model based on measurements. *Int. J. Environment and Pollution*, **5**, 375–381

Sawford, B. L. (1982): Comparison of some different approximations in the statistical theory of relative dispersion. *Quart. J. Roy. Met. Soc*., **108**, 191–206

Scire, J. S., Strimaitis, D. G., Yamartino, R. J., and Zhang, X. (1995): A user's guide for the CALPUFF dispersion model. Prepared for the USDA Forest Service, Cadillac MI, by Earth Tech, Inc., Concord, MA, USA

Smith, F. B. and Hay, J. S. (1961): The expansion of clusters of particles in the atmosphere. *Quart. J. Roy. Met. Soc*., **87**, 82–101

Stull, R. B. (1988): An introduction to boundary layer meteorology. Kluwer Academic Publishers, Dordrecht, the Netherlands

Taylor, G. I. (1921): Diffusion by continuous movements. *Proc. London Math. Soc*., Ser. 2, **20**, 196–211

Thomson, D. J. (1987): Criteria for the selection of stochastic models of particle trajectories in turbulent flows. *J. Fluid Mech*., **180**, 529–556

Thykier-Nielsen, S., Mikkelsen, T., Larsen, S.-E., Troen, I., de Baas, A. F., Kamada, R., Skupniewicz, C. and Schacher, G. (1989): A model for accidental releases in complex terrain. In: Air Pollution and its Application VII, H. van Dop (ed.), Plenum Press, New York, USA

Thykier-Nielsen, S., Mikkelsen, T. and Santabàrbara, J. M. (1994): Experimental evaluation of a PC-based real-time dispersion modelling system for accidental releases in complex terrain. Pp. 383–394 in: Air Pollution and its Application X, Gryning, S.-E. and Millan, M. M. (eds.), Plenum Press, New York, USA

Wilson, J. D. and Sawford, B. L. (1996): Review of Lagrangian stochastic models for trajectories in the turbulent atmosphere. *Boundary-Layer Meteorol*., **78**, 191–210

Yamada, T. and Bunker, S. (1988): Development of a nested grid, second moment turbulence closure model and application to the 1982 ASCOT Brush Creek data simulation. *J. Appl. Meteorol*., **27**, 562–578

Chapter 3

The Treatment of Relative Dispersion Within a Combined Puff-Particle Model (PPM)*

Abstract—The Puff-Particle Model (PPM) combines the advantages of both, puff and particle dispersion models. In short, in this approach the centre of mass of each puff is moved along a 'particle trajectory', so trying to mimic the quickly changing turbulent flow field. However, particle models account for dispersion of turbulent eddies of all sizes (1-particle statistics, absolute dispersion) while puff models use relative dispersion to describe the puff growth. Therefore, on combining these two approaches as described above, the dispersing effect of small eddies (smaller than approximately the puff's size) is accounted for twice. A method is therefore presented to correctly simulate the relative dispersion of puffs within the framework of the PPM. It is based on removing the effect of the high-frequency part of the spectrum when using a 'particle trajectory' as the trajectory of the puff centre. It is shown on the basis of tracer data, that the correct treatment and interpretation of the two contributions to the dispersion process is crucial for reproducing experimental results to a good correspondence.

Key words: dispersion modelling, puff models, particle models, relative dispersion.

3.1 CONCEPT OF THE PPM

One of the major advantages of puff models is their ability to simulate inhomogeneous and instationary conditions. In principle this allows for concentration predictions of a 'sudden release' of pollutants from a source. In such cases relative dispersion must be used to describe the growth of the puff. Relative dispersion only takes into account the dispersing effect of those turbulent eddies which are able to enlarge the size of the puff and do not move the puff as a whole without dispersing it. The use of absolute dispersion (like the widely used parametrizations of Pasquill and Turner), which accounts for the dispersing effect of turbulent

---

* this chapter has been published as:
de Haan, P., and Rotach, M. W. (1998): The treatment of relative dispersion within a combined Puff-Particle model (PPM). In: Air Pollution Modeling and Its Application XII, S.-E. Gryning and N. Chaumerliac (eds.), Plenum Press, New York, 389–396

eddies of any size, leads to underpredicted concentrations relatively close to the source due to too large a dispersion.

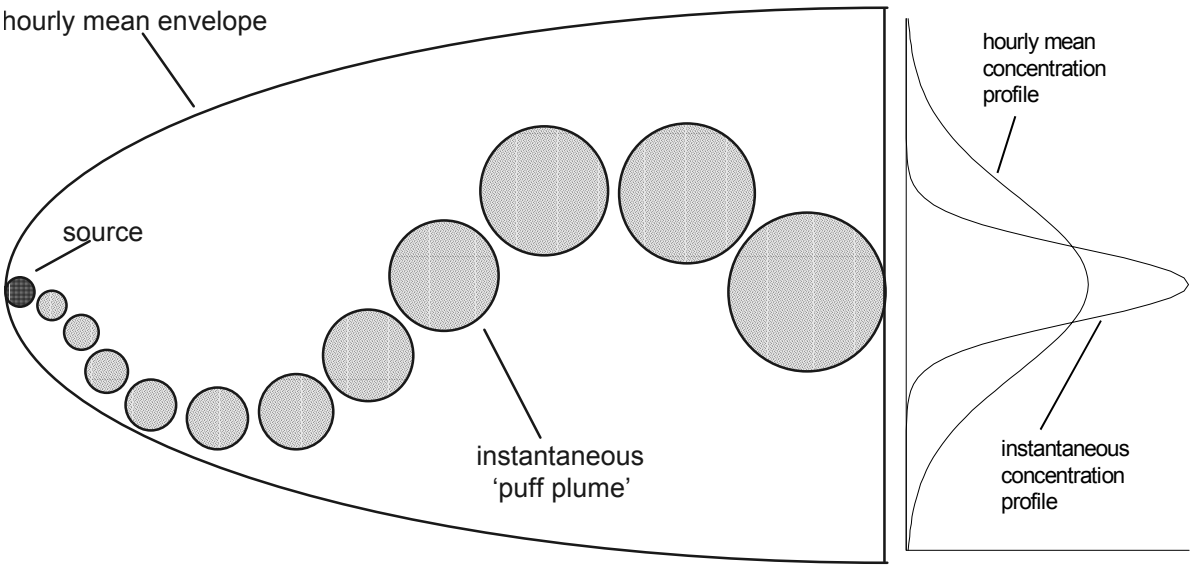

Figure 1 Conceptual sketch of the principle of the PPM. The meandering of the instantaneous 'puff plume' is modelled by moving the centre of mass of the puffs along a particle trajectory.

However, to correctly describe the dispersing effect due to the meandering of the released plume, a rather frequent updating of the flow field information is necessary. In principle, the updating of the flow field should resolve all turbulent eddies larger than the 'size' of the puff (characterized by its standard deviations). Since in practice such a frequent updating of the flow field and meteorological information is hardly possible, the puff-particle approach (de Haan and Rotach, 1995) aims at simulating the dispersing effect of plume meandering by introducing puff centre trajectories (see Fig. 1). These trajectories are determined by the low-frequency part of the turbulence spectrum, since relative dispersion only describes the effects of the high-frequency part. Clearly, as the puff's size grows, the relative dispersion covers an increasing part of the spectrum. Therefore, the trajectory of the puff's centre of mass has to simulate the effect of a decreasing amount of turbulent eddies, and thus has to become 'smoother' as puff sizes grow.

3.2 RELATIVE VS. ABSOLUTE DISPERSION

Relative dispersion corresponds to the expansion of a cluster of particles. The spread σ of an ensemble of marked passive particles from each other is

$$\sigma^2(t) = \left\langle \left(\int_0^t v(\xi) d\xi \right)^2 \right\rangle, \tag{1}$$

where $v = u - V_{cm}$, u is the absolute velocity of the particles and the velocity of the centre of mass of the cluster is denoted by V_{cm}. The overbar in Eq. (1) and hereafter denotes the average over all the particles within the puff, and the angular brackets refer to an ensemble average. In the concept of absolute dispersion, on the other hand, the spread σ is

$$\sigma^2(t) = \left\langle \left(\int_0^t u(\xi) d\xi \right)^2 \right\rangle. \tag{2}$$

For example, a turbulent eddy larger than the cluster of particles will displace the cluster as a whole. This will increase absolute dispersion, whereas the relative dispersion remains unchanged. From this it becomes clear that when using a particle model to simulate the meandering of a puff, as a surrogate for a frequently updated flow field, part of the spectrum is accounted for twice. This would cause the total dispersion to become overestimated more and more as the travel distance increases, leading to underestimated ground level concentrations far away from the source.

To separate the contribution of small eddies (contributing to an increase in puff size) for those of larger eddies (contributing to the meandering of the whole puff) the following procedure is introduced. From the actual puff sizes (i. e., the standard deviations) σ_x, σ_y, σ_z, a threshold frequency $n^*_{x,y,z} = \overline{u}(t) / (2\sigma_{x,y,z})$ is defined for each direction using Taylor's frozen turbulence hypothesis. The integral over the low frequency part of the turbulence spectrum is denoted as $\langle u_i^2 \rangle_{\text{eff}}$ $(i = u, v, w)$, where $\langle u_i^2 \rangle_{eff} = \int_{n_{\min}}^{"} S_i dn$. Then, the ratio $r_i = \langle u_i^2 \rangle_{\text{eff}} / \langle u_i^2 \rangle$ is determined (Fig. 2). The integration of the whole spectrum runs from $n_{\max} = \overline{u}/\eta$, where $\eta = (\upsilon^3/\varepsilon)^{1/4}$ is the Kolmogorov micro-scale, υ is the kinematic molecular viscosity and ε is the dissipation rate, to $n_{\min} = 1/T$, where T is the averaging time for the measurements of the turbulence statistics of the flow field.

In the present work velocity spectra models are taken from Højstrup (1981) for the unstable surface layer and Højstrup (1982) for the unstable planetary boundary layer. The model of Kaimal *et al.* (1972) is used for the neutrally stratified surface layer. For the stable surface layer, the model of Olesen *et al.* (1984) is adopted. For the upper part of the neutral and of the stable boundary layer, the same formulations as for the surface layer are used.

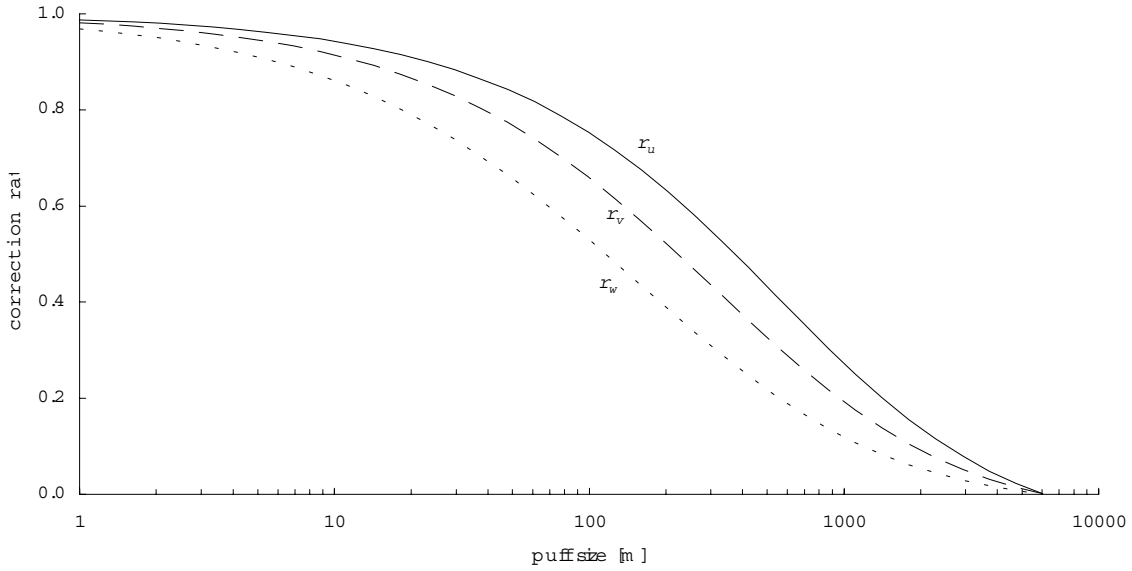

Figure 2 Plot of the correction ratios r_i *(i = u, v, w)* (*u*-component: solid line; *v*-component: dashed line; *w*-component: dotted line) as a function of puff size (conditions of forced convection; $u^* = 0.4\ \mathrm{ms}^{-1}$, $z/L = -2$, $z_i = 1000$ m, $\bar{u} = 3.4\,\mathrm{ms}^{-1}$, averaging time of flow field one hour).

3.3 REDUCTION OF THE TRAJECTORY VARIABILITY AS PUFF SIZES GROW

The combination of a puff model with a particle model representing the whole turbulence spectrum asks for the removal of the dispersing effect from the high-frequency part of the energy spectrum (i. e., the small turbulent eddies already covered by the puff model) from the particle trajectories. The procedure to remove this part of the turbulent fluctuations from the 'particle-part' of the PPM is straightforward: The time series of stochastic turbulent velocity components of each particle is smoothed. The trajectory of the centre of mass of a puff is then calculated based on these smoothed turbulent velocities. This leads to an increasingly smooth puff centre trajectory as the puff size grows.

The Kalman filter originates from the need to estimate the true value of an underlying stochastic process which can only be observed with an error, where it is assumed that the observational error is normally distributed with a standard deviation τ. Under such circumstances there is a need not to consider the measured time series of, for example, pressure, but to filter out the noise signal originating from the observational error, thus obtaining a smoothed time series as an improved, less fluctuating estimation of the quantity which originally had been measured. Often running mean values are used for such purposes, where the smoothed value is calculated as a weighted function of several values at both sides of the position for which a smoothed value has to be estimated. These running mean values

have two disadvantages with respect to the present need for smoothing the turbulent velocities calculated by a particle model: first, the future values of the turbulent velocity are not known at the moment where a smoothed value has to be estimated for use for the puff centre trajectory. This way, running mean estimations could only be based on past values of the turbulent velocities, leading to a biased estimation. Second, such a running mean makes it necessary to store an increasing number of 'past values' of the turbulent velocities of each particle, since the running mean is based on these past values.

The Kalman filter procedure, on the other hand, is computed recursively. This way, the filter estimation at the time step t is only based on the filter estimate at the time step $t-1$, the measured value at time step t and the parameters of the underlying stochastic process. Stochastic particle dispersion models generally are modelled as a so-called AR(1)-process, i. e. an auto-regressive process in which the position and velocity of a particle only depend on the velocity and position of the same particle one time-step ago.

If the underlying AR(1)-process is

$$X(t) = \alpha \cdot X(t-1) + E(t) \tag{3}$$

where X denotes the turbulent velocity vector (u', v', w'). The stochastic process from Eq. (3) has a part correlated with the turbulent velocities at the preceding time step and a uncorrelated stochastic distribution $E(t)$ which is normally distributed with zero mean and variance σ^2. The process given by Eq. (3) is our underlying, 'true' process. We assume it to be observed with a normally distributed observational error with variance τ^2. The Kalman filter estimate $\hat{X}$ for the next time step then is

$$\hat{X}_{t+1,t} = \alpha \cdot \hat{X}_{t,t} \tag{4}$$

where the filter probability density has a variance

$$R_{t+1,t} = \alpha^2 R_{t,t} + \sigma^2 \tag{5}$$

Here, the first subscript gives the time step for which the filter estimate is valid, and the second subscript indicates the time step of the last observation on which this filter estimate is based. Given the new observation at time step $t+1$, $X(t+1)$, the filter estimate is corrected to

$$\hat{X}_{t+1,t+1} = \hat{X}_{t+1,t} + \frac{R_{t+1,t}}{R_{t+1,t} + \tau^2}\left(X_{t+1} - \hat{X}_{t+1,t}\right) \tag{6}$$

with the new variance

$$R_{t+1,t+1} = \frac{R_{t+1,t} \cdot \tau^2}{R_{t+1,t} + \tau^2} \tag{7}$$

This recursive algorithm can be started as soon as initial values $\hat{X}_{0,0}$ and $R_{0,0}$ are chosen, the influence of which vanishes after just a few iterations.

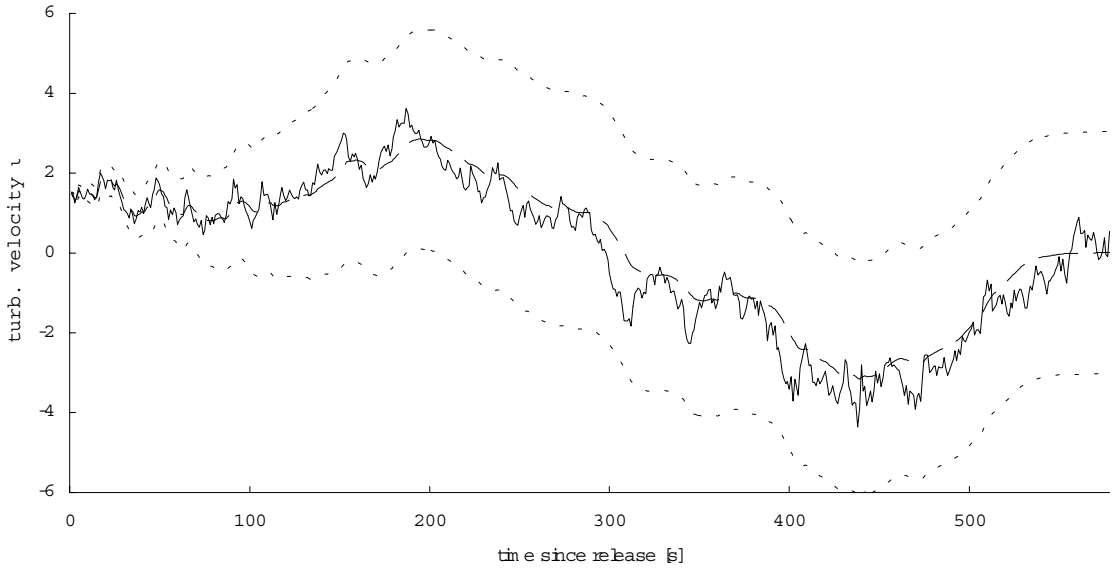

Figure 3 Smoothing of the turbulent velocity components calculated by the particle model (solid line) for use as puff centre velocities in the PPM (dashed line). The smoothing is increased as the correction ratios drop, i. e. the puff size grows. The dotted lines below and above of the smoothed turbulent velocity indicate the range $[u' - \tau, u' + \tau]$. Example for the *u*-component.

The concept used within the puff-particle approach is to consider the turbulent velocity components computed by the particle-part of the model to be 'observed values', where the 'observational error' is normally distributed with mean zero and standard deviation τ. By choosing τ proportional to the correction ratios r_i (and thus proportional to the growth of the size of the puff), increasingly smoothed time series of turbulent velocities are obtained. These smoothed velocity components are then used to calculate the trajectory of the puff's centre of mass. In the beginning, i. e. when the puff size is small and r_i approximately equals unity, τ is chosen to be zero. As puff sizes increase and the r_i decrease (Fig. 2), the high-frequency fluctuations of the turbulent velocity components are eliminated from the trajectory of the puff's centre (Fig. 3). This corresponds to the concept of relative diffusion where all fluctuations originating from turbulent eddies with sizes smaller than the size of the puff are

taken into account. As the puff size further increases, the r_i eventually drop to zero, and τ is chosen in such a way that the smoothed turbulent velocity time series remain constant.

Between the two limiting cases ($\tau_i = 0$ for $r_i = 1$ and τ_i large for $r_i = 0$),

$$\tau_i(r_i) = c\sigma \cdot \text{logit}\{d(0.5 - r_i)\} \tag{8}$$

is chosen in the PPM, where $\text{logit}(x) = \exp(x)/\{1 + \exp(x)\}$. In the present work, $c = 100$ and $d = 10$ are used. The ratios r_i are evaluated for each puff individually. As puff sizes grow, the values of the r_i decrease and eventually approach zero, leading to turbulent movements of the puff centres of very low frequency only. This allows the particle model within the PPM to be switched off as soon as r_i equals unity, and the puff centres are moved by the average flow field only. For far-field concentration predictions, this causes considerable computational savings.

Even when τ is large, the smoothed velocity fluctuation of a stochastic process will not give exactly zero. Therefore, to ensure that the smoothed turbulent velocities approach zero as $r_i \to 0$, the smoothed values are forced towards zero as soon as $r_i > 0.9$.

3.4 VALIDATION

For the prediction of concentrations averaged over approximately one hour, the puff-particle approach with smoothed puff centre trajectories should yield similar concentrations as a dispersion model based on absolute dispersion (e. g., a particle model). Therefore, the validation in this section aims at comparing the ground-level concentrations of four different models. The first model which is to be compared is a 'pure' particle model after Rotach *et al.* (1996) which fulfils the well-mixed criterion of Thomson (1987). The second and third model in this comparison are the PPM without and with additionally smoothed puff centre trajectories, respectively. The fourth model is a 'pure' puff model, in which the puffs are dispersed with relative dispersion. A second validation of the performance of the PPM with smoothed puff centre trajectories, against the data from three tracer experiments under different atmospheric conditions, can be found in de Haan and Rotach (1998).

The comparison of the predicted ground-level concentrations of these four models allows to validate the treatment of relative dispersion within the PPM. If the averaging time is one hour, the stochastic puff centre trajectories will account for almost the whole dispersing effect of plume meandering. Therefore the total dispersion will equal absolute dispersion, and this

leads to comparable ground-level concentrations predictions of both, the 'pure' particle model on the one side and the PPM with the smoothed puff centre trajectories on the other side. The PPM without the smoothing procedure, on the other hand, is expected to give too low concentration predictions, since a increasing part of the energy spectrum is taken into account twice, leading to an overestimation of the total dispersion. At the opposite, the 'pure' puff model does only cover part of the energy spectrum, leading to underestimated dispersion and hence to overpredicted ground-level concentrations.

To validate the predictions of the different models against measurements, the data from the Copenhagen tracer experiment are used. Data from 9 hours of measurements under conditions of forced convection are available. The non-buoyant tracer was released over a suburban surface at a height of 115 m. The receptors were placed on several arcs downwind of the source and hourly average measurements of the tracer concentrations were made at 2 m above ground. The mean wind speed was measured at different levels. The mixing height, the friction velocity and the Obukhov length were measured close to the release point, and measurements of the velocity statistics, $\langle u'^2 \rangle$ and $\langle w'^2 \rangle$, are available. More details about the experiment can be found in Gryning and Lyck (1984).

The simulation of the tracer experiment was performed by rebuilding the experimental set-up within the model and by predicting the concentrations at arcs of receptors at the same locations as in the tracer experiment. This allows the calculation of the cross-wind integrated concentration (CIC), the standard deviation on the arc in meters (SIGY) and of the maximum concentration occurring on an arc (ArcMax). Additionally, the ground-level concentrations in the plume centre line are predicted.

As an example, the resulting concentration profiles down-wind from the source for one of the hours of the tracer experiment are depicted in Fig. 4. The poor performance of the 'pure' puff model is completely due to the underestimated total dispersion, causing the maximum concentration to occur further down-wind and to remain on a high level as compared to the other three models as well as with the experimental data. The other three models all show very similar concentration patterns close to the source. This is due to the fact that in this early stage the relative dispersion of the puffs is only a minor contribution to the total dispersion, and also due to the fact that the 'pure' particle model is identical with the particle-part of the PPM used to calculate the stochastic puff centre trajectories. The removal of part of the

dispersing effect of these stochastic trajectories in the third model, the PPM with smoothed puff trajectories, leads to a larger predicted maximum concentration. It is similar to the maximum concentration as predicted by the 'pure' particle model. The PPM without smoothing procedure, on the other hand, predicts an about ten percent lower maximum concentration, due to the overestimation of total dispersion. Further down-wind, the concentration predictions of the particle model and of the smoothed PPM remain similar, whereas the PPM without smoothing simulates somewhat lower concentrations.

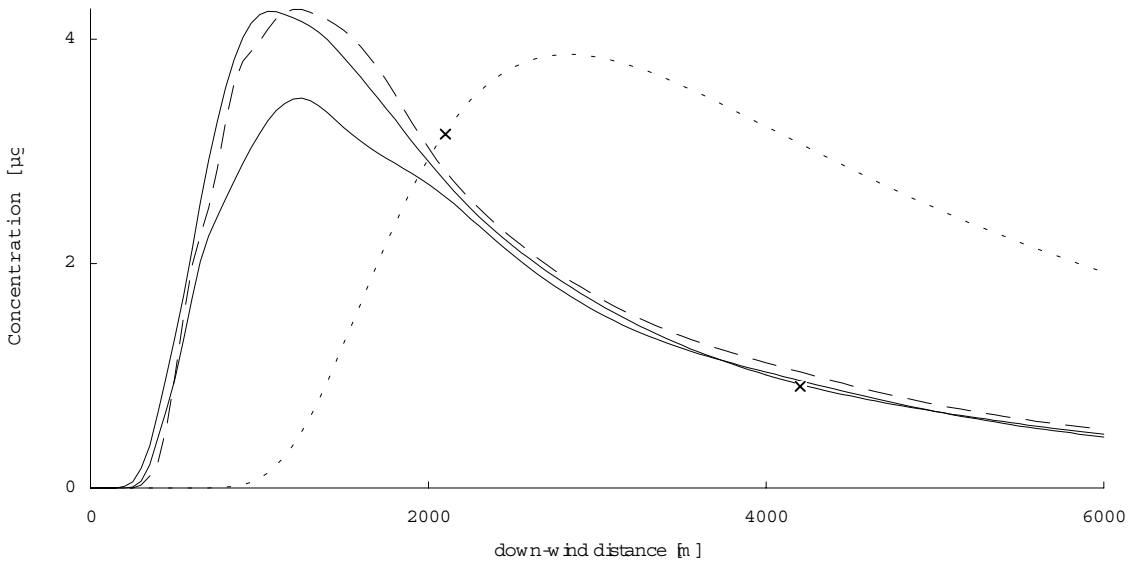

Figure 4 Example of the plume centre line concentration at 2 m above the ground for the particle model (dashed line), the puff-particle model without and with Kalman filter (lower and upper solid line, respectively) as well as for the puff model (right dashed line). Crosses depict the measurements (Copenhagen experiment from Sep. 26, 1978).

In Table 1 the following statistical measures are compared for the different simulations of the tracer experiments: the fractional bias $FB = \left(\overline{c}_{obs.} - \overline{c}_{pred.}\right) / \left\{0.5\left(\overline{c}_{obs.} + \overline{c}_{pred.}\right)\right\}$; the normalised mean square error $NMSE = \overline{\left(c_{obs.} - c_{pred.}\right)^2} \,/\, \left(\overline{c}_{obs.}\overline{c}_{pred.}\right)$; the correlation coefficient $COR = \overline{\left(c_{obs.} - \overline{c}_{obs.}\right)\left(c_{pred.} - \overline{c}_{pred.}\right)} \,/\, \left(\sigma_{obs.}\sigma_{pred.}\right)$; the percentage of simulations within a factor of two of the measurement, FAC2. $c_{obs.}$ is the observed, $c_{pred.}$ the simulated concentration.

As can be seen, the overall performance of the 'pure' particle model is better than the measures of the other three models. However, the smoothed PPM shows almost identical FB and NMSE. Additionally, the measures of the smoothed PPM are clearly improved as compared with the PPM without smoothing procedure. The puff model, finally, shows a

rather poor performance. Even the particle model, however, shows a general underprediction (a positive fractional bias). In Rotach and de Haan (1997) it is shown that taking into account the rough character of the suburban area where the tracer experiment took place leads to the vanishing of this systematic underprediction.

	ArcMax				CIC				SIGY			
	NMSE	COR	FAC2	FB	NMSE	COR	FAC2	FB	NMSE	COR	FAC2	FB
Observations	0.000	1.000	100%	0.000	0.000	1.000	100%	0.000	0.000	1.000	100%	0.000
Particle model	0.137	0.871	91%	0.029	0.189	0.700	87%	0.197	0.088	0.836	100%	0.006
PPM (Kalman f.)	0.186	0.858	87%	0.050	0.179	0.644	83%	0.123	0.091	0.879	100%	–0.08
PPM (no filter)	0.218	0.852	78%	0.047	0.180	0.654	83%	0.134	0.103	0.901	95%	–0.10
Puff model	1.687	0.255	30%	–0.47	1.057	0.029	39%	–0.12	0.388	0.947	60%	0.569

Table 1 Comparison of statistical measures (see text) for the different simulations.

It must be noted that the data from the Copenhagen experiment do not allow to validate one of the most important effects of the smoothing procedure within the PPM. The predicted maximum down-wind concentration closely resembles the predicted values from the 'pure' particle model, whereas the PPM without correction predicts lower maximum concentrations. Unfortunately, all arcs in the Copenhagen experiment were placed at relatively large distances from the source, so that the maximum concentration was not observed.

3.5 SUMMARY AND CONCLUSIONS

The puff-particle approach is suited to simulate the effect of plume meandering in absence of frequently updated meteorological and flow field information. However, the combination of a puff and a particle model leads to a double representation of the dispersing effect of part of the turbulence spectrum, dependent on the size of the individual puffs. In the present contribution, a method is proposed which corrects this overestimation of dispersion by filtering out the high-frequency part of the changes of turbulent velocity within the particle model. This filtering is realised using a Kalman filter. The extent of the smoothing depends on the proportion of the velocity spectrum of which the dispersing effect is taken into account by the puff part of the model. This way, the smoothing increases as puffs sizes grow. The validation against data from a tracer experiment and against the results of a pure particle model show than the corrected PPM (i. e., with smoothed puff centre trajectories) does not

over- nor underpredict the total dispersion and shows approximately the same results as does the particle model.

Acknowledgements—The present work was partly financed by the Swiss Federal Department of Education and Sciences (BBW) and the Swiss Federal Department of Environment, Forest and Landscape (BUWAL) through a project in the framework of COST 615 (citair), and by the Swiss National Science Foundation through Grant Nr. 21-46849.96.

REFERENCES

de Haan, P., and Rotach, M. W. (1995): A puff-particle dispersion model. *Int. J. Environment and Pollution,* **5**, Nos. 4–6, 350–359

de Haan, P., and Rotach, M. W. (1998): A novel approach to atmospheric dispersion modelling: the Puff-Particle Model (PPM). *Quart. J. Royal Meteorol. Soc..,* **124**, 2271–2292

Gryning, S.-E., and Lyck, E. (1984): Atmospheric dispersion from elevated sources in an urban area: Comparisons between tracer experiments and model calculations. *J. Clim. Appl. Met.*, **23**, 651–660

Højstrup, J. (1981): A simple model for the adjustment of velocity spectra in unstable conditions downstream of an abrupt change in roughness and heat flux. *Boundary-Layer Meteorol.,* **21**, 341–356

Højstrup, J. (1982): Velocity spectra in the unstable planetary boundary layer. *J. Atmos. Sci.,* **39**, 2239–2248

Kaimal , J. C., Wyngaard, J. C., Coté, O. R. and Izumi, Y. (1972): Spectral characteristics of surface layer turbulence. *Quart. J. Roy. Met. Soc.*, **98**, 563–589

Olesen, H. R., Larsen, S. E. and Højstrup, J. (1984): Modelling velocity spectra in the lower part of the planetary boundary layer'.*Boundary-Layer Meteorol.,* **29**, 285–312

Rotach, M. W., Gryning, S.-E. and Tassone, C. (1996): A two-dimensional stochastic Lagrangian dispersion model for daytime conditions. *Quart. J. Roy. Met. Soc.,* **122**, 367–389

Rotach, M. W. and de Haan, P. (1997): On the urban aspect of the Copenhagen data set. *Intern. J. Environment Pollution,* **8**, 279–286

Thomson, D. J. (1987): Criteria for the selection of stochastic models of particle trajectories in turbulent flows. *J. Fluid Mech.*, **180**, 529–556

Chapter 4

On the use of Density Kernels for Concentration Estimations Within Particle and Puff Dispersion Models*

Abstract—Stochastic particle models are the state-of-science method for modelling atmospheric dispersion. They simulate the released pollutant by a large number of particles. In most particle models the concentrations are estimated by counting the number of particles in a rectangular volume (box-counting). The effects of the choice of the width and of the position of these boxes on the estimated concentration is investigated. For the estimation of the concentration at a given point in space, it is shown that this numerical procedure can cause either oversmoothed predictions or too much scatter. As an alternative approach, the density kernel method to estimate concentrations is proposed, which optimizes bias and variance. It allows for a reduction of the number of particles simulated for the same accuracy. The efficiency of several density kernel shapes is compared, and methods for choosing their bandwidths are proposed. The relationship between the numerically motivated bandwidths and the description of the growth of a cluster of pollutant particles (puff dispersion) is discussed.

Key words: Kernel density estimation, box-counting, particle models, puff models, relative diffusion.

4.1 INTRODUCTION

At present, stochastic particle or random-walk models are the most advanced approach to simulate atmospheric dispersion, especially for convective atmospheric conditions (for a review, see Wilson and Sawford 1996). In such particle models, the emitted pollutant is simulated by a large number of particles, which are assumed to exactly follow the flow. This approach has several advantages over dispersion models like Gaussian plume or puff models.

---

* this chapter has been accepted for publication (editorial changes may still be made):
de Haan, P. (1999): On the use of Density Kernels for Concentration Estimations Within Particle and Puff Dispersion Models. Accepted for publication in *Atmospheric Environment*

However, simulating the emitted pollutant by many discrete particles brings up one difficulty: the correct estimation of the concentration at a certain location.

In atmospheric dispersion modelling with stochastic particle models, it is common practice to calculate such averages over a grid cell in space, i.e. by counting all particles in a box (see, f.e., Borgas and Sawford 1994; Luhar and Rao 1994; Hurley and Physick 1991; Luhar and Britter 1989; Rotach *et al.* 1996). The estimation of concentration is then obtained by multiplying the number of particles with their mass, and dividing this total mass by the size of the grid box. This way of counting the number of particles in a box is identical to calculating a three-dimensional histogram. Of course, if the volume average over such a box is what the modeler wants, such box-counting methods are most efficient.

Histogram estimations in general depend, however, on the choice of the width and the centre of the averaging interval, area or volume. To estimate point concentrations in the context of atmospheric dispersion modelling, there are no physical restrictions determining either the centre of a numerical averaging volume, or its size (besides the sampling volume of field instruments, which would lead to very small averaging volumes). This means that when choosing large averaging volumes, important details might get lost, and the estimation of the concentration density simulated by the particles will be oversmoothed. On the other hand, when choosing small averaging volumes, one runs at risk having random fluctuations in the number of particles per sampling volume.

The stochastic particle modeller will thus try to choose ”reasonable” sizes and positions of the averaging volumes. The differences in the resulting concentration predictions can be significant (see section 4.2) and of the same order of magnitude as effects which are of interest (i.e. are to be modelled). It should be stressed that this uncertainty originates from a numerical procedure only. Since atmospheric dispersion modelling already has to cope with considerable uncertainties, it is desirable to have a numerical method for concentration estimation within particle models which does not lead to much additional uncertainty.

Another approach to obtain concentrations with stochastic particle models is the backward-modelling approach of Flesch *et al.* (1995). In this approach box-counting is used, but instead of having an exact source location, the backward method has an exact receptor position (and thus sampling box position), and all backward trajectories coming ”near” to (i.e., originating from) the source are related to that source. This approach is suited for area sources together

with small receptor volumes. But even then, in principle the uncertainities related with either box-counting or kernel methods can only be circumvented when the source is located exactly at ground level, and all particles being reflected at the ground surface within the source area being related to the source. Flesch *et al.* (1995) discuss this special case into detail.

Clearly, for very high particle densities, the uncertainties of box-counting vanish; e.g. Borgas and Sawford (1994) theoretically assume the number of particles be ”high enough” for the choice of the dimensions of the particle counting box to be ”negligible”. But at present, computing power still drastically limits the number of particles which are normally emitted. With computing power currently available, only for one-dimensional models the effects might become negligible (see section 4.2).

For these reasons, another method is proposed in this paper. It relies on the concept of density distributions of different shape which are ”added” to the particle’s position, i.e. the mass represented by the particle is spread out in space. Such a density distribution around the centre of mass is called the density kernel. The kernel method has been widely applied since it was introduced in 1950 (for a good review, see Scott 1986, Ch. 6), whereas in atmospheric dispersion modelling the box-counting method is still used despite its deficiencies; Lorimer (1986) was the first, to the author’s knowledge, to use a kernel method for atmospheric dispersion modelling.

In contrary to the choice of box size and position, which makes the box-counts a bad choice for concentration estimation, the shape of the kernel and its width as a function of the particle distribution have to be specified. Of these two, the latter is chosen such that the bias and variance of the concentration estimation are minimised jointly. The number of particles normally simulated at present is more than sufficient to let this method become nearly independent of the shape of the kernel. This makes the kernel density method a suitable approach for particle modellers to estimate the concentrations simulated by their model.

The RAPTAD model of Yamada *et al.* (1987) and Yamada and Bunker (1988) combines a particle model with Gaussian shaped density kernels. They use the physical concept of absolute dispersion to estimate the appropriate size of these kernels. This approach is discussed in more detail in Section 4.6.

The box-counting method to estimate concentrations in particle models is reviewed in section 4.2. The concept of density kernel estimators is introduced in section 4.3, and the important

issue of the determination of the bandwidth of such kernels is treated in section 4.4. Different kernel shapes are compared in section 4.5. The analogy between these numerically determined density kernels and the physical description of the expansion of a cluster of particles is discussed in section 4.6.

4.2 CONCENTRATION ESTIMATION BY BOX-COUNTING

4.2.1 Box-counting in particle models

The smoothing of any given data actually is a non-parametric method to estimate the ”true” curve (being a density or a function), which is polluted by random noise. Most particle model simulations are one- or two-dimensional. The histogram (i.e., box-counting, see above) still is the commonly used density estimator for particle models. In the vertical direction, the size of the intervals (the averaging volume) is often constant with height. For their one-dimensional model, Luhar and Britter (1989) and Luhar *et al.* (1996), with 15 000 and 20 000 particles released, respectively, use vertical box heights Δz of $\Delta z/z_i = 0.05$, and a ”horizontal” extent $\Delta X = 0.1$, where X is the dimensionless travel distance, $X = w_* t/z_i$, and w_* denotes the convective velocity scale. Luhar and Rao (1994) release 12 000 particles per hour in their fully three-dimensional model, and use box dimensions $\Delta x \times \Delta y \times \Delta z$ of $200\ \mathrm{m} \times 50\ \mathrm{m} \times 10\ \mathrm{m}$ for elevated and $200\ \mathrm{m} \times 25\ \mathrm{m} \times 5\ \mathrm{m}$ for surface releases (and take the average over 1 h). Hurley and Physick (1991) have 5000 particles released in a two-dimensional model, and take $\Delta z = 25\ \mathrm{m}$ (with the inversion height $z_i = 1000\ \mathrm{m}$) and $\Delta x = 100\ \mathrm{m}$. Rotach *et al.* (1996) present a two-dimensional model and use 10 000 particles; the dimensions of the averaging boxes are $\Delta z = 20\ \mathrm{m}$ (with inversion height varying from 820 m to 1980 m) and $\Delta x = 300\ \mathrm{m}$.

The amount of additional variability of the model predictions caused by the box-counting method differs. For one-dimensional models and the use of approx. 100 000 particles, this variability seems to be small, whereas for two-dimensional particle models, this same number of particles, when applying Taylor's frozen turbulence hypothesis, has to be simulated for far longer time periods, which is about the limit of today's possibilities. For three-dimensional models, the order of magnitude of the number of particles roughly is the square of the number used in one- and two-dimensional models.

For example, Venkatram and Du (1997) report that with the simulation of 50 000 particles in a one-dimensional model, model results are not sensitive to the size of the numerical sampling

box. On the other hand, Du and Wilson (1994) (who do not mention the number of simulated particles) show concentration contour plots from a two-dimensional model where the size of the sampling volume can still be detected from the figures shown in their paper. The same holds for results from the one-dimensional particle model of Thomson and Montgomery (1994), who use 90 000 to 120 000 particles. This means that for two- and three-dimensional models, the expected increases in computing power in the near future will not be sufficient to rely on box-counting concentration estimations. Anyway, all of the box sizes used by particle modelers mentioned above are averages over volumes far larger than any receptor sampling volume.

Also, Yamada and Bunker (1988) report that determining the concentration at a given time and location by counting the particles simulated by their fully three-dimensional RAPTAD meso-scale particle model yields considerably varying results, depending on the size of the sampling volume and the number of particles used.

4.2.2 Near-source concentration estimation

Two areas can be identified where the box-counting method is most likely to be sensitive. Firstly, concentration predictions for the near-source field, where changes in the particle density are sharp and large proportions of the total number of particles might still be within the volume of few sampling boxes. Secondly, the estimation of surface concentrations, which are of interest for most air pollution simulations, but are likely to show gradients near the surface over distances similar to the vertical extent of box sampling volumes. For concentration predictions in the far field and for smooth particle probability density functions, the box-counting method will produce the same results as any other method, although the kernel method remains more efficient in these cases as well.

As an example to illustrate the variability in concentration predictions while using the box-counting method, simulations have been performed for a non-buoyant release at the height $z_s = z_i/2$, with different widths and positions of the boxes in which the particles are counted (Fig. 1). For the simulation, 1000 particles are emitted per second, the total duration of the simulation was 1000 seconds. The stochastic Lagrangian particle model used fulfils the well-mixed condition of Thomson (1987). All details of the model are outlined in Rotach *et al.* (1996).

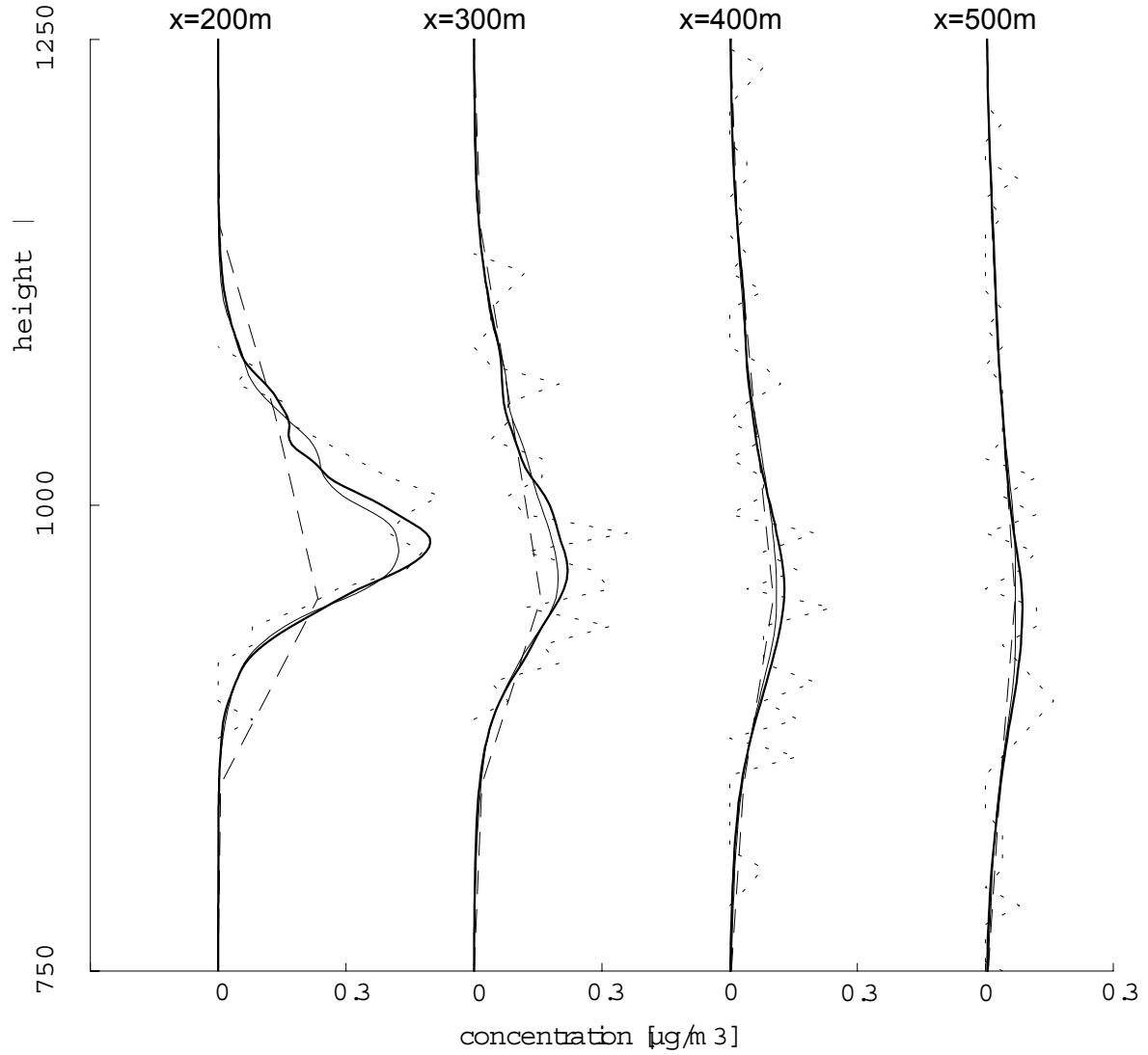

Figure 1 Vertical profiles of estimated concentration (in $\mu g \cdot m^{-3}$) for different sizes of the boxes in which the particles are counted. Profiles are taken at 200 m, 300 m, 400 m, and 500 m downwind of the source. The dashed line (– – –) shows the boxcounting prediction for vertical and horizontal box sizes of $0.05 \cdot z_i$. The dotted line (- - -) is for vertical and horizontal sizes of $0.005 \cdot z_i$. The thick line (━━) depicts the "true" concentration (see text). The thin solid line (—) shows the concentration predition using the kernel method as recommended in section 4.5.5. Release height is at $z/z_i = 0.5$; source strength $1\,g \cdot s^{-1}$; $z_i = 2000$ m, $u_* = 0.36\,m \cdot s^{-1}$, $L = -37$ m, $\overline{u}(z = 10\,m) = 2.1\,m \cdot s^{-1}$.

Concentration predictions for two sampling box sizes are shown in Fig. 1. The vertical size of $0.05 z_i$ (dashed line in Fig. 1) is often chosen by particle modellers (see above). The "true" concentration profile, based on 100 000 instead of 1000 particle trajectories, is depicted by a thick line in Fig. 1. It becomes clear that the near-source maximum concentration will be clearly underestimated for box sizes of $0.05 z_i$. The other density estimation shown in Fig. 1,

with box size $0.005z_i$ (short-dashed line), makes the concentration prediction fluctuating from one box volume to the other. However, the true value of concentration is approximated more adequately by the smaller box sampling volumes, despite the additional scatter. An additional smoothing procedure would improve the results (see, for example, Rotach *et al.* 1996). As an example, the results from a kernel density estimation following the recommendations of section 4.5.5 of this paper are also depicted in Fig. 1 (thin line).

4.2.3 Ground level concentration estimations

In Fig. 2 an example for the effects of box-counting on predicting ground-level concentrations is given. In this numerical experiment, the release took place at a height of 5 m, i.e. within the

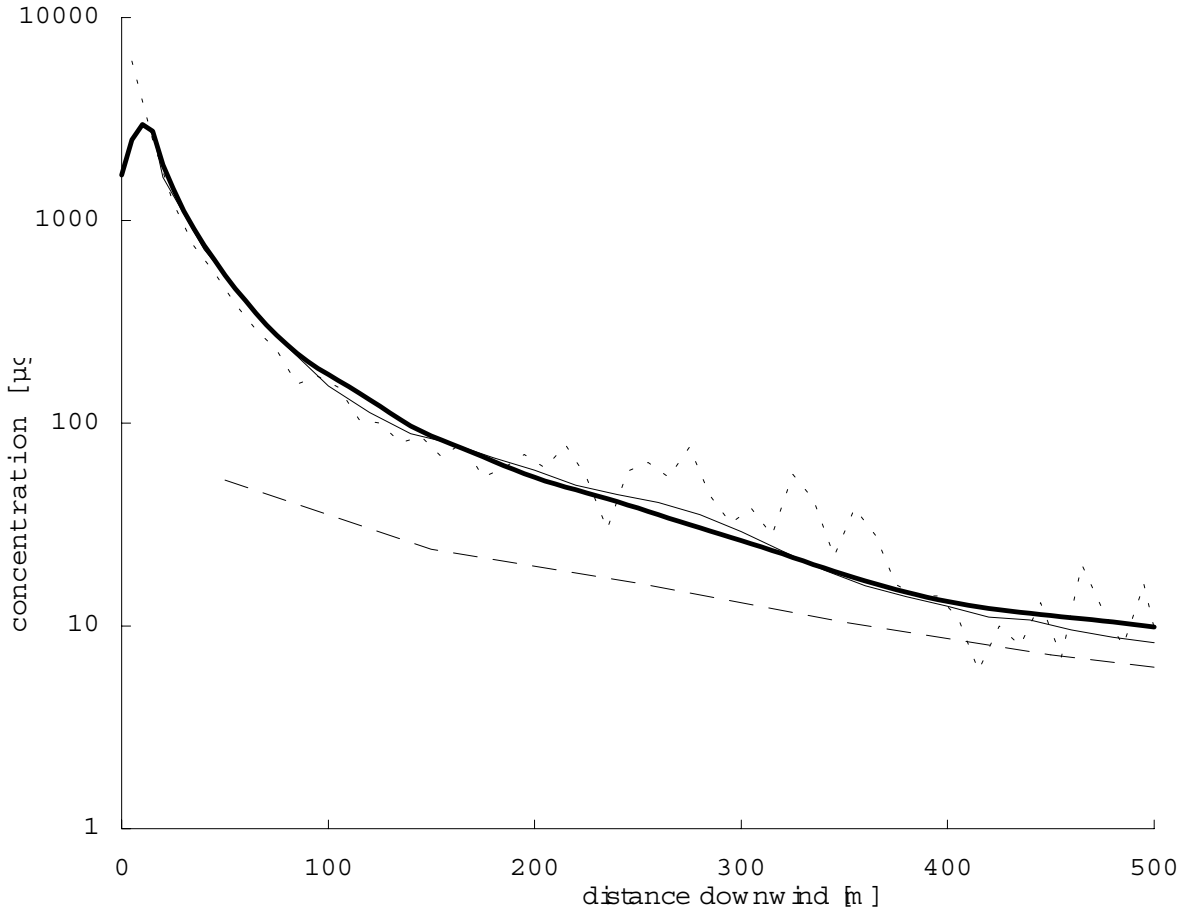

Figure 2 Same as Fig. 1, but for down-wind ground-level profiles of estimated concentration. Source is located at $z = 5$ m .

lowest sampling box. As for Fig. 1, results for vertical box sizes of $0.05z_i$ (dashed line) and $0.005z_i$ (dotted line) are depicted. Also shown are the ”true” concentration based on 100 000

particles (thick line) and the results from a triweight density kernel constructed after section 4.5.5 (thin line).

For the (widely used) $0.05z_i$ vertical box size, the ground-level concentrations, in this example, are oversmoothed, i.e. underestimated, by a factor of approximately 2 in the near-source field. The box size in the horizontal directions has been chosen equal to the vertical box size, leading to a first box center at a downwind-distance of approx. 5m ($0.005z_i$ box size) and 50m ($0.05z_i$ box size), respectively. For the smaller box with $0.005z_i$ vertical size, the estimates show a large random scatter (large variance) but no bias. The kernel estimation, on the other hand, provides a smooth estimate with almost no bias.

4.3 DENSITY KERNELS

4.3.1 Concentration estimation with density kernels

The kernel density estimator for the normalised concentration *c* of *n* given particles of equal mass at positions $\mathbf{x}_i$ is

$$c(\mathbf{x}) = \frac{1}{nh}\sum_{i=1}^{n} K\left(\frac{\mathbf{x}-\mathbf{x}_i}{h}\right), \tag{1}$$

where *h* is the width of the kernels (see section 4.4), and *K* is the kernel function, fulfilling $K(\mathbf{x}) \geq 0 \quad \forall \mathbf{x}$, and normalised so that

$$\int K(\mathbf{x})d\mathbf{x} = 1, \tag{2}$$

(thus making *c* a density distribution, i.e., $\int c(\mathbf{x})d\mathbf{x} = 1$). One of the most widely used kernels is the Gaussian kernel K_G,

$$K_G(\mathbf{r}) = \frac{1}{(2\pi)^{d/2}}\exp\left(-\frac{1}{2}\mathbf{r}^T\mathbf{r}\right), \tag{3}$$

where *d* denotes the dimension (for example, $d = 2$ for two-dimensional particle models).

The proper choice of the bandwidth *h* is of greater importance than the choice of the shape of the kernel (additional kernel shapes are introduced in section 4.3.2), since *h* plays the role of a smoothing parameter. There are several proposals for determining the value of *h* from the data. These methods aim at ”balancing” two counteracting measures, the bias (caused by the smoothing, which increases for large *h*) and the variance (increasing for small *h*).

In the following, the underlying distribution of particle positions $\mathbf{x}_i$ will be denoted as $f(\mathbf{x})$. Then, the measure on the over-all accuracy of the concentration estimate $c(\mathbf{x})$ adopted here, which is an estimator of f, is the mean integrated square error,

$$MISE(c) = \left[\int \{c(\mathbf{x}) - f(\mathbf{x})\}^2 d\mathbf{x}\right] \tag{4}$$

where the $[\ ]$-brackets denote the average over all possible data obeying $f(\mathbf{x})$. The right hand side of Eq. (4) can be formulated as

$$MISE(c) = \int \{[c(\mathbf{x})] - f(\mathbf{x})\}^2 d\mathbf{x} + \int \mathrm{var}\{c(\mathbf{x})\} d\mathbf{x} \tag{5}$$

i.e., as the sum of the integrated square bias and the integrated variance. Expressing $c(\mathbf{x})$ by Eq. (1) and taking the first term of the Taylor series expansion of $f(\mathbf{x})$, the integrated square bias can be approximated by (see Silvermann, 1986, for details)

$$\int \{[c(\mathbf{x})] - f(\mathbf{x})\}^2 d\mathbf{x} \approx \frac{1}{4} h^4 \alpha^2 \int \{\nabla^2 f(\mathbf{x})\}^2 d\mathbf{x} \tag{6}$$

and the integrated variance

$$\int \mathrm{var}\{c(\mathbf{x})\} d\mathbf{x} \approx \frac{\beta}{nh^d} \tag{7}$$

where $\beta = \int K^2(\mathbf{x}) d\mathbf{x}$ and $\alpha = \int x_1^2 K(\mathbf{x}) d\mathbf{x}$ $\left(\mathbf{x} = [x_1, x_2, x_3]^T\right)$. An "optimal" bandwidth h_{opt} for use in Eq. (1) can then be found by using the approximations (6) and (7) in Eq. (5), which becomes minimal for

$$h_{opt} = A(K) \cdot \sigma \cdot n^{-\frac{1}{d+4}} \tag{8}$$

for a particle distribution $f(\mathbf{x})$ with standard deviation σ (see section 4.4 for details). Thus the optimal bandwidth, h_{opt}, itself depends on the distribution of the data which are to be smoothed, *f*. The function $A(K)$ is defined as

$$A(K) = \left[d \frac{\beta}{\alpha^2} \left\{ \int \left(\nabla^2 f\right)^2 \right\}^{-1} \right]^{\frac{1}{d+4}} \tag{9}$$

In this paper, we assume that *f* be normal. Then,

$$\left\{ \int \left(\nabla^2 f\right)^2 \right\} = \frac{d(2+d)}{4\left(2\sqrt{\pi}\right)^d} \tag{10}$$

For Gaussian kernels K_G (Eq. 3),

$$\frac{\beta}{\alpha^2} = \left(\frac{1}{2\sqrt{\pi}}\right)^d . \tag{11}$$

So for Gaussian kernels, substituting Eqs. (10) and (11) into (9) leads to $A(K_G) = (4/[d+2])^{+1/(d+4)}$. The values of α and β for all other kernels discussed in the following sections are derived in Appendix A.

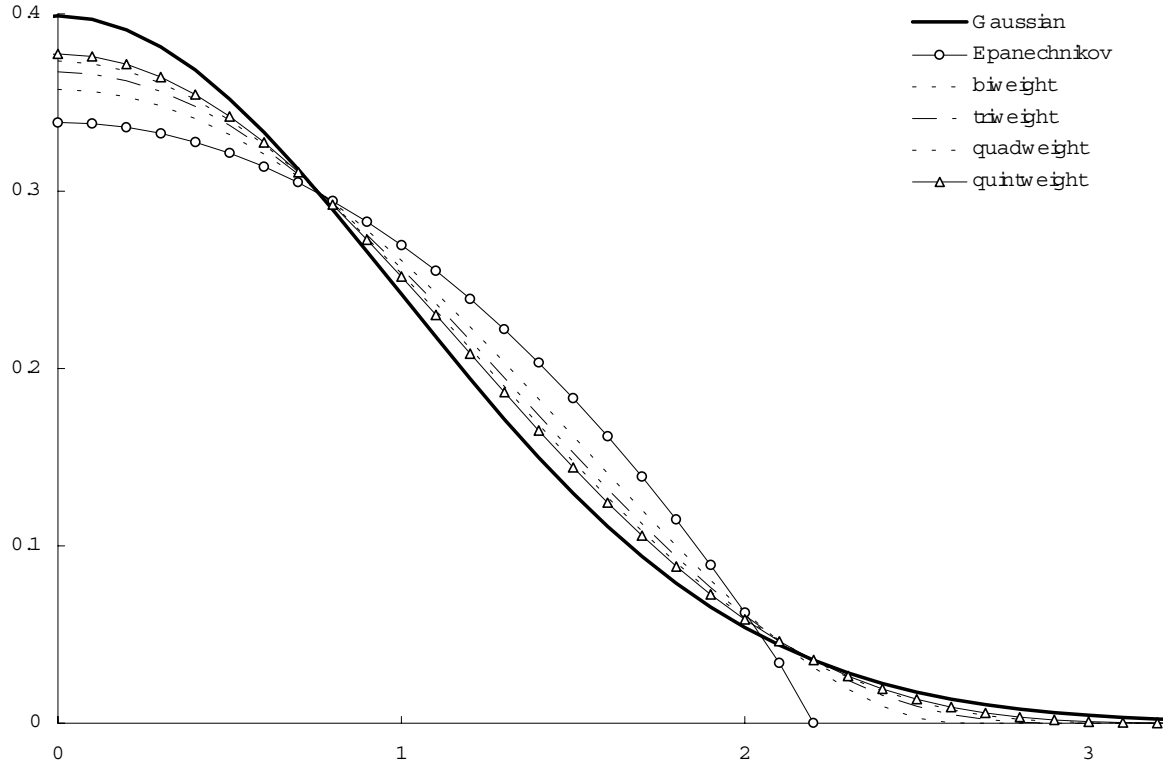

Figure 3 Comparison of one-dimensional Gaussian, Epanechnikov, bi-, tri-, quad- and quintweight kernels. The bandwidth of the Gaussian kernel is unity, and taken from Table II for the other kernels (see section 4.4.2). (Only the part for positive x is depicted; all kernels are symmetric around zero.)

4.3.2 Suitable kernels for particle models

In this paper, one family of kernels other than Gaussian is investigated, that of the form

$$K_a(\mathbf{x}) = \begin{cases} C_{d,a}\left(1 - \mathbf{x}^T\mathbf{x}\right)^a & \left(\mathbf{x}^T\mathbf{x} < 1\right) \\ 0 & \text{otherwise} \end{cases} \tag{12}$$

In Eq. (12), $C_{d,a}$ are normalising factors ensuring that $\int K_a d\mathbf{x} = 1$, which are derived in Appendix A (see Table I). For $a = 1$ up to $a = 5$, these kernels are called Epanechnikov and bi-, tri-, quad- and quintweight kernels, respectively. Figure 3 depicts their one-dimensional

form, with different bandwidths h for every kernels. The relations between values of h for different kernels having approximately the same smoothing effect are given in section 4.4.2.

$C_{d,a}$	$a=1$	$a=2$	$a=3$	$a=4$	$a=5$
$d=1$	$\frac{3}{2c_1}$	$\frac{15}{8c_1}$	$\frac{105}{48c_1}$	$\frac{945}{384c_1}$	$\frac{693}{256c_1}$
$d=2$	$\frac{2}{c_2}$	$\frac{3}{c_2}$	$\frac{4}{c_2}$	$\frac{5}{c_2}$	$\frac{6}{c_2}$
$d=3$	$\frac{5}{2c_3}$	$\frac{35}{8c_3}$	$\frac{315}{48c_3}$	$\frac{1155}{128c_3}$	$\frac{3003}{256c_3}$

Table I Normalisation constant $C_{d,a}$ (Eq. alt 9) for Epanechnikov $(a=1)$, biweight $(a=2)$, triweight $(a=3)$, quadweight $(a=4)$ and quintweight $(a=5)$ kernels for up to three dimensions ($c_1=2$, $c_2=\pi$, $c_3=4\pi/3$).

Note that the support (the *d*-dimensional interval over which the kernel function is non-zero) is infinite for the Gaussian kernel (Eq. 3) and limited for the other five types (Eq. 12). The Epanechnikov kernel ($a=1$) is optimal in minimising the MISE (Epanechnikov 1969), but its derivative is discontinuous. As can be seen from Fig. 3, the differences between the Gaussian kernel and kernels of the $\left(1-\mathbf{x}^T\mathbf{x}\right)^a$-type decrease for increasing *a*, the only significant differences occurring at the tails of the distribution. Because of the small differences between the kernel shapes, other criteria such as the ease of computation are important as well as the question, which of the kernel functions resembles most the distribution of observed turbulent wind fluctuations. The latter are generally assumed to be normally distributed (with the exception of the vertical component for convective conditions), making the Gaussian kernel the most natural choice. However, the assumption of a normal distribution of wind fluctuations attributes a non-zero possibility (though very small) to unphysically large values. This would support the choice of a kernel with a limited support interval such as, say, the triweight kernel.

Another approach is the kernel method adopted by Lorimer (1986). He uses the product of a three-dimensional Gaussian with a three-dimensional Epanechnikov kernel. Because this kernel is still defined over an infinite domain, we only compare kernels after Eq. (12) with the Gaussian kernel.

It should be kept in mind that the concentration estimation using density kernels within particle models is a numerical task, and thus any form of kernel function can be used in principle. But the analogies which show up between these numerically motivated kernel density estimators and the concept of clusters of particles as adopted in puff models is remarkable, and is further discussed in section 4.6. Recommended kernel functions which perform well numerically and have a form which can be compared to physical observations are given in section 4.5.5.

4.3.3 Three-dimensional vs. product kernels

The approach formulated in section 4.3.1 is *d*-dimensional, and thus yields a single bandwidth for *d*-dimensional kernels. Since atmospheric dispersion in the logitudinal, cross-wind and vertical directions is, from the point of view of density estimation, very similar, this approach is justified.

In other scientific areas, however, often three-dimensional density kernels are being used which are the product of one-dimensional kernels. In such so-called product kernels, instead of Eq. (1),

$$c(\mathbf{x}) = \frac{1}{n h_x h_y h_z} \sum_{i=1}^{n} \left\{ \prod_{j=1}^{3} K\left(\frac{x_i - x_{ij}}{h_j} \right) \right\} \tag{13}$$

where the bandwidths h_i of the kernel distributions in the three directions are calculated in analogy to the one-dimensional case. Product kernels have the advantage of easier mathematics, and are easier to handle in the case of data points with large differences in the standard deviations in the three directions (dimensions).

For Gaussian kernels, Eqs. 1 and 13 are identical. This relationsship does not hold any longer for Eq.-(12)-type kernels. Fig. 4 depicts the differences in density distribution between a three-dimensional triweight (using Eq. 1) and the corresponding product kernel (Eq. 13). The product kernel formulation leads to higher densities in the edges and in the center of the carrier domain, while having smaller densities in the other regions. In the field of atmospheric dispersion, diffusion is approximately equal in all directions and no “edges” with higher probabilities do exist. This means that product kernels are less suited for atmospheric dispersion data than fully three-dimensional kernels. Therefore, only the latter are investigated in this paper. But for applications where the standard deviations of the data points

substantially differ according to direction, product kernels may avoid the necessity of scale transformations.

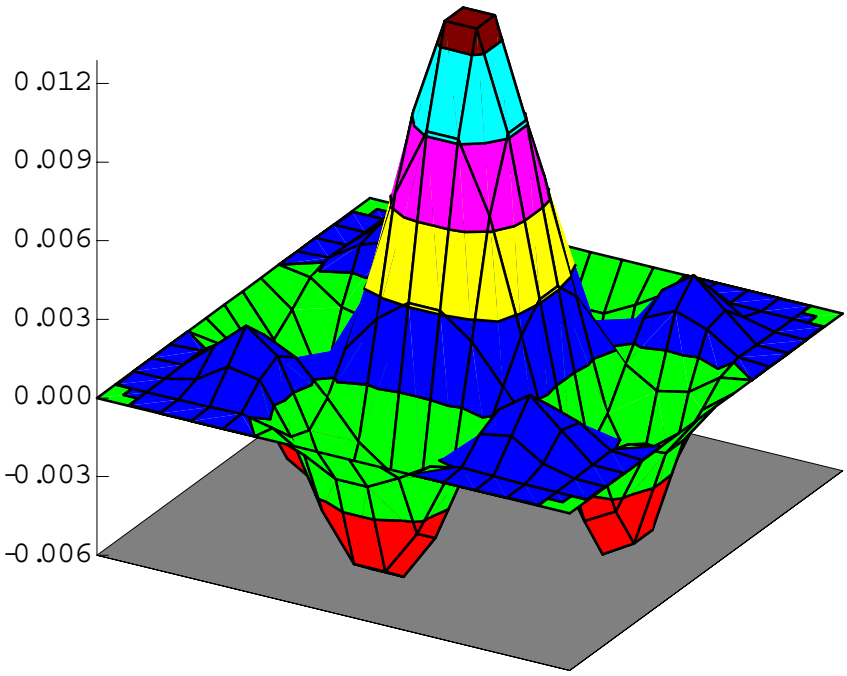

Figure 4 Density differences for a two-dimensional triweight vs. the corresponding product kernel.

4.4 BANDWIDTH ESTIMATION

4.4.1 Theory

The optimal bandwidth as given by Eq. (8) is only optimal under the assumption that the distribution of the data be normal. Therefore, more robust rules-of-thumb have been constructed. A recommended one is

$$h_{rob.} = \alpha \cdot A(K) \cdot n^{-\frac{1}{d+4}} \min\left(\sigma, \frac{R}{1.34}\right), \tag{14}$$

where R is the interquartile range, i.e. $R = R_{3/4} - R_{1/4}$, and α is taken as 0.85 in the present study. The upper quartile $R_{3/4}$ and lower quartile $R_{1/4}$ are defined as those values out of the data to be smoothed where 25% of the data has a larger or smaller value, respectively.

Lorimer (1986) used a slightly different approach to determine the kernel bandwidth. The bandwidth for the initial particle distribution was calibrated by visual comparision of the resulting density distribution. This provides an approximate value for the term $A(K)n^{-1/(d+4)}$ in Eq. (14), which remains constant. Then, Lorimer (1986) calculates the new standard deviation of the particle ensemble for every new time step, and thus calculates the bandwidth using Eq. (14).

At this point, the idea of having an estimate $\hat{\sigma}$ for the value of σ might come up. This would circumvent to some extent the fact that the optimal bandwidth depends on the density distribution of the particles to be smoothed, and would save computing time, as the standard deviation of the given particle distribution has not to be calculated. However, deriving expressions for $\hat{\sigma}$ means to theoretically solve the problem of atmospheric dispersion, and then no numerical dispersion model would be required as soon as correct, i.e. bias-free $\hat{\sigma}$ expressions (as a function of travel time or of downwind distance) are available.

4.4.2 Equivalent bandwidths for different kernels

It is possible to switch between kernels without reconsidering the optimal bandwidth. As soon as an optimal bandwidth has been chosen for one type of kernel, bandwidths for other kernels which show the same smoothing characteristics (called ”equivalent bandwidths”can be derived using Eq. (8)). The kernel dependence of the bandwidth is expressed by the function $A(K)$, and only the β/α^2 -part (Eq. 11) depends on the kernel itself. The ratio between two equivalent bandwidths for two kernels K_1 and K_2 of the same dimensionality is

$$\frac{h_1}{h_2} = \left[\frac{\beta_1/\alpha_1^2}{\beta_2/\alpha_2^2} \right]^{1/(d+4)} \tag{15}$$

For $d = 1$ and $d = 3$, Table II lists the corresponding conversion factors between equivalent kernel bandwidths.

	From/To	Gaussian	Uniform	Epanech.	Biw.	Triw.	Quadw.	Quintw.
one-	Gaussian	1	1.740	2.214	2.623	2.978	3.296	3.586
dimen-	Uniform	0.575	1	1.272	1.507	1.711	1.894	2.061
sional	Epanech.	0.452	0.786	1	1.185	1.345	1.489	1.620
	Biw.	0.381	0.663	0.844	1	1.136	1.257	1.367
	Triw.	0.336	0.584	0.743	0.881	1	1.107	1.204
	Quadw.	0.303	0.528	0.672	0.796	0.904	1	1.088
	Quintw.	0.279	0.485	0.617	0.731	0.830	0.919	1
three-	Gaussian	1	2.220	2.572	2.924	3.244	3.537	3.808
dimen-	Uniform	0.450	1	1.158	1.317	1.461	1.593	1.715
sional	Epanech.	0.389	0.863	1	1.137	1.261	1.375	1.481
	Biw.	0.342	0.759	0.880	1	1.109	1.210	1.302
	Triw.	0.308	0.684	0.793	0.901	1	1.090	1.174
	Quadw.	0.283	0.628	0.727	0.827	0.917	1	1.077
	Quintw.	0.263	0.583	0.675	0.768	0.852	0.929	1

Table II Bandwidth conversion factors for different kernel shapes. To obtain equivalent smoothing with the kernel shape K2 as with kernel K1, multiply the K1 bandwidths with the factor from row K1, column K2. Also shown are results for a uniform kernel.

4.4.3 Kernels with variable bandwidth

The use of individual bandwidths for every kernel rather than using the same h_{opt} for all kernels allows for adequate smoothing where particle density is high, whilst minimising the variance of the estimation in regions of low simulated particle densities. This is of special use for near-source as well as ground level concentration estimations, e.g. the most natural field of use of density kernels in atmospheric dispersion modelling.

For every kernel an individual bandwidth $h \cdot \lambda_i$ is used. To obtain the λ_i, a first-guess estimator $\hat{c}(\mathbf{x})$ is used (for example using h_{opt} from Eq. 8). The λ_i are then chosen proportional to $\hat{c}(\mathbf{x}_i)^{-\alpha}$, where $\mathbf{x}_i$ denotes the position of the *i*-th particle. Silvermann (1986) recommends a value $\alpha = 0.5$. However, such variable bandwidths are not investigated in this paper.

4.5 KERNEL SENSITIVITY

4.5.1 Kernel shape comparison

The effect of different shapes of density kernels is investigated and compared to the ”true” concentration prediction within a Lagrangian particle model. This ”true” concentration is obtained by using a very large number (500 000) of particle trajectories for the full three-

dimensional model simulation. For 500 000 particles, the effect of kernel shape vanishes (no difference larger than 1.1%), and the arithmetric mean of the bi-, tri- and quadweight kernel results has been used as the ”true” estimate. These ”true” concentration predictions are then compared to estimations by different kernel methods, for different numbers of particles released (500, 5000 and 50 000).

The meteorological conditions and the set-up of the Copenhagen tracer experiment are used for comparison. This experiment took place under atmospheric conditions of forced convection. Measurements of wind speed, friction velocity, wind fluctuation standard deviations, Obukhov length and mixing layer depth are available (see Gryning and Lyck, 1984, for more details on the experiment). The tracer was released from a 115 m high stack, and sampled at arcs of ground-level receptors typically 2 to 6 km down-wind from the source. The averaging time is one hour. For the present kernel shape comparison, the simulated concentrations have been evaluated for those locations where the receptors have been placed during the Copenhagen experiment. This was done to obtain a typical application for a Lagrangian particle dispersion model.

For the numerical simulation, the Lagrangian particle model of Rotach *et al.* (1996) is used, which has a probability density function (pdf) suitable for neutral to convective conditions. It has been extended to three dimensions (de Haan and Rotach 1998b) and fulfils the well-mixed condition of Thomson (1987). However, in the validation discussed in this section, the focus is not on finding the kernel shape obtaining the highest correspondence with the measured concentration values. Instead, the kernel concentration estimates are compared to the ”true” concentrations yielded for the simulation of 500 000 particles (see above). This way, we will be able to know which kernel shape has the lowest bias for a given number of released particles, and is best suited for telling the particle modeller what the model actually predicted. The near-source field is investigated in section 4.5.3, and the intermediate field (roughly between 1 and 6 km down-wind from the source) in section 4.5.4.

4.5.2 Experimental set-up

The simulations are performed by essentially rebuilding the experimental set-up. At the mixing height z_i as well as at the ground, perfect reflection without any entrainment or deposition of pollutants is assumed. To ensure that the inverse of the time steps for the simulation lies in the inertial subrange for the particle part of the model, the criteria after

Rotach *et al.* (1996) are applied. The mean wind profile was determined based on an approach by Sorbjan (see Rotach *et al.* 1996 for details).

To ensure mass conservation, for the kernel concentration distributions belonging to each particle, image sources are assumed below the ground and above the inversion height. For Gaussian shaped kernels K_G (Eq. 3), six image sources were placed, i.e., at $z = -h_s$, $2z_i - h_s$, $-2z_i - h_s$, $4z_i + h_s$ etc., where h_s is the actual height of the particle. This is necessary to ensure that no mass gets lost (maximum loss is 0.10%). For the non-Gaussian kernel shapes with a limited carrier interval, only 4 image sources (2 below the ground, 2 above z_i) are needed at maximum (maximum loss is 0.06%).

For the present comparison, all data from the Copenhagen experiment (9 runs) have been simulated.

4.5.3 Near-source predictions

In Fig. 5 results are shown for one of the experimental runs. The ”true” estimate based on 500 000 particles acts as ”reference”. The effect of the number of particles upon the ground-level concentrations is larger than the choice of kernel shape. This result had to be expected, since a kernel, and its shape, is only a numerical method of translating particles positions into concentrations, whereas a tenfold increase in the number of simulated particles is likely to significantly increase model performance.

The kernel method will always produce ”smooth” concentration profiles, even for very low numbers of particles, because the kernel bandwidths adapt to the number of particles. For a similar effect using the box-counting method, it would be necessary to automatically determine the sampling box size from the number of particles. But the amount of unwillingly introduced additional smoothing (bias), i.e., artificial dispersion, will be higher for lower particle numbers. This will lead to an earlier and steeper increase of ground-level concentration near the source, and a faster decline of ground-level concentration after reaching the concentration maximum (Fig. 5).

The interesting question is which kernel shape approaches the ”true” estimate faster, that is, performs best for a given number of particles. To assess the near-source prediction performance, four ratios are calculated: The ratio of predicted to ”true” maximum ground-level concentration, $R_1 = \chi^{\max}_{pred.} \big/ \chi^{\max}_{'true'} - 1$: the corresponding ratio of down-wind distances,

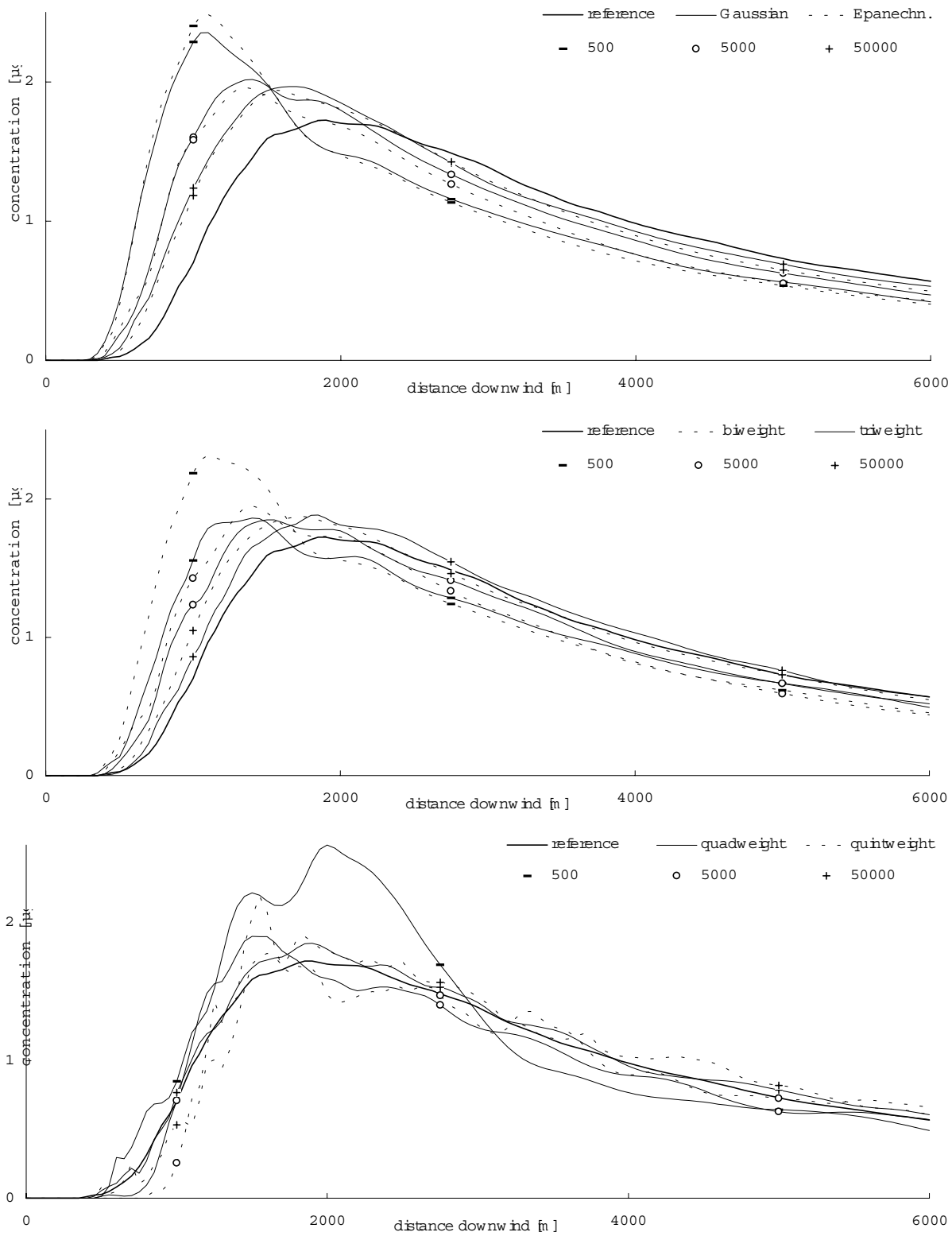

Fig. 5 Intercomparison of estimated ground-level concentration for different kernel types and numbers of particles. (a) Gaussian and Epanechnikov kernels; (b) bi- and triweight kernels; (c) quad- and quintweight kernels. Thick solid line (━): estimate for 500 000 particle trajectories using triweight kernels. Simulations with 500 particles are marked with minus signs (–), 5000 particles with circles (o), 50 000 particles with plus signs (+). Copenhagen exp. from Jun. 27, 1979 ($z_i = 1850$ m, $u_* = 0.64\ \mathrm{m \cdot s^{-1}}$, $L = -104$ m, $\overline{u}(z = 10\ \mathrm{m}) = 4.1\ \mathrm{m \cdot s^{-1}}$).

$R_2 = x_{pred.}^{\max} \big/ x_{'true'}^{\max} - 1$ (where the distances are defined by $\chi\left(x_{pred.}^{\max}\right) = \chi_{pred.}^{\max}$ and $\chi\left(x_{'true'}^{\max}\right) = \chi_{'true'}^{\max}$); the ratio of the down-wind plume-centerline integrated "over-/underpredicted" concentration to the total down-wind integrated "true" concentration, i.e.,

$$R_3 = \int_0^\infty \left|\chi_{pred.}(x) - \chi_{'true'}(x)\right| dx \Big/ \int_0^\infty \chi_{'true'}(x)\,dx \tag{16}$$

and a ratio which measures the "smoothness" of the prediction,

$$R_4 = \int_0^\infty \left|\frac{\partial}{\partial x}\chi_{pred.}(x)\right| \Big/ \int_0^\infty \left|\frac{\partial}{\partial x}\chi_{'true'}(x)\right| - 1 \tag{17}$$

Unity is subtracted from R_1, R_2 and R_4 so that all ratios are zero for a perfect prediction.

The cross-wind integrated plume-centerline groundlevel concentrations for experiment 7 of the Copenhagen data set were compared. The resulting ratios are listed in Table III. Two groups can be distinguished: the Gaussian, Epanechnikov and quintweight kernel on the one hand, and the bi-, tri- and quadweight kernels on the other hand. However, the first group is heterogeneous, since the performance of the Gaussian and Epanechnikov kernels is worsened because of "oversmoothing" (the maximum concentration is overpredicted, and too close to the source, which leads to higher values of R_1 and R_2, respectively). The performance of the quintweight kernel is most influenced by its "undersmoothing", i.e., the oscillating prediction (scatter) (see Fig. 5c).

Out of Table III, two tendencies can be distinguished. First, for an increasing number of particles, the quadweight kernel takes over the role of best predicting kernel from the triweight kernel. Second, the influence of the shape of the kernel vanishes for higher numbers of simulated particles, and is in fact negligible for the simulation of 50 000 particles. As a result, the triweight kernel can be recommended as the best kernel shape for near-source predictions; for high numbers of particles, the quadweight kernel performs slightly better.

4.5.4 Intermediate-field predictions

The intermediate-field prediction performance of the different kernel shapes is compared by calulating widely used statistical measures. From the predicted concentrations at the individual receptor locations, the arcwise maximum concentration and the cross-wind integrated concentration (on the arc) are determined. As statistical measures to describe the model performance, the fractional bias, $FB = \left(\overline{C}_{\text{"true"}} - \overline{C}_{\text{pred.}}\right) \Big/ \left(0.5\left(\overline{C}_{\text{"true"}} + \overline{C}_{\text{pred.}}\right)\right)$, and the

		Gaussian	Epanechn.	Biweight	Triweight	Quadw.	Quintw.
500 part.	R_1	0.3138	0.3875	0.2939	**0.0407**	0.4342	0.1836
	R_2	–0.4268	–0.4157	–0.3846	–0.2564	**0.0623**	0.1201
	R_3	0.2987	0.3441	0.2439	**0.0941**	0.1196	0.1379
	R_4	0.4182	0.5085	0.3792	**0.0762**	0.5844	1.1997
	sum	1.4575	1.6558	1.3017	**0.4674**	1.2006	1.6413
5000 part.	R_1	0.1270	0.0951	0.0889	**0.0331**	0.0641	0.2274
	R_2	–0.2654	–0.2829	–0.2564	–0.2102	**–0.2033**	–0.2267
	R_3	0.1076	0.1180	0.0801	0.0447	**0.0289**	0.0344
	R_4	0.1798	0.1525	0.1409	**0.0533**	0.0963	0.4377
	sum	0.6798	0.6486	0.5663	**0.3413**	0.3926	0.8762
50000 part.	R_1	0.0984	0.0438	0.0461	0.0528	**0.0350**	0.0634
	R_2	–0.1236	–0.2033	–0.0705	–0.0173	**0.0092**	–0.0273
	R_3	0.0488	0.0488	0.0241	0.0126	**0.0091**	0.0170
	R_4	0.1261	0.0703	0.0581	0.0581	**0.0300**	0.2055
	sum	0.3968	0.3661	0.1988	0.1408	**0.0833**	0.3132

Table III Ratios for the near-source performance of different concentration estimation kernel methods (using Gaussian, Epanechnikov, bi-, tri-, quad- and quintweight kernels) for the release of 50 000, 5000 or 500 particles, respectively. The reference estimation was obtained by releasing 500 000 particles. For definitions of $R_1 - R_4$ see text. The lowest absolute value in each row is shown in bold typeface. The sum denotes the sum of the absolute values of the ratios.

normalised mean square error, $NMSE = \overline{\left(C_{\text{"true"}} - C_{\text{pred.}}\right)^2} \Big/ \left(\overline{C}_{\text{"true"}} \overline{C}_{\text{pred.}}\right)$, are determined, where $C_{\text{"true"}}$ is the "true" (reference) concentration and $C_{\text{pred.}}$ the simulated one.

The behaviour found for the single run 7 as depicted in Fig. 5 can be found for all 9 runs. In Table IV, the NMSE and FB statistical measures for the performance on the whole data set are listed. Note that the statistical measures are given relative to the "true" estimate, not to field measurements.

Several conclusions can be drawn from the results in Table IV. First, even for 500 particles, the NMSE and FB values resulting are not that large. Other assumptions underlying the dispersion model could cause effects of a comparable magnitude. This means that for intermediate to far-field concentration predictions with particle models, a few thousand particles will do the job even in three-dimensional models (with kernel density estimation). Second, for all three different numbers of simulated particles, the quadweight kernel performs best, and the triweight kernel second best. These two kernel shapes also performed well in the near-source assesment. Third, for 50 000 simulated particles, the differences in performance

between different kernel shapes are minor, and certainly not significant anymore: regarding the low values of NMSE and FB, it is hard to determine which kernel actually performs best.

		ArcMax		CIC	
		NMSE	FB	NMSE	FB
500 000	reference	0.000	0.000	0.000	0.000
50 000	Gaussian	0.009	0.014	0.014	–0.008
	Epanechnikov	0.008	0.045	0.004	0.011
	biweight	0.005	0.029	0.002	0.008
	triweight	0.004	–0.021	0.002	–0.026
	quadweight	0.003	–0.039	0.001	–0.021
	quintweight	0.019	–0.083	0.006	–0.057
5000	Gaussian	0.020	0.068	0.007	0.001
	Epanechnikov	0.034	0.101	0.011	0.042
	biweight	0.022	0.069	0.007	0.029
	triweight	0.013	0.020	0.003	0.007
	quadweight	0.010	–0.003	0.003	0.007
	quintweight	0.060	–0.129	0.003	–0.034
500	Gaussian	0.136	0.253	0.033	0.107
	Epanechnikov	0.151	0.261	0.036	0.104
	biweight	0.101	0.206	0.026	0.084
	triweight	0.037	0.116	0.016	0.060
	quadweight	0.033	0.007	0.010	0.007
	quintweight	0.184	–0.249	0.019	–0.023

Table IV Statistical measures for the performance of different concentration estimation kernel methods (using Gaussian, Epanechnikov and bi-, tri-, quad- and quintweight kernels) for the release of 50 000, 5000 or 500 particles, respectively. The reference estimation is the arithmetic mean of the results obtained for 500 000 particles for bi-, tri- and quadweight kernels.

The results listed in Table IV show that the NMSE and FB values are reduced by a factor between 2 and 4 by simulating the tenfold number of particles. For 5000 particles, the NMSE and FB caused by the kernel procedure are already neglibible. This statement holds for concentration predictions at down-wind distances like those where the receptor arcs in the Copenhagen experiment were located (2 to 6 km down-wind from the source). For near-source predictions, before the maximum ground-level concentration occurs, this number probably is inaccurate, as can be seen in Fig. 5, but a number of 50 000 simulated particles should give a high accuracy. When conducting particle simulations for down-wind distances so near to the source that even a number of 50 000 particles (using the kernel estimate

method) could be considered insufficient, parametrizations within the particle model (e.g., for turbulence, the timestep and the pdf) are likely to have an even larger impact.

4.5.5 Recommended scheme

The triweight kernel approaches the near-source ”true” estimate faster than the other kernel shapes investigated (see previous sections). For intermediate to far-field estimations, the quadweight kernel is best. For the Copenhagen experiment, the simulation of 5000 particle trajectories has been shown to be more than sufficient when using a fully three-dimensional stochastic particle model. The same number has also been used by the author to simulate other tracer experiments which took place under stable and fully convective conditions. In fact, when the measurements available took place further down-wind than the location at which the ground-level concentration has its maximum (as is the case for the Copenhagen experiment), 500 particles together with quadweight kernels produce very good results.

It also is recommended to use the more robust formulation of Eq. (14) instead of Eq. (8). This produces clearly better predictions especially in situations where the assumption of normal distribution of the particle positions cannot be justified, i.e., for fully convective conditions, as well as for the vertical direction after the release has become well-mixed over the entire boundary layer (not shown). In future work, the use of kernels with variable bandwidths, as briefly outlined in section 4.4.3, will be further refined. This technique will eventually allow for more robust and even more efficient concentration predictions.

4.6 ANALOGY OF DENSITY KERNELS AND PUFFS

4.6.1 Interpretation of density kernels as clusters of particles

When interpreting density kernel distributions as models for clusters of pollutant particles (puffs), one has to be aware of the fact that the kernel approach originates from the need for a numerical non-parametric regression method. To fullfil this numerical task best, the bandwidths of density kernels should be chosen according to the procedure outlined in section 4.3. With the corresponding Eqs. (8) and (14), for the simulated particles obeying the same density distribution, kernels obtain smaller bandwidths as the particle number increases.

Density kernel bandwidths formulations derived from some physical description of cluster growth must not depend on the number of particles within the cluster, but only on the size of

the latter. The growth rate of such a cluster of particles depends on its size, i.e., the range of eddies small enough to be capable of dispersing the cluster.

Numerically obtained kernel bandwidths, on the other hand, depend on the number of particles released (Eq. 8). This fundamental difference could lead to the assumption that no relation can be established between cluster growth and kernel bandwidth, although such a relation would be desirable in order to be able to ”blend” puff and particle models. One way to indeed blend puff and particle models, which uses kernels with physically motivated sizes taken from dispersion theory, is the Puff-Particle approach by de Haan and Rotach (1998b).

4.6.2 Bandwidth estimates taken from dispersion theory

It should be distinguished between absolute and relative dispersion: Relative dispersion accounts for the dispersing effect of all turbulent eddies smaller than the separation of two particles, since these eddies will be able to enlarge their mean distance. Absolute dispersion describes the spread of a release with respect to a fixed point in space, and thus accounts for the dispersing effect of eddies of all sizes.

As the growth of a cluster of particles is described by relative dispersion, parametrisations of this growth, e.g. as a function of cluster size, could also be used as bandwidths of density kernels. Relative dispersion is applied in puff dispersion models which use frequently updated wind fields to account for all dispersion originating from eddies larger than the size of an individual cluster (thus not yet covered by the relative dispersion for such a cluster).

However, the size of a relatively dispersed cluster (i.e., puff) differs fundamentally from the numerical bandwidth for a density kernel. This can easily be verified by looking at two hypothetical cases: First, doubling the number of simulated particles will reduce the numerical bandwidth according to Eq. (8); the physical size of a cluster under the given turbulent conditions is not affected. Second, kernel bandwidths will only increase when the mean distance between particles increases, whereas relatively dispersed clusters grow with every timestep.

4.6.3 Use of absolute dispersion to describe kernel bandwidths

The RAPTAD model of Yamada *et al.* (1987, 1989) and Yamada and Bunker (1988) combines a particle model with Gaussian shaped density kernels. They use the physical concept of absolute dispersion to estimate the appropriate bandwidth of these kernels. This is

a physical constraint determining the size, in contrast to the numerically motivated bandwidths as outlined in section 4.4.

For a sufficiently high number of particles, the bandwidths of the numerical kernel will be smaller than the size of relatively dispersed puffs (see preceding section). This adds dispersion to the dispersion model as a whole, i.e. it widens the predicted concentration distribution. Therefore, this additional dispersion has to be removed from the particle model, by modifying (reducing) the turbulent energy spectrum representing the stochastic particle trajectories. This approach is realised in de Haan and Rotach (1998a), where a low-pass filter depending on the size of the relatively dispersed puff filters out dispersion from the particle trajectories.

Note that the ”dispersion” added to the model by the numerical kernel bandwidths should not be filtered out of the particle model. It is the smoothing necessary to interpolate between particle positions, and tends to zero as the number of particles approaches infinity (whereas the overdispersion caused by the physical sizes remains constant).

4.7 SUMMARY AND CONCLUSIONS

A method is proposed to estimate concentrations from stochastic Lagrangian particle models. Traditionally, most particle modellers use the box-counting method, where concentration is estimated by counting particles in imaginary sampling boxes. Using such box-averaged concentrations as an estimation for point concentrations, if boxes are chosen too small, the concentration distribution becomes noisy (having a large variance); if they are too large, the concentration is oversmoothed (having a large bias). It is shown for two hypothetical source-receptor configurations that the choice of box sizes can cause large differences in the predicted concentration, especially for near-field and ground level predictions. Only large particle numbers can minimize these effects.

The kernel density estimation method is proposed as an alternative which minimizes the sum of the variance and the bias of the predicted concentration distribution. This allows for the number of particles to be reduced by an order of magnitude as compared to predictions made with the box-counting method. The most important parameter, the bandwidth of the kernels, is determined from the standard deviations of the particle position distribution.

The effectiveness of six different kernel shapes in concentration estimation is investigated. The so-called quadweight kernel, used with a robust parametrisation for the calculation of

bandwidth, has optimal performance. It yields optimal results even if only a few thousand particle trajectories are simulated. The use of dispersion theory to describe kernel bandwidths, allowing an interpretation of the kernels as physically meaningful clusters of particles, is only possible if the corresponding amount of dispersion which has been added by the bandwidths of the kernels is removed from the stochastic particle trajectories (de Haan and Rotach 1998a).

Acknowledgements—The comments of Dr. R. Yamartino on a first draft of this paper have been very helpful. Thanks go to Dr. P. Manins for drawing my attention to the work of G. Lorimer. The present work was partly financed by the Swiss Agency of Education and Sciences (BBW) and the Swiss Agency of Environment, Forest and Landscape (BUWAL) through a project in the framework of COST 615 (citair), and by the Swiss National Science Foundation through Grant Nr. 21-46849.96.

APPENDIX—DETERMINATION OF $C_{d,a}$, α AND β

The normalizing factor $C_{d,a}$ for kernels of the form $\left(1-\mathbf{x}^T\mathbf{x}\right)^a$ (introduced in Eq. 12) is calculated by integrating in d dimensions the non-normalized kernel. Alternatively, the d-dimensional rotational volume can be calculated, $C_{d,a}{}^{-1} = c_d \int_0^\infty \left[K_a{}^{-1}(y)\right]^d dy$, with the substitution $y = \left(1-x^2\right)^a = K_a(x)$ and $K_a{}^{-1}(y) = \left(1-y^{1/a}\right)^{1/2}$:

$$C_{d,a} = \left\{\int \left(1-\mathbf{x}^T\mathbf{x}\right)^a d\mathbf{x}\right\}^{-1} = \left\{c_d \int_0^1 \left(1-y^{1/a}\right)^{d/2} dy\right\}^{-1} \tag{A1}$$

where c_d is the volume of the unit d-dimensional sphere (i.e. $c_1 = 2$, $c_2 = \pi$, $c_3 = 4\pi/3$). For $a = 1$, this gives $C_{d,1}{}^{-1} = 2c_d/(d+2)$, and the general solution is

$$C_{d,a} = \left\{\pi^{d/2} \frac{\Gamma(a+1)}{\Gamma(a+1+d/2)}\right\}^{-1} = \frac{\prod_{i=1}^{a}(d+2i)}{c_d \cdot 2^a \cdot a!} \tag{A2}$$

For the kernel functions used in this paper and for up to three dimensions, the corresponding normalising factors are listed in Table I.

The determination of the value of $\beta = \int K^2(\mathbf{x}) d\mathbf{x}$ (introduced in Eq. 9) is straightforward using the above method and result, yielding

$$\beta = C_{d,a}^2 \int \left(1 - \mathbf{x}^T \mathbf{x}\right)^{2a} d\mathbf{x} = C_{d,a}^2 \left\{ \pi^{d/2} \frac{\Gamma(2a+1)}{\Gamma\left(2a+1+d/2\right)} \right\} = C_{d,a}^2 \frac{c_d 2^{2a} (2a)!}{\prod_{i=1}^{2a} (d+2i)} \tag{A3}$$

To obtain $\alpha = \int x_1^2 K(\mathbf{x}) d\mathbf{x}$ $\left(\mathbf{x} = \left[x_1, x_2, x_3\right]^T\right)$, we calculate

$$\begin{aligned} \alpha &= C_{d,a} \int_{-1}^{1} \left(\int_{-\sqrt{1-x_1^2}}^{\sqrt{1-x_1^2}} \left(\int_{-\sqrt{1-x_1^2-x_2^2}}^{\sqrt{1-x_1^2-x_2^2}} x_1^2 \left(1 - \mathbf{x}^T \mathbf{x}\right)^a dx_3 \right) dx_2 \right) dx_1 \\ &= \frac{\Gamma(a+1)\pi^{(d-1)/2}}{\Gamma\left(a+(d+1)/2\right)} \int_{-1}^{1} t^2 \left(1 - t^2\right)^{(2a+d-1)/2} dt \end{aligned} \tag{A4}$$

With the solution

$$\alpha = C_{d,a} \frac{2^a a! c_d}{\prod_{i=1}^{a+1} (d+2i)} \tag{A5}$$

which has been proved for $d \le 3$ and $a \le 5$. Combining Eqs. (A4) and (A5) with Eq. (10), $A(K)$ from Eq. (9) can then be calculated.

REFERENCES

Batchelor, G. K. (1952): Diffusion in a Field of Homogeneous Turbulence—Part II: The Relative Motion of Particles. *Proc. Camb. Philos. Soc.*, **48**, 345–362

Borgas, M. S. and Sawford, B. L. (1994): A Family of Stochastic Models for Two-Particle Dispersion in Isotropic Homogeneous Stationary Turbulence. *J. Fluid. Mech.*, **279**, 69–99

Du, S., and Wilson, J. D. (1994): Probability Density Functions for Velocity in the Convective Boundary Layer, and Implied Trajectory Models. *Atmospheric Env.*, **28**, 1211–1217

Epanechnikov, V. K. (1969): Non-parametric Estimation of a Multivariate Probability Density. *Theory Probab. Appl.*, **14**, 153–158

Flesch, T. K, Wilson, J. D. and Yee, E. (1995): Backward-Time Lagrangian Stochastic Dispersion Models and Their Application to Estimate Gaseous Emissions. *J. Appl. Meteorology*, **34**, 1320–1332

Gryning, S.-E. and Lyck, E. (1984): Atmospheric Dispersion from elevated sources in an urban area: Comparison between tracer experiments and model calculations. *J. Clim. Appl. Met.*, **23**, 651–660

de Haan, P., and Rotach, M. W. (1998a): The Treatment of Relative Dispersion within a combined Puff-Particle Model (PPM). In: Air Pollution Modeling and Its Application XII, S.-E. Gryning and N. Chaumerliac (eds.), Plenum Press, New York, 389–396

de Haan, P., and Rotach, M. W. (1998b): A novel approach to atmospheric dispersion modelling: The puff-particle model (PPM). *Quart. J. Roy. Meteorol. Soc.*, **124**, 2771–2792

Hurley, P. and Physick, W. (1991): A Lagrangian Particle Model of Fumigation by Breakdown of the Nocturnal Inversion. *Atmospheric Env.,* **25A**, 1313–1325

Hurley, P. and Physick, W. (1993): A skewed homogeneous Lagrangian particle model for convective conditions. *Atmospheric Env.,* **27A**, 619–624

Lorimer, G. S. (1986): A kernel method for air quality modelling – I: Mathematical foundation. *Atmospheric Env.*, 20, 1447–1452

Luhar, A. K., and Britter, R. E. (1989): A Random Walk Model for Dispersion in Inhomogeneous Turbulence in a Convective Boundary Layer. *Atmospheric Env.*, **23**, 1911–1924

Luhar, A. K., and Rao, K. A. (1994): Lagrangian Stochastic Dispersion Model Simulations of Tracer Data in Nocturnal Flows over Complex Terrain. *Atmospheric Env.*, **28**, 3417–3431

Luhar, A. K., Hibberd, M. F., and Hurley, P. J. (1996): Comparison of Closure Schemes used to Specify the Velocity PDF in Lagrangian Stochastic Dispersion Models for Convective Conditions. *Atmospheric Env.*, **30**, 1407–1418

Mikkelsen, T., Larsen, S. E. and Pécseli, H. L. (1987): Diffusion of Gaussian Puffs. *Quart. J. Roy. Met. Soc.*, **113**, 81–105

Rotach, M. W., Gryning, S.-E. and Tassone, C. (1996): A Two-Dimensional Stochastic Lagrangian Dispersion Model for Daytime Conditions. *Quart. J. Roy. Met. Soc.,* **122**, 367–389

Scott, D. W. (1992): *Multivariate Density Estimation: Theory, Practice, and Visualisation*. Wiley, New York

Silverman, B. W. (1986): *Density Estimation*. Chapman and Hall, London

Thomson, D. J. (1987): Criteria for the Selection of Stochastic Models of Particle Trajectories in Turbulent Flows. *J. Fluid Mech.*, **180**, 529–556

Thomson, D. J., and Montgomery, M. R. (1994): Reflection Boundary Conditions for Random Walk Models of Dispersion in Non-Gaussian Turbulence. *Atmospheric Env.*, **28**, 1981–1987

Venkatram, A., and Du, S. (1997): An Analysis of the Asymptotic Behavior of Cross-Wind-Integrated Ground-Level Concentrations using Lagrangian Stochastic Simulation. *Atmospheric Env.*, **31**, 1467–1476

Wilson, J. D. and Sawford, B. L. (1996): Review of Lagrangian Stochastic Models for Trajectories in the Turbulent Atmosphere. *Boundary-Layer Meteorol.*, **78**, 191–210

Yamada, T., Bunker, S., and Niccum, E. (1987): Simulations of the ASCOT Brush Creek data by a Nested-Grid, Second-Moment Turbulence Closure Model and a Kernel Concentration Estimator. AMS 4th Conference on Mountain Meteorology, 25–28 Aug. 1987, Seattle, WA.

Yamada, T. and Bunker, S. (1988): Development of a Nested Grid, Second Moment Turbulence Closure Model and Application to the 1982 ASCOT Brush Creek Data Simulation. *J. Appl. Meteorol.*, **27**, 562–578

Yamada, T., Jim Kao, C.-H., and Bunker, S. (1989): Airflow and Air Quality Simulations over the Western Mountainous Region with a Four-Dimensional Data Assimilation Technique. *Atmospheric Env.*, **23**, 539–554

Chapter 5

Prediction of Higher Moments of Near-Source Concentration by Simulating the Meandering of Pollutant Puffs*

Abstract—A method to estimate the higher moments of near-source concentrations for different averaging times is presented. Puff dispersion models using so-called „absolute dispersion“ predict one-hour-averaged concentrations. In order to be able to predict the higher moments of concentration (the probability density function), the „absolute dispersion“ has to be separated in its puff-growth part and the additional contribution from the meandering of the plume during the averaging time. The Puff-Particle Model (PPM) has been developed as such a puff-meandering model. The PPM aims at combining the advantages of both, puff and particle dispersion models by moving the center of mass of each puff along a trajectory which mimics the quickly changing turbulent flow field (artificial meandering). This trajectory is derived from the low-frequency part of trajectories as simulated by a Lagrangian stochastic particle model. These puff center trajectories are stochastically independent, which allows only for the evaluation of instantaneous concentration variances. A puff-plume meandering scheme is proposed which introduces spatial correlation between puffs which simulate a continuously emitting source. With this approach, the PPM can also be used to compute the probability density function for any other given averaging time. The PPM has been introduced as a sub-model into the CALPUFF Lagrangian puff dispersion model. The combination of CALPUFF and PPM improves the prediction of the highest possibly occurring near-source concentration, as well as the distance down-wind from the source where it occurs, while retaining the advantages of the CALPUFF model.

Key words: concentration pdf, puff models, plume meandering, relative dispersion.

---

* this chapter is an enhanced compilation of two publications:

de Haan, P., and Scire, J. S. (1999): Prediction of higher moments of near-source concentration by simulating the meandering of pollutant puffs. Preprints 13th Conference on Boundary Layers and Turbulence, Jan. 10–15, 1999, Dallas TX. American Meteorological Society, Boston, USA

de Haan, P., Scire, J. S., Strimaitis, D. G, and Rotach, M. W. (1999): Introduction of a Puff-Particle approach for near-source dispersion into the CALPUFF model. In: Air Pollution Modeling and Its Application XIII, S.-E. Gryning and E. Batchvarova (eds.), Plenum Press, New York

5.1 INTRODUCTION

When modeling pollutant transport and dispersion using gridded meteorological flow fields on an hourly basis, significant parts of the turbulence spectra are not resolved in space and time. Parameterizations of puff or plume dispersion commonly account for this by estimating one-hour averaged dispersion (so-called “absolute dispersion”).

For risk assessments and odor impact analyses, the highest possibly occurring concentration during a time considerably shorter than one hour is more decisive than one-hour average values. For this, the probability density function of concentration for a given location and a specific averaging time is required.

Within the field of dispersion modeling, puff models show a variety of advantages compared to Gaussian plume models. They can take into account the spatial variability of meteorological and dispersion conditions, causality effects, wet and dry deposition, low wind speed dispersion, etc. Lagrangian stochastic particle models, on the other hand, are the state-of-science of dispersion modeling, especially for the simulation of inhomogeneous (convective) turbulence. However, their demand of computing time generally limits their application to the simulation of short episodes rather than a full year. Furthermore, physical processes like dry and wet deposition, buoyant plume rise, and chemical transformations within a cluster, are much easier to implement within the framework of a puff model.

To estimate concentration probability density functions, the absolute dispersion has to be split up into its two components, i. e. the instantaneous puff/plume growth (“relative dispersion”) and the dispersion caused by meandering of the puff during the time averaging period. The first of these two components is driven by the turbulent eddies being smaller than the size of the puff, which are thus able to increase the mean distance between particles within the puff. The second component accounts for the effect of eddies larger than the puff; they displace the puff without enlarging it.

Assessment of flammability or toxicity on the basis of ensemble-averaged concentrations can be seriously in error. These effects depend on short temporal- and spatial-scale fluctuations and thus the variance is essential for these predictions (Sykes 1988). Short temporal scale effects call for short (concentration) sampling times. This violates a basic assumption of many common air pollution models, since such averaging times are considerably shorter than the

spectral gap (approximately one hour). Most models assume that the sampling time is a time long enough to include most of the turbulent energy spectrum (Hanna 1982, p. 278).

In practice it is difficult to provide the flow field at a sufficiently high temporal rate to resolve all meandering motions, especially for small puffs. This means that the effect of meandering has to be simulated. For this, in the Puff-Particle Model (PPM) (de Haan and Rotach 1998a), a „cluster dispersion“ puff model using relative diffusion, the meandering of the puffs' centers of mass is generated artificially. These meandering trajectories simulate the effect of all those eddies not resolved by the flow field but still larger than the puff.

The present contribution calculates concentration fluctuations with a plume meandering model. This can be applied to near-source cases, since the internal (i. e., within the puff) fluctuations are neglected; internal fluctuations become important when the release becomes approximately well-mixed in the vertical direction (Hanna 1984, 1986).

Savunen and Rantakrans (1999) present an odor model based on the assumption of a log-normal probability density function of concentration (denoted hereafter as C-pdf), based on Gifford (1959) and Hanna (1986). Its second moment is estimated as the standard deviation of the meandering motion or, when the plume becomes well-mixed, as the standard deviation of turbulent velocity. Sykes *et al.* (1984) present a second-order turbulence closure scheme which accurately describes the near-field meandering and is able to predict the concentration variance along with the ensemble-mean concentration.

Borgas (1998) and Wilson and Hildermann (1999) focus on the prediction of the highest occurring concentration caused by internal fluctuations. Borgas (1998) uses theoretical relative dispersion considerations to derive the higher moments of the C-pdf, whereas Wilson and Hildermann (1999) use a stochastic Markov process to emulate the time series of internal concentration fluctuations, when the moments of the C-pdf are supplied by any plume meandering model.

Several models have been developed based on Gifford's (1959) meandering plume concept to separate the dispersing effect of instantaneous plume (or puff) growth and of meandering (e.g. Hanna 1984, 1986; Savunen and Rantakrans 1997; Sykes 1988). They all have in common that a certain shape of the probability density function of concentration is assumed and that the variance of concentration fluctuations is derived from the properties of turbulence. SCIPUFF (Sykes 1997) uses a second-order turbulence closure scheme predicting both the

mean concentration and its variance. In contrast, the PPM aims at simulating a realistic three-dimensional meandering of the puffs, which allows for the direct determination of the higher moments of concentration, while enabling the individual puffs to account for inhomogeneous conditions.

In the next section, the concepts of absolute and relative dispersion are used to distinguish between two different so-called puff model families. The basic philosophy and major features of the CALPUFF and PPM puff models are summarized (sections 5.3 and 5.4). The puff-plume meandering scheme, which is proposed to simulate the meandering behavior of a continuously emitting source within the PPM, is introduced in section 5.5. The introduction of the PPM as a sub-model within CALPUFF is described in section 5.6. By interpreting any single meandering puff trajectory as a possible realization, a C-pdf can be computed, which is done for a tracer experiment (section 5.7). Finally. the form of such concentration pdf's for different down-wind distances and averaging times is discussed (section 5.8).

5.2 RELATIVE AND ABSOLUTE DISPERSION

The well-known "absolute" dispersion (so-called 1-particle statistics, or ensemble averaged dispersion), is the ensemble-averaged particle separation with respect to a fixed point in space (Taylor 1921). Richardson (1926) was the first to introduce the concept of relative dispersion, defined as the ensemble averaged separation between pollutant particles released together, i.e. the dispersion around the cluster's center. Gifford (1957a, 1957b) first pointed out that the instantaneous growth of puffs is governed by the concept of relative instead of absolute dispersion. Within the concept of relative dispersion (i.e. 2-particle statistics), turbulent eddies smaller than the actual puff size will contribute to its growth (increasing the ensemble 2-particle separation), while larger eddies move the puff as a whole (without changing the separation of the particles). Thus absolute dispersion is the sum of relative dispersion and meandering during the averaging time (Mikkelsen *et al*. 1987; de Haan and Rotach 1998a).

The missing link between relative and absolute dispersion is the dispersing effect of meandering over time-scales shorter than the averaging time for which the absolute dispersion parameterization used applies. Most formulations of absolute dispersion correspond to an ensemble averaging time of roughly one hour, corresponding to the spectral gap between synoptic and turbulent frequencies.

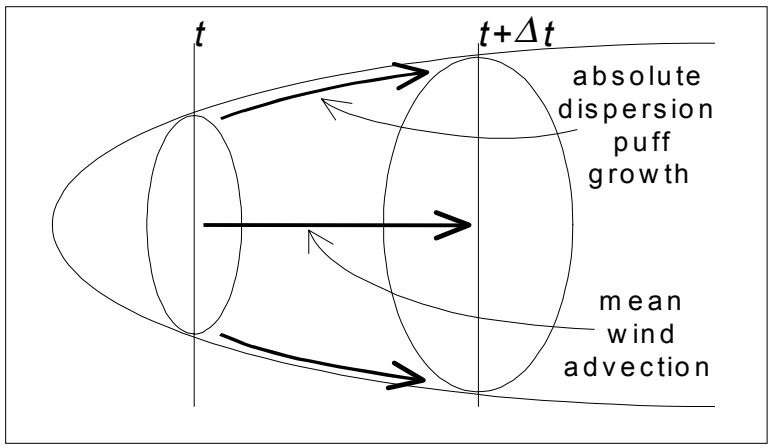

Figure 1 Principle of plume segment models, using puffs as a segment of the ensemble averaged plume.

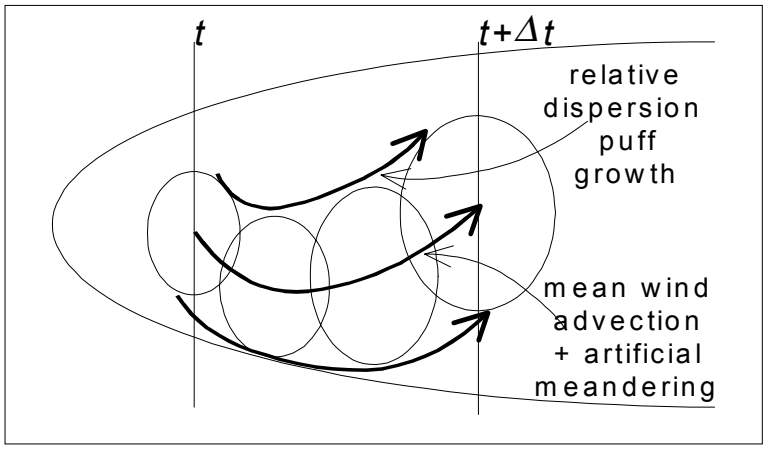

Figure 2 Principle of cluster dispersion models, using puffs as clusters (clouds) of pollutants.

Hence, there are two different kinds of puff models: On the one hand, plume segment models (see **Figure 1**), which describe a segment of an ensemble averaged plume by using a puff; their absolute dispersion scheme accounts for the ensemble averaged dispersion (from cluster growth and cluster meandering) during the averaging time T between two consecutive updates of the mean flow field. On the other hand, there are cluster dispersion models (see **Figure 2**), which interpret a puff as being an instantaneous cluster of pollutants. The spectral gap between turbulent eddies covered by the flow field and those covered by the relative dispersion scheme is simulated with artificial meandering.

Within the framework of these 'plume segment' puff models, a puff (consisting of a center of mass, the actual velocity of the puff, and a 3D distribution of the total mass around the center)

stands for the ensemble average of the concentration distribution belonging to a „piece“ (in time) of the pollutant release. These puffs do not correspond to a single cluster in nature, but are an ensemble average over many individual clusters. Such models generally assume that there is no gap between the averaging time of the measurements from which the dispersion scheme has been derived, and the time interval between two consecutive updates of the flow field within the model.

‘Cluster dispersion’ puff models identify the puff with an individual, physically realistic cluster of particles. They use the concept of relative dispersion (i. e. 2-particle statistics; Gifford 1957a,b; Borgas and Sawford 1994; Thomson 1990): turbulent eddies smaller than the actual puff size will contribute to its growth (increasing the ensemble 2-particle separation), while larger eddies move the puff as a whole (without changing the separation of the particles). Hence, absolute dispersion is the combined effect of relative diffusion and of the meandering of the puff respective to a fixed point, caused by turbulent eddies larger than the puff.

The PPM represents the second group of cluster dispersion models. It uses relative dispersion to describe the instantaneous growth of the cluster (puff); the range of turbulent eddies covered by the relative dispersion depends on the size of the cluster. Eddies larger than the cluster will displace the cluster as a whole without dispersing it. This meandering has to be simulated separately.

When computing ensemble averaged concentrations, both model approaches will yield similar results, though not identical: the meandering of puff centers allows for the advection of different parts of the ensemble average plume by the local flow. Especially near the ground, this will lead to differences in ground concentrations. For elevated releases, the meandering concept will cause some puffs to come close to the ground, where wind velocities are lower, and will thus lead to an somewhat earlier and steeper increase of the concentration profile in the plume center line.

Figure 3 compares the two concepts of puff dispersion. The most pronounced difference occurs for travel times of several minutes. For small (newly released) puffs, absolute dispersion is dominated by meandering rather than by puff-growth. Therefore, in contrast to „cluster dispersion“ models, „plume segment“ puff models are not suited to give correct concentration predictions for a single (instantaneous) release, especially in the intermediate field.

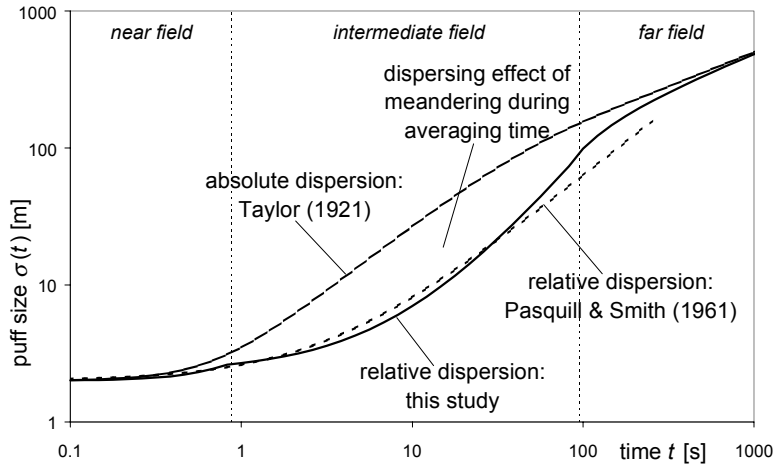

Figure 3 Puff spread as a function of travel time t. The upper, long-dashed line is calculated from Taylor's single particle diffusion theory. Figure adapted from de Haan and Rotach (1998a).

5.3 THE CALPUFF MODEL

The CALPUFF model (Scire *et al.* 1995, 1997) is a non-steady-state Lagrangian puff dispersion model for pollutant transport simulations under inhomogeneous and non-stationary conditions for periods of one year or more with a one-hour time step. Among its main fields of application are pollutant transport simulations for inhomogeneous and non-stationary conditions. CALPUFF is a member of the 'plume segment' puff model family. Using parameterizations like the Pasquill-Gifford-Turner scheme, it yields an ensemble averaged dispersion (i.e. 'absolute dispersion', cf. section 5.2). Together with the flow fields of its meteorological model, CALMET, CALPUFF is applicable to complex terrain and coastal situations.

The user-defined grid size allows for high-resolution simulation of episodes as well as for runs of one year or more with a one-hour time step for environmental impact assessments, and studies of air quality and pollutant transport on regional scales. By its puff-based formulation, it can account for a variety of effects such as spatial variability of meteorological and dispersion conditions, causality effects, dry deposition, plume fumigation, low wind speed dispersion, pollutant transformation, wet removal, and complex terrain effects. It has various algorithms for parameterizing dispersion processes, including the use of turbulence-based dispersion coefficients derived from similarity theory or observations.

The CALPUFF modeling system consists of several parts: The meteorological model CALMET, which is a diagnostic flow field model producing mass consistent and diagnostic

3D flow, temperature and turbulence fields on an hourly basis, based on measurements. Currently, three different dispersion models are designed to use the output of CALMET: CALPUFF, CALGRID, and KSP. CALGRID is a photochemical grid model (Yamartino *et al.* 1992). The Kinematic Simulation Particle model (KSP) (Yamartino *et al*. 1996) is using artificial turbulent eddies of different wave lengths to simulate turbulence.

Evaluation studies of CALPUFF have been done for long range transport distances (for the CAPTEX experiment; U.S. EPA 1995), intermediate distances (Inel data; Irwin 1998) and short to intermediate distances (SF6 data from Kincaid and SO_2 data from Lovett power plants; Strimaitis *et al.* 1998).

5.4 THE PUFF-PARTICLE MODEL (PPM)

The fact that instantaneous releases require puff models using relative dispersion, but that at the same time, the update frequency of the flow field information in almost all applications is too low to resolve all those turbulent eddies not covered anymore by the relative dispersion concept, gave rise to the development of the Puff-Particle Model (PPM). It represents the group of so-called „cluster dispersion“ puff models. The PPM in its current version is a research model for tracer pollutants, focusing on near-source dispersion, and neglecting deposition and chemical processes. It features a full stochastic Lagrangian particle dispersion model, which fulfills the well-mixed criterion (Thomson 1987). For convective conditions, the vertical component of the pdf is the same as in Luhar and Britter (1989). To provide a perfectly smooth transition between stable/neutral Gaussian turbulence to convective skewed turbulence, the transition function of Rotach *et al.* (1996) has been adopted. Further details on the PPM can be found in de Haan and Rotach (1998a).

Every puff within the PPM follows a turbulent puff trajectory derived from a stochastic particle trajectory. The kinematic turbulent energy belonging to those eddies which are smaller than the puff's size-already covered within the concept of relative dispersion-is removed from the particle trajectories. For this, a Kalman low-frequency filter is used, where the cut-off frequency depends on the size of the puff (de Haan and Rotach 1998b). Hence, every puff carries along its own position as well as the position and turbulent velocity components of the stochastic particle it 'belongs to'. The effect of meandering (caused by turbulent eddies larger than the puff but not resolved by the flow field) is simulated by the

puff center trajectories, yielding a complete description of dispersion. It has been shown on the basis of tracer data, that the correct treatment and interpretation of the two contributions to the dispersion process is crucial for reproducing experimental results to a good correspondence (de Haan and Rotach 1998a).

In order to avoid the double-counting of dispersion, only the low-frequency part of the trajectory is used by applying a low-pass Kalman filter (see de Haan and Rotach, 1998b, for details). The principle of this method is depicted in **Figure 4**.

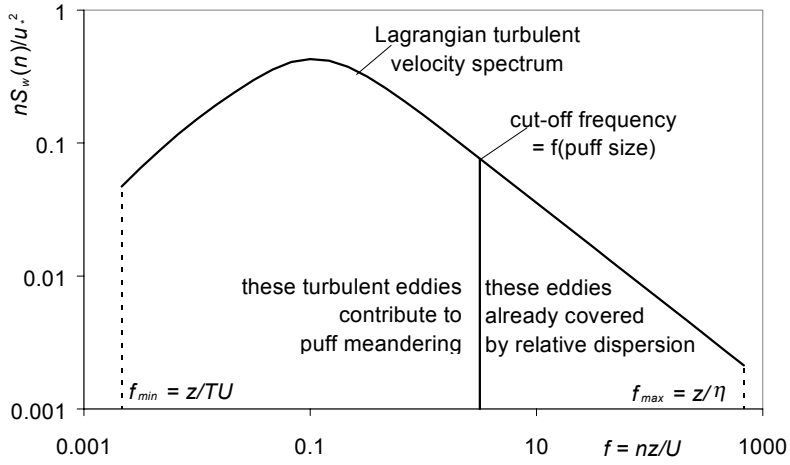

Figure 4 Basic principle to compute stochastic movements of puff centers in the PPM.

5.5 THE PUFF-PLUME MEANDERING SCHEME

Gifford's (1959) meandering plume dispersion model neglects dispersion in the direction of the mean wind, leading to a 'spreading disk' plume dispersion model. The mean concentration distribution as predicted by Gifford's (1959) model is identical with predictions from ensemble-averaged plume models. Additionaly, it predicts statistical properties like the variance of point concentrations. The 'split' between instantaneous plume growth and dispersion due to meandering is a function of down-wind distance, i.e. is different for each 'disk' of the fluctuating plume. These 'disks' do not actually move; it is the statistical property of their movement that is predicted. From this it follows that the statistical properties of concentration as predicted by the Gifford (1959) approach apply to instantaneous (point) concentrations, i.e. with zero averaging time.

For a non-zero, arbitrary concentration averaging time, however, the correlation of the meandering movements between two neighboring 'disks', or puffs, has to be taken into

account. Even though the statistical properties of concentration fluctuations for each point are correct, the statistical properties of concentration *averages* over time differ from non-correlated to correlated meandering. Sykes (1984) and Sykes and Gabruk (1997) present an extension to the Gifford (1959) model, introducing an autocorrelation function for concentration fluctuations. This allows for the computation of the influence of averaging time on the concentration variances.

Within the PPM, the puffs use stochastic paths to artificially produce the correct meandering behavior. This way, the ensemble mean concentration together with its higher moments can be computed for a puff release, for any user-specified averaging (i.e. sampling) time. To obtain correct C-pdf's for continuous plume releases, however, these stochastic puff meandering trajectories are not sufficient. They are derived from Lagrangian particle trajectories which are stochastically independent. But 'neighbor' puffs (i.e. subsequently released puffs) should show 'similar' meandering: the spatial and temporal correlation of turbulence has to be taken into account. If this is neglected, the most extreme concentration events will be underestimated, and the C-pdf will not be correct.

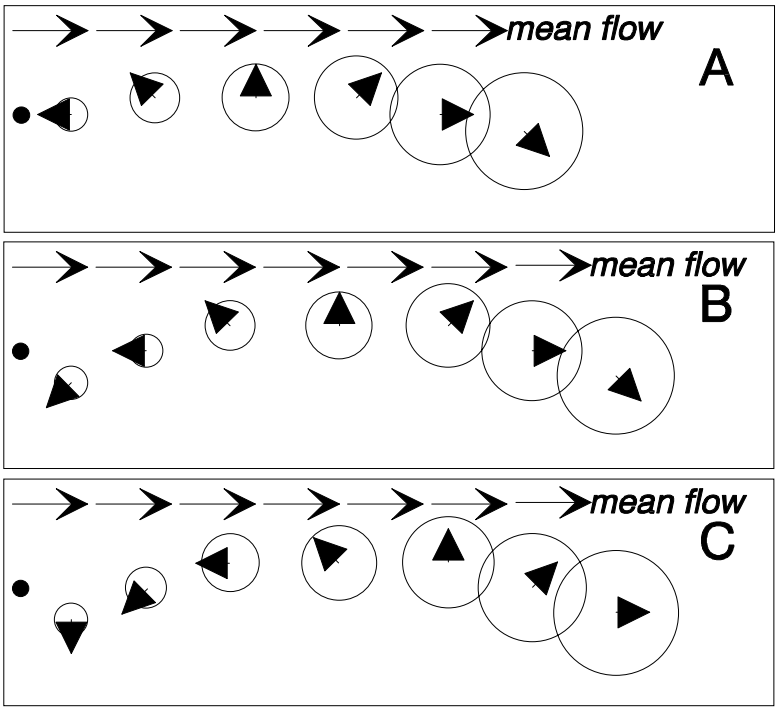

Figure 5 Scheme to produce artificially meandering puff-plumes. The source location is indicated by a solid black dot. The solid triangles depict the stochastic velocity of the puff centers (2D in the figure, but 3D in the model), without the mean wind flow component. For explanations of steps A to C, see text.

The PPM employs a plume meandering scheme based on the puff meandering scheme. Plumes are described as threads of puffs which are correlated in their turbulent movements to their next neighbors in the puff-plume. The PPM puff-plume meandering scheme is illustrated in **Figure 5** and consists of three steps:

- *Step A:* At the beginning of the time-step, each puff has its initial 3D stochastic velocity components.
- *Step B:* After moving the puff-plume with the mean flow and by the stochastic velocities, the newest puff is released. Its stochastic velocities are correlated with those of the second-newest puff (its „mother“ puff) by copying the mother's turbulent velocities and computing a puff trajectory over a time which corresponds to the spatial separation from this second-last puff to the source
- *Step C:* The size of the puffs is enlarged using relative dispersion, and new stochastic velocity components are computed (again, by computing a puff trajectory starting with the turbulent velocities from the „mother“ puff). The first (most distant from the source) puff of the puff-plume follows a normal (non-correlated) PPM puff-center trajectory.

This meandering scheme can be illustrated by thinking of a spectrum of turbulent eddies „rolling back“ towards the source along the puff-plume with the average mean wind speed (introducing the spatial correlation). Such a spectrum of eddies is „released towards the origin“ from the front of the plume every time step, based on the puff path of the front puff (temporal correlation). **Figure 6** and 7 show examples of such meandering puff-plumes.

The Lagrangian particle model within the PPM yields a Lagrangian spectrum, when the turbulent velocity of a particle is followed over time. It has the correct „–1“ slope of the inertial subrange, in contrast with the „–2/3“ slope required for Eulerian spectra. The current approach will thus give a „–1“ instead of a „–2/3“-inertial subrange slope when considering the turbulence at a fixed point in space. However, since these spectra are filtered and only their low-frequency part is used, this shortcoming has only a minor influence. The main difference between Eulerian and Lagrangian spectra is the location of the maximum of the spectrum, $f_{max,E}$ and $f_{max,L}$, respectively. This is corrected by shifting the Lagrangian spectrum towards higher frequencies by a factor $\beta = f_{max,E} / f_{max,L}$. So the turbulent velocities of a puff with a separation x to its „mother“ are computed as a puff trajectory over a time $\beta \cdot x/U$ rather than x/U.

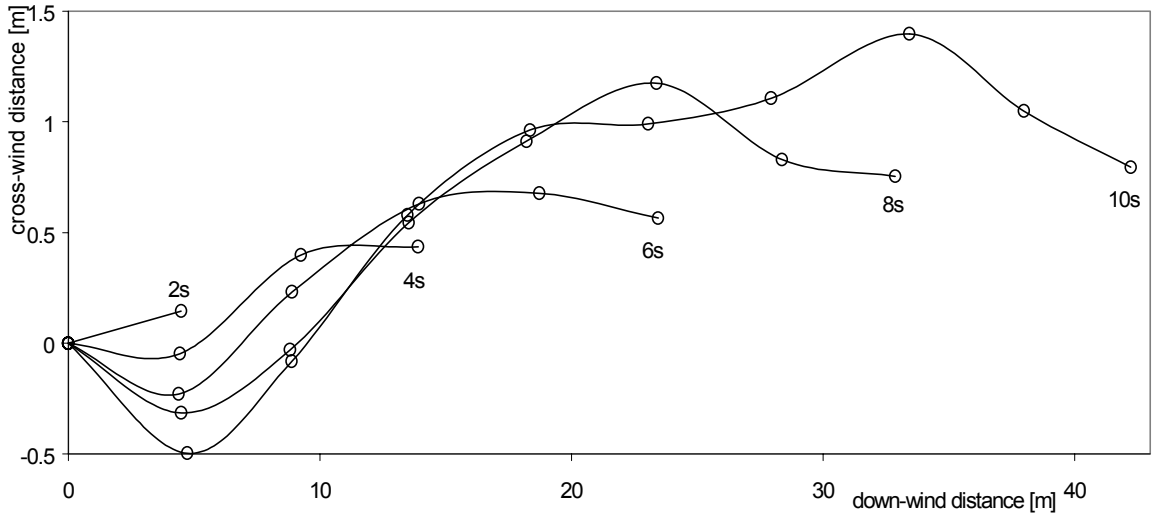

Figure 6 Illustration of the meandering puff-plume scheme. The released puff-plume is depicted 2, 4, 6, 8 and 10 seconds after its release. Puffs belonging to the same puff-plume are connected by a thin line. Circles indicate the position of the center of each puff (not the puff size). View from above.

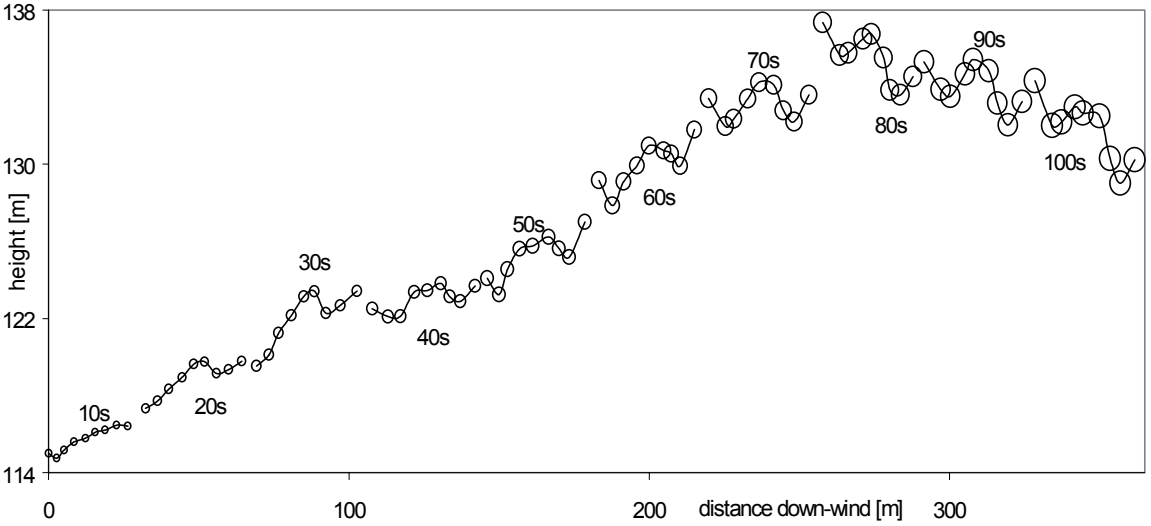

Figure 7 Possible evolution of a plume (consisting of 9 puffs released with a one second interval) over time, when using PPM's meandering puff-plume scheme. The position of the plume's puffs is shown every ten seconds. Example for convective conditions, release height 115 m. View from the side.

5.6 INTRODUCTION OF THE PUFF-PARTICLE MODULE INTO CALPUFF

The CALPUFF model has been developed for a broad range of applications, from micro-scale to meso-scale, from short-term to long-term, with treatments of wet and dry deposition, chemistry, coastal interactions, complex terrain, visibility impacts, etc. The PPM will be one

additional option in this list, providing additional information on the near-source concentration moments. Due to the flexibility of the CALPUFF model on the side of the user, its code has reached a high grade of complexity. Therefore, one of the main objectives for the implementation of the Puff-Particle module into CALPUFF was to introduce as few interactions between the CALPUFF code and the PPM option as possible, in keeping with the module coding concept. Thus, the underlying thought of the concept adopted was that CALPUFF's puff treatment will not change; it is only within the Puff-Particle module that the simulation of artificial meandering of relatively dispersed puffs is computed.

Because CALPUFF and PPM each belong to a different family of puff models (see section 5.2), no interference should occur between CALPUFF's puffs and those of PPM. This is done by attaching so-called "mirror ensembles" of PPM puffs to every newly released CALPUFF "parent puff", which are advected in a "parallel universe" by the PPM-module. Whereas CALPUFF uses sampling steps ensuring that the puffs are advected within each grid cell on their path, the PPM has an internal time step between 1 and 10 s only. At the end of the CALPUFF basic time step, position and size of the "parent puff" are recomputed based on its mirror ensemble's moments.

Figure 8 illustrates the basic set-up of the PPM within CALPUFF:

- To every newly released puff, a so-called 'mirror ensemble' is attached. Such a mirror ensemble consists of a user-defined number, *N*, of puff-particles.
- In order to take into account the information from all grid cells through which the puff will pass in one hour, CALPUFF divides the one hour model time step into a varying number of sampling steps for each puff. For the duration of the sampling step of the parent puff within CALPUFF's main routine, the mirror-ensemble is advected with an internal user-defined PPM-timestep between, say, 1 and 10 seconds. For every internal PPM-timestep, new particle trajectories are computed, from which puff trajectories are derived. Additionally, the puff-particles are advected by the mean flow.
- At the end of the sampling step, from the mirror ensemble's first and second moments of the mass distribution, the position and size of the parent puff are calculated and handed back to CALPUFF's main routine. CALPUFF may then compute any physical process possibly changing the (parent) puff's mass or chemical composition, but not its size or location. The mirror ensemble remains in existence for use in the next sampling step.

- After a certain time, the size of the relatively dispersed particle-puffs in the mirror ensemble will be such that the largest part of the energy spectrum of turbulent eddies will be 'within' the puff-particle. This means that the relative and absolute dispersion for that ensemble become similar. The artificial meandering will show only little variation of the particle-puff's paths. Then, the 'parent puff' location and size is recomputed, the mirror ensemble deleted and the parent puff restored, which from then on is treated with the common absolute dispersion within the CALPUFF model.

The initial position of the particle-puffs at the time of creation of a mirror ensemble is taken randomly from a three-dimensional Gaussian distribution with mean at the center of the parent puff, and the standard deviations of the parent puff being the second moments of the Gaussian distribution. Analogously, the initial turbulent velocity components of the puff-particles of the mirror ensemble are taken from a three-dimensional Gaussian distribution with zero mean and with the ambient turbulence $\left(\overline{u_i'^2}, i = 1,2,3\right)$ as the second moments.

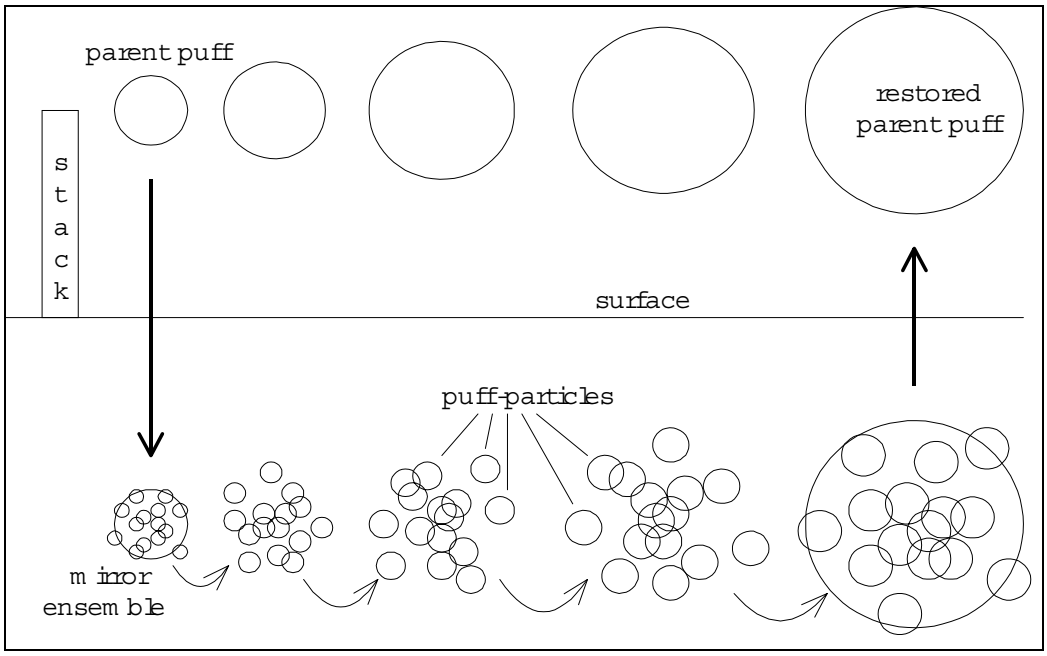

Figure 8 Illustration of the embeddement of the PPM into the CALPUFF model. The procedure for one sampling time step is depicted. After 'restoring' the new location and size of the parent puff, the mirror-ensemble remains stored for use at the beginning of the next sampling step of the same puff, until the puff reaches a mature stage where the mirror-ensemble will be deleted.

5. 7 DETERMINATION OF CONCENTRATION PROBABILITY DENSITY FUNCTIONS

The puff-particle approach gives a realistic picture of the transport (caused by the mean wind, provided by the flow field updates), the amount of meandering (covered by the stochastic puff center trajectories) and the diffusion of the release (caused by eddies smaller than the puff, and taken into account by relative diffusion). For each parent puff, an ensemble of mirror puff-particles is released. Since the meandering part of their motion is reigned by random particle motion, their trajectories will not be identical. Each of them is a possible realization of what might have happened to the parent puff in reality.

To obtain the mean (ensemble averaged) concentration at any receptor, the average over all mirror puff-particles can be taken, where each realization is assumed to represent $1/N$ of the total mass of the parent puff. In theory, the ensemble average concentration thus obtained should be close to the concentration estimation obtained by using the parent puff only, together with absolute dispersion. Of course, in practice, minor differences will appear. To let these differences vanish, it would be necessary to use the same set of parameterized spectra of turbulent energy as a foundation of the absolute as well as the relative dispersion parameterization and at the same time derive the particle pdf within PPM's particle model from this set of spectra.

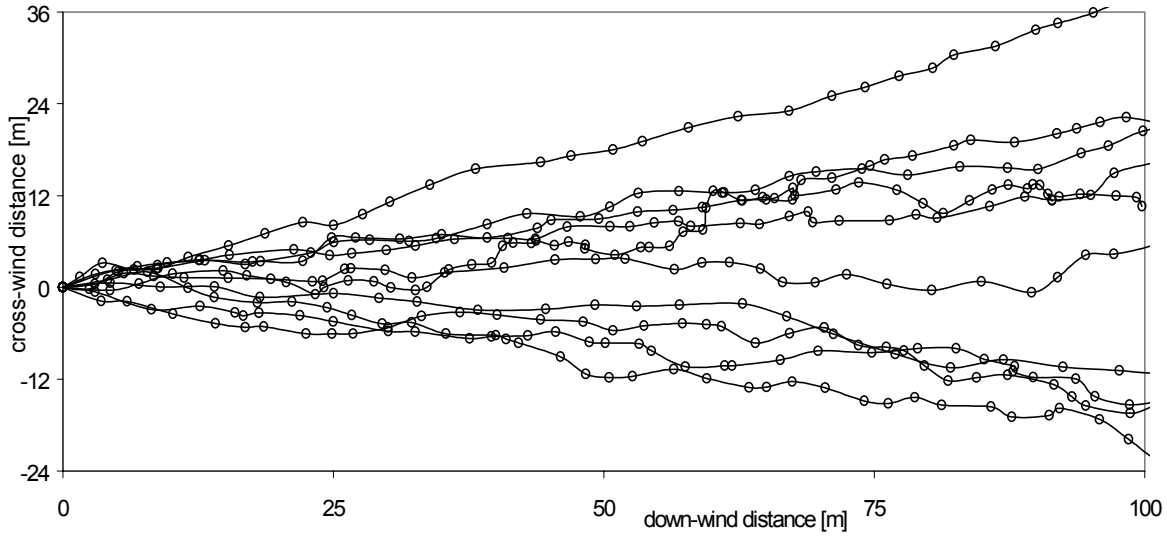

Figure 9 Method to construct a C-pdf. Many individual meandering puff-plumes are simulated. Each is treated as one possible realization that could actually have happened for the given meteorological data. The sorted concentration impacts (for a user-determined averaging time) at specified receptor locations from these many realizations constitute the C-pdf.

To obtain the pdf of concentration at such a receptor, every realization (i. e. mirror puff-particle) carries the whole mass of the parent puff, and the concentration due to this particular realization is computed (**Figure 9**). This leads to *N* possible concentrations, from which the concentration pdf easily can be derived. Of course, to make the concentrations thus computed comparable to the standard CALPUFF results, these *N* possible concentrations have to be computed using all puffs in the modeling domain impacting the receptor, whether they possess a mirror-ensemble or not. In the intermediate to far field, this will lead to a narrowing of the concentration pdf, reflecting the fact that well dispersed pollutant clusters will indeed lead to a higher degree of determination of the corresponding concentration. Therefore, the PPM option within CALPUFF will produce valuable results mainly in the near field, where the differences in puff position due to meandering potentially are of the same order of magnitude as the size of the puff.

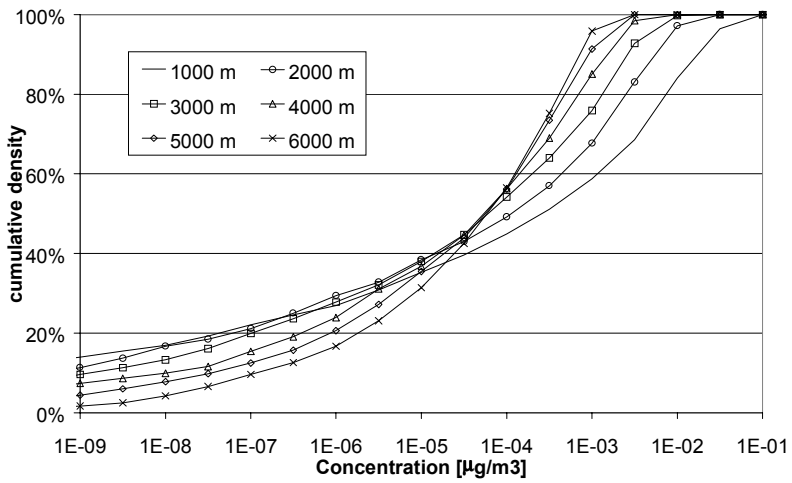

Figure 10 Cumulative concentration pdf's for the plume center line position at six distances down wind from the source; averaging time 60 s. Release height 115 m, conditions of forced convection.

As a first example of the application of PPM's puff-plume meandering scheme, Figure 10 depicts cumulative C-pdf's for the Copenhagen tracer experiment (Gryning and Lyck 1984) for $N = 1000$ for an averaging time of 60 s. 60 s averages are considered representative for odor problems here. For the example of 1000 m down wind plume centerline concentrations, the chance that the "true" concentration will not exceed the average is 74%. In 5% of all cases, the actual concentration will be higher than 5 times the ensemble average.

The precision of the form of the C-pdf at its lower and upper tails is related directly to N, and to the averaging time *T*. However, it should be kept in mind that the "highest occurring concentration" can only be specified for a given averaging time *T*. Choosing *T* shorter than, say, 30 s, will call for a drastic increase in *N* and thus in computational resources, in order to avoid that extreme events become ill-defined because only very few puffs will impact on the receptor location during such short averaging times.

5.8 CHARACTERISTICS OF CONCENTRATION PDF'S

Observations (Fackrell and Robins 1982) show that the most pronounced plume concentration fluctuations are produced very near to the source, and the form of the pdf changes from a near-source exponential to a intermediate-field normal distribution. Despite these forms, the ratio of peak to ensemble-averaged concentrations seems to remain constant. The relative amount of meandering (with respect to ensemble-averages dispersion) depends on atmospheric stability. For stable (night-time) conditions, for example, Hanna (1983) observed very high lateral plume meandering.

When looking at the changes in the form of the C-pdf for increasing down-wind distances (**Figure 11**), two effects are occurring simultaneously. First, a shift of the mean (and the maximum) to the left, i. e. to lower ensemble average concentrations. Second, a narrowing of the C-pdf: the slopes to the left and to the right of the maximum are getting steeper. This means that the ensemble average becomes „better defined", due to the fact that the relevant time scales of fluctuation at these distances are much larger than the averaging time.

The form of the C-pdf also is a function of the averaging time *T*. Whereas a short averaging time of 60 s leads to a wide-spread C-pdf, the C-pdf narrows for larger averaging times (without changing its mean, i. e. ensemble concentration). Additionally, C-pdf's for stable conditions are wider than for convective conditions, because more dispersion leads to a more well-defined ensemble mean, hence a narrowing of the C-pdf.

The form of the C-pdf often is assumed to be log-normal. For most models predicting concentration fluctuation probabilities, this is an input rather than a result. The results from the present model, however, suggest that the C-pdf is log-skewed towards lower concentrations.

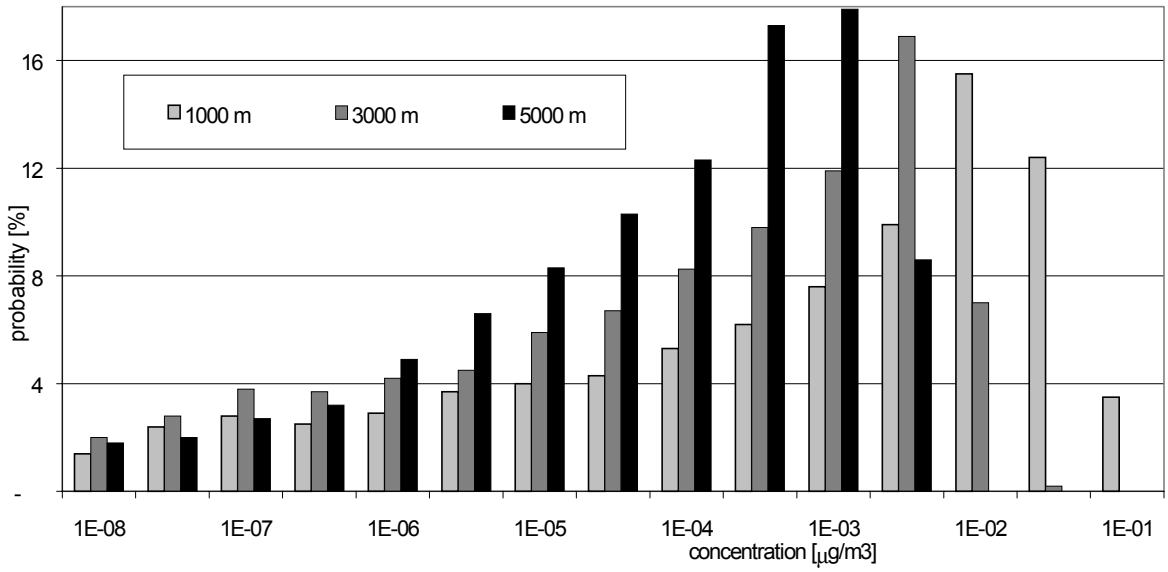

Figure 11 Example of C-pdf's for the plume centerline position at three distances down-wind from the source; averaging time 60 s. Example for the Copenhagen experiment (release height 115 m, conditions of forced convection).

5.9 SUMMARY AND CONCLUSIONS

Hazardous gases and odor complaints show a highly non-linear relationship between their impact and the average concentration. The total dose or the peak concentration are more relevant. To assess such releases, short averaging times are needed as well as the higher moments of concentration, i. e., a C-pdf.

For this, the sub-averaging time and sub-grid meandering of the pollutant release has to be modeled separately from the dispersion itself. Using the PPM, the present contribution shows a method to simulate the meandering of puffs while dispersing the puffs with relative dispersion. For every emitted pollutant puff, an ensemble of puffs is simulated within the PPM. Every individual meandering puff path is interpreted as one possible realization of the dispersing, meandering and transport of the pollutant puff. The C-pdf then is based on the estimated concentration impacts of the individual realizations from the ensemble.

The particle model incorporated within the PPM, upon which the puff meandering is based, assumes that the particle trajectories be stochastically independent. This allows for the computation of concentration variances for an instantaneous (i.e., puff) release. For any continuous release, however, the correlation between subsequently emitted puffs has to be

taken into account. In order to correctly mimic this spatial and temporal correlation, a puff-plume meandering scheme has been introduced.

The puff- and plume-meandering approach is suited to calculate near-source C-pdf's for any user-specified averaging time. For the estimation of far-field concentration fluctuations, the effect of internal fluctuations has to be taken into account as well. This way, the PPM is especially suited for the simulation of accidental hazardous releases. The artificial meandering scheme allows identifying worst-case scenarios.

The combination of the PPM with an operational, user-friendly Lagrangian puff model, CALPUFF, which uses a different approach to describe the dispersion of pollutants, allows for the combination of the advantages of the CALPUFF model, with additional information on the higher moments of the concentration distribution at near-field receptors from the PPM module. This allows for an additional assessment of concentrations that actually could be observed at a given receptor, together with the corresponding probability. This additional feature is particularly useful for the assessment of hazardous pollutants, where the question of the ensemble-averaged exposure is less relevant than the highest exposure which could actually occur under the given meteorological conditions.

Acknowledgements—The present work was partly financed by the Swiss Agency of Education and Sciences (BBW) and the Swiss Agency of Environment, Forest and Landscape (BUWAL) through a project in the framework of COST 615 (citair), and by the Swiss National Science Foundation through Grant No 21-46849.96.

REFERENCES

Borgas, M. S. and Sawford, B. L. (1994): A family of stochastic models for two-particle dispersion in isotropic homogeneous stationary turbulence. *J. Fluid. Mech*., **279**, 69–99

Borgas, M. S. (1998): The variability of pollutant doses in atmospheric plumes. Presented at 14th Clean Air & Environment Conf., Oct. 18–22, 1998, Melbourne, Australia

Fackrell, J. E., and Robins, A. G. (1982): Concentration fluctuations and fluxes in plumes from point sources in a turbulent boundary layer. *J. Fluid. Mech.*, **117**, 1–26

Gifford, F. A. (1957a): Relative atmospheric diffusion of smoke puffs. *J. Meteorol.*, **14**, 410–414

Gifford, F. A. (1957b): Further data on relative atmospheric diffusion. *J. Meteorol.*, **14**, 475–476

Gifford, F. A. (1959): Statistical properties of a fluctuating plume dispersion model. *Adv. Geophys.*, **6**, 117–138

Gryning, S.-E. and Lyck, E. (1984): Atmospheric dispersion from elevated sources in an urban area: Comparison between tracer experiments and model calculations. *J. Clim. Appl. Met*., **23**, 651–660

de Haan, P., and Rotach, M. W. (1998a): A novel approach to atmospheric dispersion modelling: the Puff-Particle Model (PPM). *Quart. J. Roy. Meteorol. Soc*., **124**, 2771–2792

de Haan, P., and Rotach, M. W. (1998b): The treatment of relative dispersion within a combined Puff-Particle Model (PPM). In: Air Pollution Modeling and Its Application XII, S.-E. Gryning and N. Chaumerliac (eds.), Plenum Press, New York, 389–396

Hanna, S. R. (1982): Applications in air pollution modeling. In: Atmospheric turbulence and air pollution modelling, Nieuwstadt, F. T. M, and van Dop, H. (eds.). Kluwer Academic Publishers, Dordrecht, Netherlands, 275–310

Hanna, S. R. (1983): Lateral turbulence intensity and plume meandering during stable conditions. *J. Clim. Appl. Meteorol.*, **22**, 1424–1430

Hanna, S. R. (1984): Concentration fluctuations in a smoke plume. *Atmos. Environ.*, **18**, 1091–1106

Hanna, S. R. (1986): Spectra of concentration fluctuations: The two time scales of a meandering plume. *Atmos. Environ.*, **20**, 1131–1137

Irwin, J. S. (1998): A comparison of CALPUFF modeling results with 1977 Inel field data results. In: Air Pollution Modeling and Its Application XII, S.-E. Gryning and N. Chaumerliac (eds.), Plenum Press, New York, 143–151

Luhar, A. K. and Britter, R. E. (1989): A random walk model for dispersion in inhomogeneous turbulence in a convective boundary layer. *Atmospheric Env.*, **23**, 1911–1924

Mikkelsen, T., Larsen, S. E. and Pécseli, H. L. (1987): Diffusion of Gaussian puffs, *Quart. J. Roy. Meteorol. Soc*., **113**, 81–105

Richardson, L. F. (1926): Atmospheric diffusion shown on a distance-neighbour graph. *Proc. Royal Soc*., Series A, **110**, 709–737

Rotach, M. W., Gryning, S.-E. and Tassone, C. (1996): A two-dimensional stochastic Lagrangian dispersion model for daytime conditions. *Quart. J. Roy. Meteorol. Soc.*, **122**, 367–389

Savunen, T., and Rantakrans, E. (1999): Description and application of an odour dispersion model. Presented at 23rd NATO/CCMS ITM, Bulgarian, 1998. To be published in: Air Pollution Modeling and Its Application XIII, S.-E. Gryning and E. Batchvarova (eds.), Plenum Press, New York.

Scire, J. S., Strimaitis, D. G., Yamartino, R. J., and Zhang, X. (1995): A user's guide for the CALPUFF dispersion model. Prepared for the USDA Forest Service, Cadillac MI, by Earth Tech, Inc., Concord, MA 01742, USA

Scire, J. S., Strimaitis, D. G., Yamartino, R. J., and Insley, E. M. (1997): A user's guide for the CALPUFF dispersion model (Version 5.0). Earth Tech, Inc., Concord, MA 01742, USA.

Strimaitis, D. G., Scire, J. S., and Chang, J. C. (1998): Evaluation of the CALPUFF dispersion model with two power plant data sets. Preprints 10th Joint Conf. Appl. Air Poll. Meteorology, 11–16 Jan. 1998, Phoenix, Arizona

Sykes, R. I., Lewellen, W. S., and Parker, S. F. (1984): A turbulent-transport model for concentration fluctuations and fluxes. *J. Fluid. Mech.*, **139**, 193–218

Sykes, R. I. (1984): The variance in time-averaged samples from an intermittent plume. *Atmos. Env.*, **18**, 121–123

Sykes, R. I. (1988): Concentration fluctuations in dispersing plumes. In: Lectures in air pollution modeling, A. Venkatram and J. C. Wyngaard (eds.), American Meteorological Society, Boston, USA

Sykes, R. I., and Gabruk, R. S. (1997): A second-order closure model for the effect of averaging time on turbulent plume dispersion. *J. Appl. Met.*, **36**, 1038–1045

Sykes, R. I. (1997). PC-SCIPUFF version 1.0 technical documentation. Technical report, Titan Corp., Princeton NJ, USA

Taylor, G. I. (1921): Diffusion by continuous movements. *Proc. London Math. Soc.*, Ser. 2, **20**, 196–211

Thomson, D. J. (1987): Criteria for the selection of stochastic models of particle trajectories in turbulent flows. *J. Fluid Mech*., **180**, 529–556

U. S. Environmental Protection Agency (1995): Testing of meteorological and dispersion models for use in regional air quality modeling. U. S. EPA, Research Triangle Park, NC.

Wilson, D. J., and Hilderman, T. L. (1999): Stochastic reconstruction of intermittent zero concentration periods in plumes for accidental toxic and flammable releases. Presented at 23rd NATO/CCMS ITM, Bulgaria,

1998. To be published in: Air Pollution Modeling and Its Application XIII, S.-E. Gryning and E. Batchvarova (eds.), Plenum Press, New York

Yamartino, R. J., Scire, J. S., Carmichael, G. R., and Chang, Y. S. (1992): The CALGRID mesoscale photochemical grid model–I. Model formulation. *Atmos. Environ.,* **26A**, 1493–1512

Yamartino, R. J., Strimaitis, D. G., Scire, J. S., Insley, E., and Spitzak, M. (1996): Final report on the Phase I development of the Kinematic Simulation Particle (KSP) atmospheric dispersion model. Earth Tech report 1274-3, prepared for Free University of Berlin and Umweltbundesamt, Berlin, FRGs

Chapter 6

Extension of an Operational Short-Range Dispersion Model for Applications in an Urban Environment*

Abstract—When operationally modelling dispersion of air pollutants over a city, 'conventional' dispersion models are often used with modifications in some of the parameters such as the roughness length. However, the presence of a roughness sublayer (RS) is usually neglected, although its turbulence structure is different from that in the surface layer. Therefore, in the present work a roughness sublayer for urban applications is introduced. The principle of the modification has already been tested by simulating two tracer experiments using a Lagrangian particle model and it was shown that the introduction of an RS clearly improves the model performance for both experiments. In this paper, it is shown that the same holds for the introduction of the RS in the multi-source/multi-receptor Gaussian OML model. Its performance is furthermore investigated for the city of Zurich in the year 1990, when a detailed emission inventory and observations at 29 stations are available. It is concluded that the introduction of the RS increases the physical significance of the model in urban environments and thus the credibility of its predictions.

Keywords: dispersion modelling, urban turbulence, rough surfaces, urban air pollution, roughness sublayer

6.1 INTRODUCTION

Air pollution modelling in urban areas suffers from the discrepancy between the explicit need for dispersion simulations due to the high emission densities on the one hand, and a deficit concerning the knowledge on the flow and turbulence structure due to the complicated building structure on the other hand. The presence of tall roughness elements (buildings, trees, etc.) with irregular spacing leads to the formation of a roughness sublayer (RS), which ranges from the physical surface up to 2–5 times the average roughness element height (Raupach *et*

* this chapter has been published as:
de Haan, P., Rotach, M. W., and Werfeli, M. W. (1998): Extension of an operational short-range dispersion model for applications in an urban environment. *Int. J. Vehicle Design*, **20**, 105–114

al., 1991), i. e. it includes the urban canopy layer (see Fig. 1). Within this RS the flow and turbulence structure is different from that of the surface layer (Högström *et al.*, 1982; Rotach, 1993a, b; Roth and Oke, 1993; Roth, 1993; Oikawa and Meng, 1995), which latter usually constitutes the lowest part of applied (operational) dispersion models.

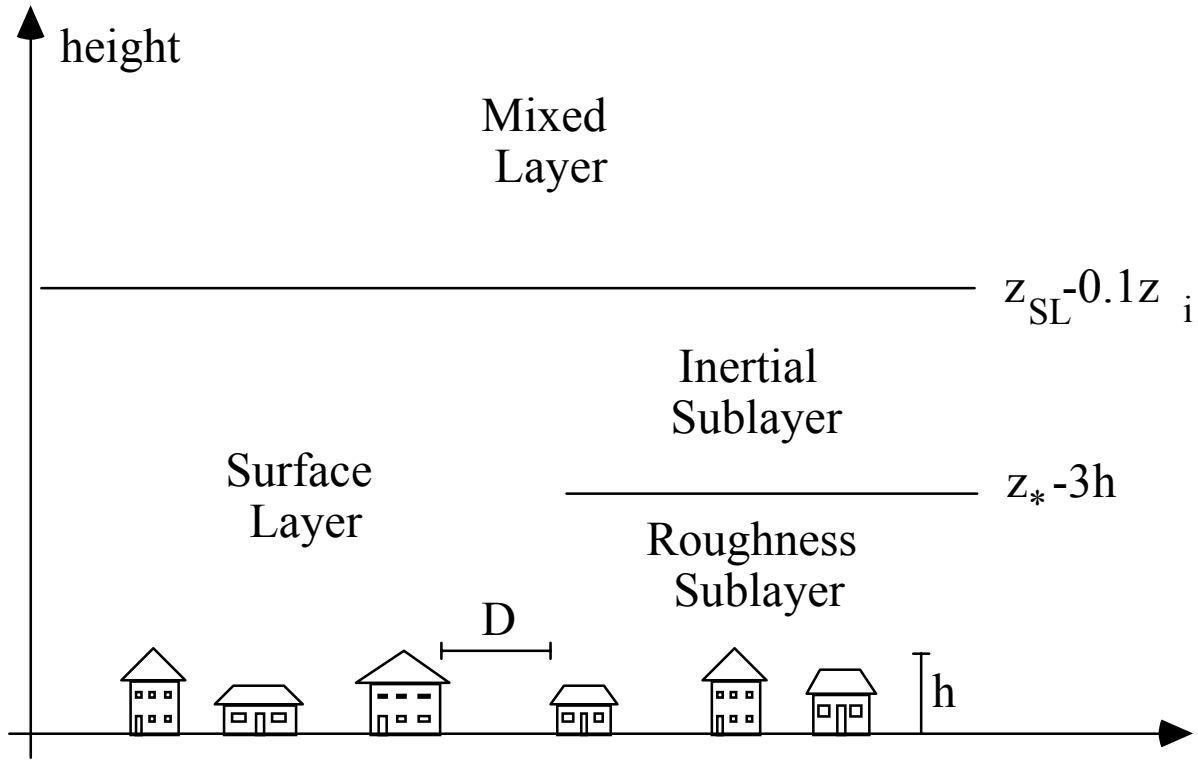

Figure 1 Conceptual sketch of the lowest layers within the boundary layer over an urban surface. The left hand side of the figure shows the situation as it is conventionally used in applied dispersion models ('non-urban' in the present terminology), while the right hand side depicts the actual situation with a roughness sublayer adjacent to the surface (referred to as 'urban' in the text).

The most striking difference is the fact that the turbulent fluxes of momentum (and heat) are not constant with height (cf. the identification of the surface layer as a 'constant flux layer'). For momentum, Rotach (1993a) hypothesised that the non-constant turbulent flux within the urban RS is most likely due to a mean horizontal pressure gradient, as it is characteristic for a flow over a warm (cf. the urban heat island) and rough surface. The non-constant Reynolds stress within the RS leads to a smaller gradient of mean wind speed as compared to the 'logarithmic profile' of the surface layer (Rotach, 1993a) and the necessity to revise the scaling concept for the turbulence statistics such as velocity variances (Rotach, 1993b). Both these features are likely to modify dispersion characteristics and hence surface concentrations

over urban surfaces, and this modification may be severe due to the relatively large vertical extension of an urban RS.

In a recent comparison study, the performance of five operational dispersion models was compared with respect to three tracer data sets (Olesen, 1995). Two of these tracer experiments were conducted in the cities of Copenhagen (Gryning and Lyck, 1984) and Lillestrøm (Haugsbakk and Tønnesen, 1989), i. e. over (sub)urban surfaces. The intercomparison showed that in both cases all the participating operational models underestimated the surface concentrations on average (Olesen, 1995). Using a Lagrangian particle dispersion model, Rotach (1997b), for a hypothetical near-surface source and Rotach and de Haan (1997), for the tracer experiment of Copenhagen showed that this underestimation is likely to be due to neglecting the flow and turbulence structure of the urban RS. In both these studies the model is run in an 'urban' mode and in a 'non-urban' mode: the former takes into account the effect of the rough surface by explicitly using the turbulence characteristics of the RS (corresponding to the right side of Fig. 1) and the latter uses surface layer characteristics at the bottom of the model domain (cf. the left side of Fig. 1) as it is common for essentially all applied dispersion models.

In the present contribution it is investigated how the modified turbulence structure for simulating dispersion over an urban surface can be introduced into an operational dispersion model. It is shown that the modification improves the model performance for the case of the ('ideal') tracer experiments (Section 6.2). When simulating yearly averages of pollutant concentrations from 'real sources' (traffic, domestic and industrial heating) over the area of a whole city (Section 6.3) a similar improvement is observed, but other effects such as the treatment of plume rise tend to mask the improvement of the physically more consistent 'urban' type simulation.

6.2 THE MODIFICATION OF AN OPERATIONAL MODEL

6.2.1 The OML Model

The so-called OML is the basic atmospheric dispersion model for environmental impact assessments in Denmark. Besides the scientific multi-source/multi-receptor version used in the present work, OML-Multi, a single-source version for regulatory purposes is available (OML-Point). The OML is a Gaussian plume model, but in contrast to many regulatory

models its physical description is not based on the traditional discrete stability categories (Pasquill-Turner stability classes). Instead, the model uses basic boundary layer scaling parameters (see below). It is intended to be used for distances up to about 20 km from the source. It requires information on emission and meteorology on an hourly basis, and returns a time series of concentrations calculated at user-specified receptor points. For a more detailed description of the model and the associated meteorological preprocessor, see Olesen *et al.* (1992). The lower boundary of the model domain in vertical direction equals the roughness length, z_0. Perfect reflection without deposition is assumed. This is done by placing a mirror source below the ground.

6.2.2 Modification for urban environments

In the OML model the determination of the standard deviations of the plume dimensions in cross-wind and vertical direction, σ_y and σ_z, respectively, is based on a simplified Lagrangian theory. As input parameters, some of the boundary layer turbulence statistics are required and these, in turn, are parametrised based on similarity theory with the friction velocity, the convective velocity scale and the Obhukov length as scaling variables. This part of the OML is called its meteorological preprocessor. In our modification of the OML for urban environments, the parametrisations in the lower part of the surface layer, i. e. the roughness sublayer, are modified according to the observations which were briefly introduced in Section 6.1. Specifically, this means that due to the decreasing Reynolds stress (in connection with the concept of local scaling) the velocity variances become smaller than they would be in a surface ('constant flux') layer, and the same is true for the gradient of mean wind speed. Additionally, the lower boundary of the modelling domain is lifted up to the zero plane displacement *d* in order to avoid the physically dubious use of a Gaussian dispersion model between the roughness elements.

The 'urban modification' of the OML model only requires one additional step, which slightly modifies the results of its meteorological preprocessor. This is, in general, the simplest way of modifying operational dispersion models for urban environments. No major changes are needed in the code of the program itself. It is important to notice that our distinction between 'urban' and 'non-urban' has nothing to do with the possible contrast between urban and rural. 'Urban' in our context simply means that the RS turbulence structure is correctly taken into account, while 'non-urban' denotes a simulation in which this is not the case. More details

about the modification of the meteorological input to dispersion models for application in urban environments can be found in Rotach (1997a).

6.2.3 'Urban' vs. 'non-urban' simulations

The modification of the OML is validated using the two tracer experiments in Copenhagen and Lillestrøm (see Section 6.1). These tracer experiments are widely used for the validation of models for regulatory purposes. Here, the results of two different simulations of the Copenhagen and Lillestrøm experiments are presented. In the 'non-urban' version, all meteorological input parameters are used as in the original papers (for Copenhagen: Gryning and Lyck, 1984; for Lillestrøm: Haugsbakk and Tønnesen, 1989). For the Copenhagen experiment, mixing layer depths are available from radio soundings; for the Lillestrøm experiment, however, no measurements of the inversion layer height are available, so that a parametrisation has to be used. In this study the formulation of Zilitinkevitch (1972) with a proportionality constant of 0.28 is applied. (Note that since no details on the parametrisation employed are provided in Olesen (1995), we are unable to *exactly* reproduce these results for the 'non-urban' case.)

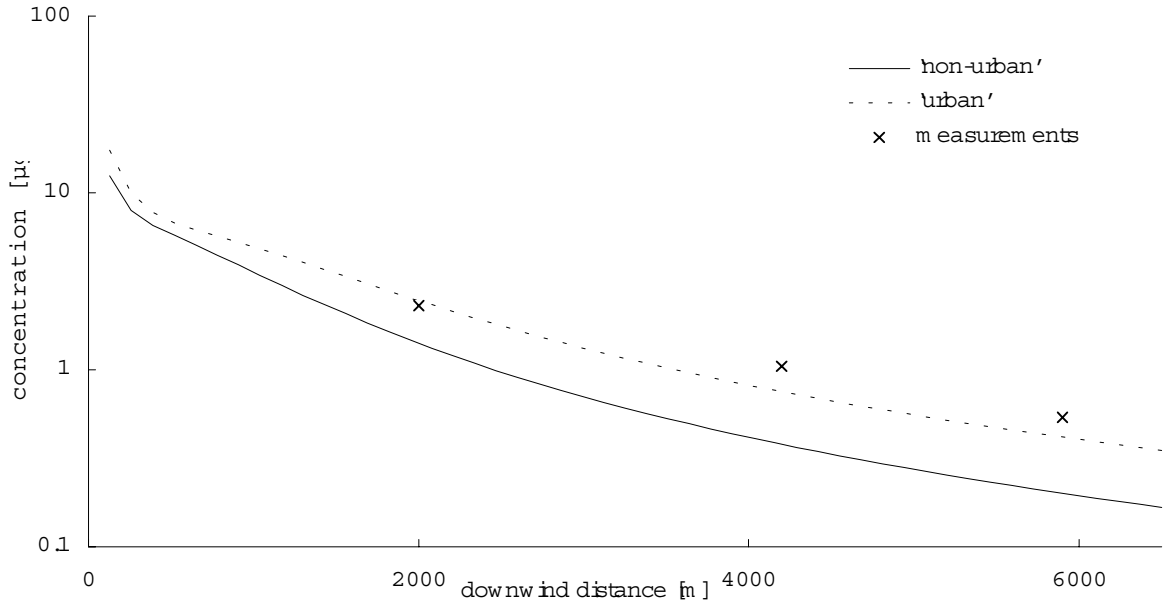

Figure 2 Example of the plume centre line concentration at 2 m above the ground for the 'original' (i. e., 'non-urban') version of the OML and the 'urban modification'. Crosses depict the measurements (Copenhagen experiment from April 30, 1979).

For the 'urban' simulations, the zero-plane displacement has to be estimated from the available information on the average building height and the density of the roughness elements (for details see Rotach, 1997a). For Copenhagen and Lillestrøm, these estimated values for the zero-plane displacement height are 1.0 m and 0.9 m, respectively. In both experiments the friction velocity was measured (or determined from other measurements) at a nominal height of 10 m, i. e. within the RS. Therefore, the parametrised profile of Reynolds stress within the RS (Rotach, 1997a) was used to determine a friction velocity for the inertial sublayer, u_*^{IS}, and this value was input to the OML.

The main effect on the surface concentrations of the modification of the OML with the urban preprocessor is illustrated in Fig. 2. The profile of Reynolds stress within the RS and the associated profiles of the velocity variances give rise to a reduced dispersion as compared to a surface layer assumption ('non-urban' in our notation), thus leading to larger ground-level concentrations downwind of the maximum concentration.

In Table 1 the following statistical measures are compared for the two different simulations of the two tracer experiments:

FB the fractional bias: $FB = (\overline{C}_{\text{obs.}} - \overline{C}_{\text{pred.}}) \big/ (0.5(\overline{C}_{\text{obs.}} + \overline{C}_{\text{pred.}}))$

NMSE the normalised mean square error: $NMSE = \overline{(C_{\text{obs.}} - C_{\text{pred.}})^2} \big/ (\overline{C}_{\text{obs.}} \overline{C}_{\text{pred.}})$

COR the correlation coefficient: $COR = \overline{(C_{\text{obs.}} - \overline{C}_{\text{obs.}})(C_{\text{pred.}} - \overline{C}_{\text{pred.}})} \big/ (\sigma_{\text{obs.}} \sigma_{\text{pred.}})$

FAC2 percentage of simulations within a factor of two of the measurement

Here, $C_{\text{obs.}}$ is the observed concentration and $C_{\text{pred.}}$ the simulated one. These statistical measures are calculated for the maximum concentration (plume centre line) measured on an arc of receptors placed cross-wind at a constant distance from the source, at 2 m above the ground, and for the cross-wind integrated concentration, CIC.

		arcwise maximum conc.				cross-wind integrated conc.			
		NMSE	COR	FAC2	FB	NMSE	COR	FAC2	FB
Copenhagen	Observations	0.00	1.000	100%	0.000	0.00	1.000	100%	0.000
	OML 'non-urban'	1.03	0.798	22%	0.743	0.49	0.852	57%	0.577
	OML 'urban'	0.37	0.737	87%	0.247	0.41	0.836	74%	0.519
Lillestrøm	Observations	0.00	1.000	100%	0.000	0.00	1.000	100%	0.000
	OML 'non-urban'	0.47	0.811	47%	0.427	2.10	0.572	37%	0.960
	OML 'urban'	0.38	0.751	58%	0.131	1.15	0.502	58%	0.514

Table 1 Comparison of statistical measures for the 'urban' and 'non-urban' simulations for the two tracer experiments from Copenhagen and Lillestrøm.

As can be seen from Table 1, the results of the OML are improved when using the 'urban' modification. In the case of the Copenhagen experiment, all statistical measures show a clear improvement, with the exception of the correlation coefficient, which slightly decreases but still remains relatively high. In general, the improvements are more pronounced in the statistical measures for the arcwise maximum concentration than for those of the CIC.

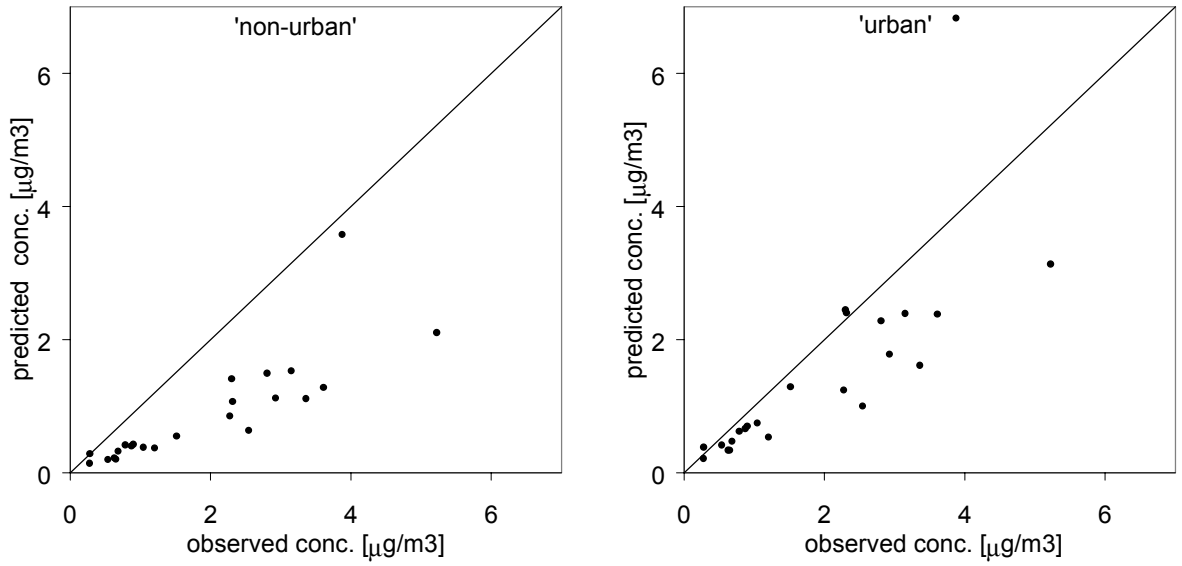

Figure 3 Scatter plot of all observed arcwise maximum concentrations vs. predictions (Copenhagen experiment). Total number of data points is 23. a) 'non-urban' simulation, and b) 'urban' simulation.

A scatter plot of observed vs. simulated arcwise maximum concentrations for the Copenhagen experiment is presented in Fig. 3. As can be seen, the underprediction from the non-modified version of the OML is clearly reduced. Only in one case the 'urban' modification causes a previously underpredicted value to become overpredicted. For all other observed values, the predictions improve when using the 'urban modification'. This leads to the significantly improved statistical measures in Table 1, with the most remarkable changes for the ArcMax predictions, with the FB and NMSE measures becoming almost three times smaller. For the Lillestrøm experiment, the statistical measures show similar improvements, but are most pronounced for the CIC predictions, with FB and NMSE dropping by almost 50%. Again, the correlation coefficient shows a slight decrease. With the 'urban modification', however, the performance of the OML becomes comparable to the performance of more advanced scientific dispersion models (Olesen, 1995).

6.3 APPLICATION TO THE CITY OF ZURICH, 1990

In the previous section, the importance of the roughness sublayer turbulence structure was demonstrated for an 'ideal' setting of a tracer experiment. For this type of experiment the source is well defined and its strength is exactly known, no effects of plume rise have to be taken into account and the receptor density is usually high. In contrast, when using an operational dispersion model such as the OML for the simulation of, e. g., the spatial distribution of the annual mean surface concentrations over the area of a whole city, these conditions are not fulfilled. In the following we present first results from such an attempt, namely the simulation of the surface concentration of NO_x in the year 1990 for the city of Zurich. For this year a detailed (100 m x 100 m resolution) emission inventory was constructed (Werfeli, 1995). It takes into account traffic (number of vehicles per day and estimated speed on the 152 largest roads of the city; additionally, estimates of short-distance traffic not using major roads), domestic and commercial heating and the 35 largest industrial sources (treated as point sources in the model).

This emission inventory sums up to over 4300 SO_2 sources and over 4300 NO_x sources, where the line sources (roads) are split up and added to area sources. To simulate the time dependence of source strength, the amplitude of the traffic sources is modulated according to the hour of the day and the day of the week, and the strength of the heating sources depends on the hour of the day and on the month. The emission data of the heating sources was collected very carefully (0.01% missings in the number of sources) and the traffic emissions were modelled using numerous results from actual traffic census data. The emission factors used for the calculation of the overall emissions for each source type and pollutant were checked with in-site monitoring measurements. With this procedures the overall accuracy of the emission data is estimated at ±5% for heating sources (SO_2 and NO_x) and at ±20% for NO_x and ±25% for SO_2 for emissions from traffic sources. This amounts to a total maximum estimated error in the emission data of 6.3% for SO_2 and, due to the larger contribution of traffic sources, of 14.3% for NO_x. For details concerning the emission inventory see Werfeli (1999).

In addition, for the year of 1990, a total of 29 stations spread all over the city, yielded observational data of surface pollutant concentrations for comparison to the simulations. Besides from five continuously monitoring stations (hourly averaged concentrations for the

whole year), pollutant concentrations were measured over shorter time periods (covering all seasons) at the remaining 24 stations, from the results of which annual average concentrations were estimated by statistical means.

For the configuration of the model and the definition of the required model input, one has to be aware that several assumptions are likely to have a significant influence on the resulting ground level concentrations. The approaches chosen for the most sensitive parametrisations are outlined in the following:

- Plume rise plays an important role in determining surface concentrations for real sources. The commonly used plume rise schemes of Briggs (1984) are designed for large point sources. For the present purpose, these schemes are translated for use in connection with domestic heating and traffic area sources by choosing average stack heights above roof level and above the street level, respectively. Instead of specifying values for vertical exit velocity and source radius, averaged buoyancy fluxes are assigned to the individual sources depending on the source strength (being a function of time and of space). The temperature of the emissions is set to a constant level and not to an constant excess with respect to the ambient temperature. This has been done in order to reflect the more or less constant burning temperature of engine vehicles and of heatings.
- The well known Gaussian plume solution to atmospheric dispersion does not apply close to the source, since all parametrisations of the vertical and lateral plume standard deviation, $\sigma_y(x)$ and $\sigma_z(x)$, respectively, approach zero near the source. This causes the ground level concentration prediction of Gaussian plume models to approach infinity for $x \to 0$, since both $\sigma_y(x)$ and $\sigma_z(x)$ appear in the denominator of an exponential expression. Therefore, Gaussian plume models only apply for $x > 100\,\mathrm{m}$ (Briggs, 1973). Hence, Gaussian dispersion models tend to overestimate the surface concentrations close to the source. To circumvent the problem that typically small sources, which are located in the vicinity of any receptor in an urban environment, promote an average (potentially large) overestimation due to this flaw of Gaussian dispersion models, the groundlevel concentration predictions caused by the individual sources is set to zero for the near-field $(x < 100\,\mathrm{m})$ (note that for the tracer experiments discussed in the previous section the closest measurement arc was far enough from the source so that this problem did not occur).

- The definition of the model surface is another key factor in determining the model performance. In order to avoid the use of a (relatively simple) Gaussian model for dispersion estimates *between* the roughness elements, where its application can certainly not be justified, a model surface corresponding to the zero displacement height (see Rotach, 1994) rather than the physical surface $(z = 0)$, is used.

First results of the simulation of the annual mean NO_X surface concentrations for 1990 for the city of Zurich at the 29 measurement stations are shown in Fig. 4. The simulation with the parametrisations and the set-up as outlined above, is denoted 'non-urban' (see Fig. 4a). This 'non-urban' simulation results in a fractional bias of 0.17, i. e. an underestimation of 17% (Fig. 4a). As for the tracer experiment in the previous section, the 'urban' simulation improves the performance (Fig. 4b). In particular, the fractional bias is reduced, and does not any more differ significantly from zero on a 5% level, whereas the scatter (the normalised mean square error) and the correlation coefficient do not change significantly.

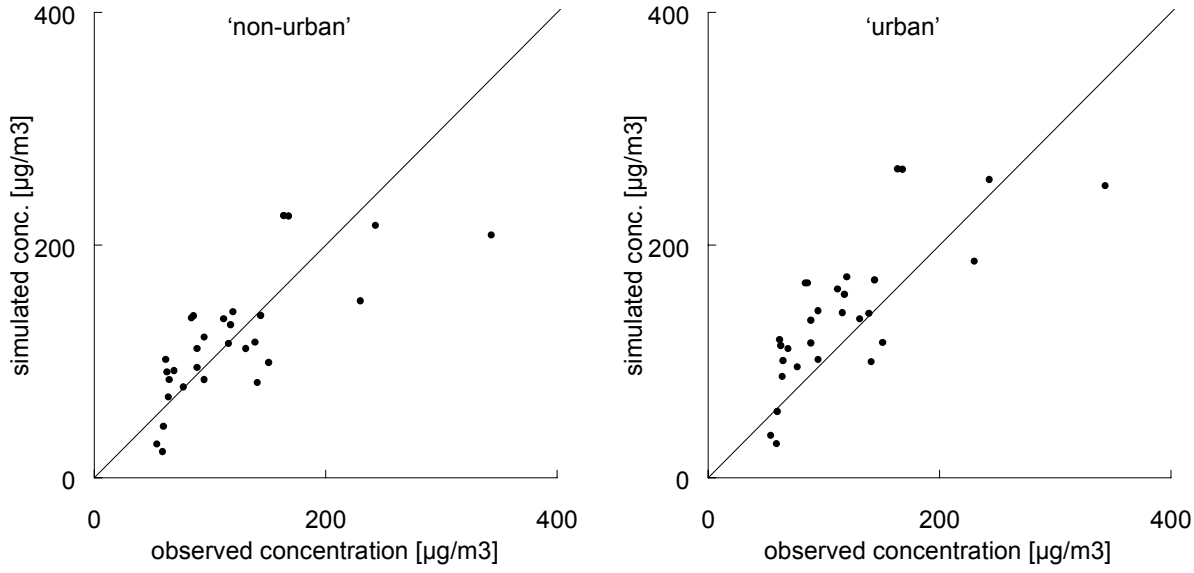

Figure 4 Comparison of observed vs. modelled yearly averages of NOx groundlevel concentration in at 29 surface observation stations in the city of Zurich (1990). a) 'non-urban' simulation, and b) 'urban' simulation.

In future work, an attempt for further refinements will be made, especially concerning the improvement of the near-field correction of the Gaussian plume model. Additionaly, the background concentration of SO_2 and NO_X in the city of Zurich will be assumed to consist of two contributions: firstly, the natural concentration measurable at remote rural stations, and,

secondly, the contribution from sources near the city of Zurich, but not accounted for in the emission inventory, which only covers sources within the community of Zurich, and not the whole urban agglomeration. Nevertheless, the preliminary results presented here show clearly that the main effect of introducing a RS in a conventional Gaussian dispersion model leads to higher annual average ground level concentrations of between 10–20%, thus compensating the underestimation most models show over urban environments. The other statistical performance measures of the modified dispersion model in question, the OML, remained approximately unchanged for the case of a real emission scenario over an European city.

6.4 SUMMARY AND CONCLUSIONS

To obtain a proper modification of operational (Gaussian) dispersion models for use within urban environments, the concept of an urban meteorological preprocessor has been introduced. Its basic principle is to use similarity theory based on local fluxes for the parametrisation of the turbulence structure within the urban roughness sublayer. The first validation step of this concept has been reported on elsewhere (Rotach and de Haan, 1997) and was performed by use of a Lagrangian particle dispersion model (research model) for the simulation of two tracer experiments, which took place in (sub)urban environments. A clear improvement of the predictability was the result. This indicates that the urban preprocessor is able to better take into account the rough character of the surface at the sites where these experiments took place. As a second validation step the performance of the operational Gaussian multi-source dispersion model OML for these two experiments also shows an improvement of the correspondence between the simulated and the measured concentrations if the urban preprocessor is applied. Therefore, the concept of the urban preprocessor can be used within operational Gaussian dispersion models to improve the model's prediction ability over urban surfaces. First results for the case study of the surface pollution concentration (NO_x) in the city of Zurich in the year 1990, for which a very detailed emission inventory (100 m x 100 m resolution) is available, also show an improved model performance after introduction of the roughness sublayer.

Acknowledgements-The present work was partly financed by the Swiss Federal Department of Education and Sciences (BBW) and the Swiss Federal Department of Environment, Forest

and Landscape (BUWAL) through a project in the framework of COST 615 (citair), and by the Swiss National Science Foundation through Grant Nr. 21-46849.96.

REFERENCES

Briggs, G. A. (1973): Diffusion estimation for small emissions. 1973 Annual Report, Air Resources Atmos. Turb. and Diffusion Lab., Environmental Lab., Report ATDL-106, USDOC-NOAA

Briggs, G. A. (1984): Plume Rise and Buoyancy effects. Atmospheric Science and Power Production (ed. by Randerson D.), DOE/TIC 27601. Department of Commerce, Springfield, U. S. A.

Gryning S.-E., and Lyck E. (1984): Atmospheric Dispersion from Elevated Sources in an Urban Area: Comparisons between Tracer Experiments and Model Calculations. *J. Clim. Appl. Meteorol*., **23**, 651–660

Haugsbakk I. and Tønnesen D. A. (1989): Atmospheric Dispersion Experiments at Lillestrøm. 1986–1987. Data Report NILU OR 41/89. Available from Norwegian Inst. for Air Research, PO Box 100, N-2007 Kjeller, Norway

Högström U., Bergström H. and Alexandersson H. (1982): Turbulence Characteristics in a Near-Neutrally Stratified Urban Atmosphere. *Boundary-Layer Meteorol*., **23**, 449–472

Oikawa S. and Meng Y. (1995): Turbulence Characteristics and Organized Motion in a Suburban Roughness Sublayer. *Boundary-Layer Meteorol*., **74**, 289–312

Olesen H. R., Løfstrøm P., Berkowicz R. and Jensen A. B. (1992): An improved dispersion model for regulatory use: the OML model. In van Dop H. and Kallos G. (eds.), Air Pollution Modelling and its Applications IX, Plenum Press, New York

Olesen H. R. (1995): The Model Validation Exercise at Mol: Overview of Results. *Int. J. Environ. Poll*., **5**, 761–784

Raupach M. R., Antonia R. A. and Rajagopalan S. (1991): Rough-Wall Turbulent Boundary Layers. *Appl. Mech. Rev*., **44**, 1–25

Rotach M. W. (1993a): Turbulence Close to a Rough Urban Surface Part I: Reynolds Stress. *Boundary-Layer Meteor*ol., **65**, 1–28

Rotach M. W. (1993b): Turbulence Close to a Rough Urban Surface Part II: Variances and Gradients. *Boundary-Layer Meteorol.,* **66**, 75–92

Rotach, M. W. (1994). Determination of the Zero Plane Displacement in an Urban Environment. *Boundary-Layer Meteorol*., **67**, 187–193

Rotach M. W. (1997a): Towards Meteorological Preprocessing for Dispersion Models in an Urban Environment. *Intern. J. Environment Pollution*, **8**, 548–556

Rotach M. W. (1997b): The Turbulence Structure in an Urban Roughness Sublayer, in: Perkins, R. J. and Belcher, S. E. (Eds): Flow and Dispersion through Groups of Obstacles, Clarendon Press, Oxford, 143–155

Rotach M. W. and de Haan P. (1997): On the Urban Aspect of the Copenhagen Data Set. *Intern. J. Environment Pollution*, **8**, 279–286

Roth M. and Oke T. R. (1993): Turbulent Transfer Relationships over an Urban Surface. I: Spectral Characteristics. *Quart. J. Roy. Meteorol. Soc*., **119**, 1071–1104

Roth M. (1993): Turbulent Transfer Relationships over an Urban Surface. II: Integral Statistics. *Quart. J. Roy. Meteorol. Soc*., **119,** 1105–1120

Werfeli M. (1995): Modelling Surface Pollutant Concentrations (SO2 and NOx) in the City of Zürich. *Int. J. Environ. Poll*., **5**, 575–584

Werfeli M. (1999): Modellierung von Luftschadstoff-Immissionen in Siedlungsgebieten am Beispiel der SO2- und NOx-Immissionen in der Stadt Zürich. Ph.D. Swiss Federal Institute Zurich, Switzerland

Zilitinkevich S. S. (1972): Determining the Height of the Nocturnal Boundary Layer. *J. Appl. Meteorol*., **17**, 28–33

Chapter 7

Modification of an Operational Dispersion Model for Urban Applications*

Abstract—An operational multi-source, multi-receptor Gaussian dispersion model, the Danish regulatory model OML, has been modified for applications in urban environments. A so-called roughness sublayer has been introduced into the model to represent the turbulence characteristics of the lowest part of the surface layer over rough surfaces like cities. The meteorological preprocessor was enhanced to take into account an urban energy budget. The performance of the resulting OML-Urban has been validated for NO_x and SO_2 for the city of Zurich for the year 1990. For this year, a detailed emission inventory as well as continuous hourly measurements at four stations are available. The air pollution monitoring stations used for validation have been divided into different groups, depending on local influences from nearby roads. The urban modification (roughness sublayer and changes in the met. preprocessor) results in a 25–35% increase of the annual mean surface concentration. OML-Urban shows a good reproduction of the probability density function of predicted concentrations, and the simulated yearly averaged concentrations show a good correspondence to observations.

Key words: dispersion modeling, urban turbulence, rough surfaces, urban air pollution, roughness sublayer

7.1 INTRODUCTION

Air pollution modeling in urban areas is different from the traditional single high stack source dispersion problem in many ways. The air pollution level in agglomerations often is dominated by a countless number of small, not well determined emission sources. The inhomogeneity of the built-up area often causes concentration measurements to be

---

* this chapter will be submitted for publication in *J. Appl. Met.*:
de Haan, P., Rotach, M. W., and Werfeli, M.: Modification of an operational dispersion model for urban applications.

locally influenced. Almost all emission sources and (human) receptors are situated within the lowest tens of meters.

Although crucial to micro-scale dispersion modeling, relatively little is known concerning the flow and turbulence structure over built-up areas. Irregularly spaced tall roughness elements such as buildings induce a roughness sublayer (RS), which ranges from ground-level to several times the average building height (Raupach *et al*. 1991), as displayed in Figure 1. The existence of a roughness sublayer is not specific to urban surfaces but, unlike to the case of smoother terrain, its vertical extension cannot be neglected. Within this RS the flow and turbulence fields are different from that of the surface layer above (Högström *et al.* 1982; Rotach 1993a, b, 1997b; Roth and Oke 1993; Roth 1993; Oikawa and Meng 1995).

Gaussian plume models represent a valid (analytical) solution to the diffusion equation only for idealized circumstances. Stationarity and homogeneity of the turbulence characteristics are requested. In practice, none of these conditions is fully satisfied, but Gaussian plume dispersion models have been successfully used for rural configurations. Extensive validation has been done on tracer experiments conducted e.g. in Kincaid and Prairie Grass (see e.g. Olesen 1995; Carruthers *et al.* 1992). Gaussian plume models have also been tested against tracer experiments in urban surroundings like the Indianapolis experiment (Hanna and Chang 1993). Especially, for the prediction of yearly averaged concentration based on hourly meteorological data, Gaussian plume models are still the method of choice. Also, Gaussian plume dispersion models have been applied to multi-source, multi-receptor situations in inhomogeneous urban environments (e.g. Gryning and Lyck 1984; Häggkvist 1997; Härkönen *et al.* 1998).

The question addressed in this paper is which changes should be made in order to apply Gaussian plume models to urban environments:

1. changes to the computing code of the dispersion model and its meteorological pre-processor (to take into account the turbulence characteristics and the energy balance over urban surfaces)
2. changes in the set-up of the model (emission height of sources and receptor heights within the urban canopy layer)

3. changes in model validation by classifying measuring sites into different groups depending on the influence of nearby roads and building structures.

Rotach (1997a) proposed a method to introduce the RS into dispersion models by using an 'urban meteorological preprocessor'. Since one of the main characteristics of a RS is the fact that the turbulent fluxes are not constant with height, the urban meteorological preprocessor allows for a non-constant Reynolds stress in the RS. This leads to higher wind speeds as compared with a logarithmic wind-profile (Rotach 1993a), and the concept of local scaling is used to determine turbulence statistics such as velocity variances (Rotach 1993b). If the dispersion model uses similarity theory instead of stability classes, the concept of local scaling within the RS needs to be implemented in the dispersion model itself. The parameterizations on urban stability and urban heat balance affect the meteorological pre-processor only.

The treatment of the Roughness Sublayer (RS) after Rotach (1997a) proved to be successful in improving the performance of dispersion models: For a Lagrangian stochastic particle model, Rotach and de Haan (1997) showed that the OML underprediction of surface concentrations for the Copenhagen tracer experiment vanishes (Olesen 1995). De Haan *et al.* (1998) introduced the RS concept into an operational Gaussian dispersion model (which is much more suited to handle multi-source, multi-receptor problems), the Danish regulatory model OML (cf. section 7.2.1). A similar performance improvement for the Copenhagen and, in addition, for the Lillestrøm tracer data set has been achieved.

The present contribution focuses on this modified version of the OML with an urban pre-processor, hereafter called 'OML-Urban', and presents the application to an entire city. The concept of the RS and other necessary changes to the OML meteorological pre-processor and dispersion model are presented (sections 7.2.2 and 7.2.3). The resulting OML-Urban is validated using an extensive data set from the city of Zurich. Measurements of NO_x and SO_2 are available at 28 different sites, which are divided into groups of different quality (section 7.3). It is shown that the concept of the urban modification leads to a clear improvement of the predictions of the OML model. The resulting simulated surface concentrations are very accurate (section 7.4).

7.2 ADAPTATION OF THE OML DISPERSION MODEL TO URBAN CONDITIONS

7.2.1 OML dispersion model

The so-called OML (Operationelle Meteorologiske Luftkvalitetsmodeller) is the basic atmospheric dispersion model for environmental impact assessments in Denmark. Besides the scientific multi-source/multi-receptor version used in the present work, OML-Multi, a single-source version for regulatory purposes is available (OML-Point). The OML is a Gaussian plume model, but in contrast to many regulatory models its physical description is not based on the traditional discrete stability categories (Pasquill-Turner stability classes). Instead, the model uses basic boundary layer scaling parameters (see below).

The OML is intended to be used for distances up to about 20 km from the source. It requires information on emission and meteorology on an hourly basis, and returns a time series of concentrations calculated at user-specified receptor points. For a more detailed description of the model see Olesen *et al.* (1992). The lower boundary of the model domain in the vertical direction equals the roughness length, z_0. Perfect reflection without deposition is assumed. This is done by placing a mirror source below the ground.

The meteorological preprocessor accompanying the OML is based on the resistance method (Berkowicz and Prahm 1982a). The method used is one-dimensional, i. e. neglecting heterogeneous surface conditions and topography. A description can be found in Olesen and Brown (1992).

7.2.2 Characteristics of the Roughness Sublayer

Within this RS the flow and turbulence structure is different from that of the surface layer, which latter usually constitutes the lowest part of applied (operational) dispersion models. The most striking difference is the fact that the turbulent fluxes of momentum (and heat) are not constant with height (cf. the identification of the surface layer as a 'constant flux layer'): observations show an increase of the Reynolds Stress, τ, with

height (Rotach 1993a; Oikawa and Meng 1995; Feigenwinter *et al.* 1998; Rafailidis 1997). The non-constant Reynolds stress within the RS leads to a smaller gradient of mean wind speed as compared to the 'logarithmic profile' of the surface layer (Rotach 1993a) and the necessity to revise the scaling concept for the turbulence statistics such as velocity variances (Rotach 1993b). Instead of using a constant value of the friction velocity to scale velocity variances, within the RS Rotach (1993b) uses local scaling with the height-dependent friction velocity.

Both these features are likely to modify dispersion characteristics and hence surface concentrations over urban surfaces, and this modification may be severe due to the relatively large vertical extension of an urban RS:

- Within the meteorological pre-processor, for all observed friction velocity values from measurements within the RS, a 'reference' friction velocity, u_{*r}, representative for the inertial sublayer (IS) is computed (Rotach 1993a, his eq. (16))
- In the dispersion model, velocity variances are scaled with u_{*r} in the IS. In the RS below, a height dependent local friction velocity $u_*(z)$ is used (again using Eq. (16) from Rotach (1993a)). The same local scaling approach applies to the mean wind speed profile within the RS.

7.2.3 Introduction of an urban energy balance into the meteorological pre-processor

In this section, the modification of the original meteorological preprocessor of the OML (Olesen and Brown 1992) to take into account an urban energy budget is described. Meteorological preprocessing usually makes use of parameterizations based on measurements in rural environments. The main differences between rural, vegetated and surfaces of cities are a reduced evaporation, because of the fast run-off and built-up areas, and a limited storage capacity for water. This causes the latent heat flux to be much smaller as compared to rural environments. Furthermore, the roughness is much higher as compared to rural surfaces, often comparable to the roughness of forests.

The meteorological preprocessor accompanying the OML computes descriptive surface turbulence parameters using the resistance method of Berkowicz and Prahm (1982). The parameters are heat flux, friction velocity, Obukhov length and net radiation. The resistance method assumes analogy with Ohm's law when accounting for, on the one

hand, the resistance of the surface to evaporation, and on the other hand, the flux of heat and water vapor through the surface layer. Parameters have to be determined from data for the description of the stomatal resistance. This has been done in Berkowicz and Prahm (1982) for three types of grass vegetation only, making it impossible to adapt the resistance method model to urban situations. Therefore, the surface fluxes of heat, *H*, and water vapor, *LE*, were calculated by incorporating the scheme of Holtslag and van Ulden (1983). Their scheme, following the Penman-Monteith approach (Monteith 1981), also depends on two empirical parameters, α and β'; the sensible heat flux is parameterized as

$$H = \frac{(1-\alpha)+\gamma/s}{1+\gamma/s}\left(Q^* - G\right) - \alpha\beta' \tag{1}$$

and the latent heat flux by

$$LE = \alpha\left(\frac{1}{1+\gamma/s}\left(Q^* - G\right) + \beta'\right) \tag{2}$$

where Q^* denotes the net radiation, G the ground heat flux, $s = \partial q_s/\partial T$, q_s the saturation specific humidity; $\gamma = C_p/\lambda$, C_p is the specific heat of air at constant pressure, and λ the latent heat of water vaporization.

The value of α can be computed from observations; it depends on the surface moisture condition. For bare soil, $\alpha = 0$, so that $LE = 0$. For the Prairie Grass experiment, $\alpha = 0.45$ (Holtslag and van Ulden 1983). For vegetated surfaces with enough water to evaporate, $\alpha = 1$. Because of the reduced water storage capacity and the fast run-off, the following parameterization has been introduced into OML's preprocessor for use over urban surfaces:

$$\alpha = \begin{cases} 1 & \text{hours with rain reported} \\ 0.45 & \text{first hour after rainfall} \\ 0.2 & \text{accumulated net radiation} < 300\ \text{Wh}\cdot\text{m}^{-2} \\ 0 & \text{otherwise} \end{cases} \tag{3}$$

The accumulated net radiation is calculated as the sum of the net radiation for each hour since rain fall stopped. With Eq. (3), the parameter α is not a constant anymore, and the urban energy budget becomes a function of the accumulated net radiation.

The net radiation (Eqs. 1 and 2) is calculated with OML's routine which is based on the scheme of Nielsen *et al*. (1981). For daytime hours, this scheme calculates Q^* as a function of the global radiation; for nighttime hours, Q^* is a function of the difference between incoming and outgoing radiation, cloud cover and albedo. Transition of night- to daytime hours and vice versa is defined by the sign change of the solar elevation angle. The albedo is set to 0.16 (Oke 1988). For snow covered surfaces, the albedo ranges from 0.95 for fresh snow to 0.40 for old snow (Stull 1998, p. 258; Oke 1987, p. 12). In this study, 0.60 has been chosen as averaged snow albedo value, reflecting the fact that within cities, the snow normally is removed from major streets almost immediately, and gets dirty soon.

The ground heat flux G (Eqs. (1) and (2)) is parameterized as a function of the net radiation. Oke and Cleugh (1987) derived the following expression for a suburban area:

$$G = \begin{cases} 0.25\left(Q^* - 27\,\mathrm{Wm^{-2}}\right) & \text{(daytime)} \\ 0.67Q^* & \text{(nighttime)} \end{cases} \tag{4}$$

Irregularly spaced, large roughness elements affect the stability regime. Such elements cause additional mechanical turbulence. This leads to a tendency for the atmospheric night-time stability towards neutral conditions, when compared to the rural areas surrounding the city. During day-time, the same roughness elements counteract the development of large convective eddies as well as a pronounced negative potential temperature gradient. This causes a trend of the day-time stability regime towards neutral conditions as well.

The default minimum value of the Obukhov length within the OML preprocessor is $100z_0$, i.e. roughly equal to ten times the average obstacle height. For cities with a roughness length of order 1 m, this leads to a minimum value of L of 100 m. Hanna and Chang (1992; 1993) use minimum L values over urban terrain as well, being a function of the height of the roughness elements, h. For the present work, OML's minimum value has been applied to unstable atmospheric stability as well, i. e.,

$$\left|L\right|_{\min} = 100z_0 \tag{5}$$

In addition, the minimum value of the friction velocity, which has an original minimum value of $0.001\,\mathrm{ms^{-1}}$ within the OML, has been raised to $u_{*,\min} = 0.1\,\mathrm{ms^{-1}}$ for urban areas.

7.2.4 Modification of the dispersion model

Plume rise plays an important role in determining surface concentrations for real sources. Within cities, almost all emissions originate from combustion processes (road traffic, domestic heating, waste incineration, etc.) and thus have a buoyancy induced plume rise. On the aggregated level of gridded emission inventories, the individual characteristics of stacks (like diameter, temperature excess, and vertical exit velocity) are of no importance. But the over-all effect of plume rise should be parameterized and included in the model.

Within the OML, the commonly used plume rise schemes of Briggs (1984) are implemented, which express the final rise height of the buoyant release as a function of, among other parameters, the buoyancy flux, the mean wind speed at the stack tip, and the friction velocity. For the present purpose, these schemes are translated for use in connection with domestic heating and traffic area sources by choosing average stack heights above roof level and above the street level, respectively. Instead of specifying values for vertical exit velocity and source radius, averaged buoyancy fluxes are assigned to the individual sources depending on the source strength (being a function of time and of space). The temperature of the emissions is set to a constant level and not to a constant excess with respect to the ambient temperature. This has been done in order to reflect the more or less constant burning temperature of engine vehicles and of heating.

The well known Gaussian plume solution to atmospheric dispersion does not apply close to the source, since all parameterizations of the vertical and lateral plume standard deviation, $\sigma_y(x)$ and $\sigma_z(x)$, respectively, approach zero near the source. This causes the ground level concentration prediction of Gaussian plume models to approach infinity for $x \to 0$, since both $\sigma_y(x)$ and $\sigma_z(x)$ appear in the denominator of an exponential expression. The minimum source-receptor distance depends on the difference between release and receptor height as well. For example, Briggs (1973) mentions $x > 100\,\mathrm{m}$ as the range of applicability of the Gaussian plume equation. Therefore, many applied Gaussian plume models either impose a lower limit on $\sigma_y(x)$ and $\sigma_z(x)$, or an upper limit on the near-source concentration.

When using Gaussian plume models together with gridded emission inventories of a finer scale, the Gaussian plume expression has to be replaced by another model for the near-source field, in fact yielding a hybrid dispersion model. Otherwise, small sources, which are located in the vicinity of any receptor in an urban environment, may promote an average (potentially large) overestimation of concentration.

Within the OML dispersion model, there is no special near-source dispersion model for point sources, but for area sources, a lower limit of half the horizontal extension of the area source applies to $\sigma_y(x)$ and $\sigma_z(x)$. This effectively prevents the near-source concentration from going to infinity. However, the OML scheme yields a different lower limit to $\sigma_y(x)$ and $\sigma_z(x)$ when, for example, a 100 m x 100 m area source is numerically replaced by four 50 m x 50 m sources with one fourth the original emission rate each.

Therefore, in the present study, the ground level concentration prediction is subject to an upper boundary

$$C_{\max} = \frac{Q}{\Delta x \Delta y \overline{U}} \tag{6}$$

Here, $\overline{U}$ denotes the average mean wind speed representative for the area source, as used in the well-known Gaussian dispersion equation. Equation (6) means that the concentration within the area of the source is set equal to the concentration which would be in place within an ”infinite” area source, with source strength Q (in units g·s^{-1}) per area of size $\Delta x \times \Delta y$, regardless of atmospheric stability.

Although Eq. (6) does not explicitly take into account the boundary of the area source (Eq. 6 being applied to all distances down-wind from the source), the transition is smooth and takes places in the proximity of the boundary of the area source. Figure 2 shows a comparison between the original OML area source near-field scheme, and Eq. (6). As can be seen, Eq. (6) yields the identical upper concentration limit, since it depends on the normalized emission rate. The original OML scheme, on the other hand, is an explicit function of the source size, and thus yields different results when the resolution of an emission inventory is changed from, for example, a 1 km grid to a 100 m grid.

7.3 ZURICH 1990 CASE STUDY

7.3.1 Zurich 1990

The city of Zurich has approx. 370 000 inhabitants and covers an area of 88 km^2. This area consists of 4226 ha natural surface (forests, parks, agricultural areas, cemeteries, water) and 4548 ha covered surface (buildings, roads, infrastructure, industry). Figure 3 depicts the land use of the city of Zurich aggregated into six main categories.

Data from a meteorological station from the national weather service are available which is situated within the city. This station covers all ground observations needed. As an example, the wind rose for the entire year 1990 is depicted in Figure 4. For the determination of the mixing height, the OML preprocessor requires vertical profiles of temperature and density. For this, the radio soundings (twice daily) from the Payerne station, 200 km away from Zurich, have been used. The Payerne site is the only meteorological station in Switzerland conducting radio soundings.

7.3.2 Classification of concentration measurement locations

For the year of 1990, a total of 28 stations spread all over the city, yielded observational data of surface pollutant concentrations for comparison to the simulations. Besides from 4 continuously monitoring stations (hourly averaged concentrations for the whole year), pollutant concentrations were measured at the remaining 24 stations during 40 to 45 periods of 24 hours each (covering all seasons, and all days of the week), from the results of which annual averaged concentrations were estimated. Figure 5 shows the position of the air pollution monitoring stations from which data have been used for model validation in the present study.

Due to the use of gridded emission inventories, we are able to predict area averaged concentrations only. The measured concentrations, however, will essentially be point concentrations. These point concentrations may be influenced by local emission sources (like major roads), or they may not (yielding the urban background concentration). If local influences are present, they may either be resolved by the emission inventory, or they may not.

The representativeness of measurement stations depends on the local influence from roads or near-by buildings. In the present study, the model performance validation is

done separately for three groups, as defined in Table 1 (urban background, influenced by major roads with or without local influences). To determine the specific group, all measurement sites have been investigated in detail.

To describe the immediate and local environment of each measurement site, the surroundings have been identified from maps, and the locations were visited in the field where necessary. The details of the environment description scheme used are given in Table 2. Table 3 gives some additional details on the concentration monitoring sites, along with the coordinates as depicted in Figure 5. The boundary for the so-called "immediate" environment has strictly been set to 100 m, that of the "local" environment to 1 km. For stations situated near major roads, the daily traffic volume is given as well. The resulting station classification in the groups Q1, Q2 and Q3, respectively, as adopted in this study (listed in Table 3), is mainly influenced by the "immediate" environment.

Any dispersion model would be expected to perform best in predicting the urban background (Q1 data in this study), second-best in predicting concentrations where roads are adequately resolved in the emission inventory (Q2), and to show considerable error when local effects are present on scales smaller than the spatial concentration sampling scale (Q3).

When a concentration measuring unit is positioned such that strong local influences exist (for example in a street canyon), the measured concentration may strongly depend, for example, on the mean wind direction. Then, the stationarity condition, and the ensemble-average approach, only allow for concentration sampling times of 24 hours and longer to be compared with the corresponding model predictions. They also do not allow for the comparison of the distribution of hourly concentration, i.e. of quantile-quantile plots of predicted vs. observed concentration, as a model validation tool for such sites with local influences.

7.3.3 Emission inventory

The emission rate of a single large source can easily be measured, but estimating the total emissions of an agglomeration is more difficult. Uncertainties exist on the emission level of road traffic as well as the traffic volume itself, on the emission level for the various other fossil burning processes, etc. Although no dispersion model prediction can

be more accurate than the emission inventory it relies upon, these inherent uncertainties of urban emission inventories are not addressed here. The focus is on the modeling of dispersion.

For the city of Zurich in the year 1990, a detailed (100 m x 100 m resolution) emission inventory was constructed (Werfeli 1995). It takes into account traffic (number of vehicles per day and estimated speed on the 152 largest roads of the city; additionally, estimates of short-distance traffic not using major roads), domestic and commercial heating and the 33 largest industrial sources (treated as point sources in the model).

This emission inventory sums up to over 4300 SO_2 sources and over 4300 NO_x sources, where the line sources (roads) are split up and added to area sources. To simulate the time dependence of source strength, the amplitude of the traffic sources is modulated according to the hour of the day and the day of the week, and the strength of the heating sources depends on the hour of the day and on the month. Among the observational data, traffic frequency data at four sites within the city are available, which have been used to construct average hourly and daily frequency cycles.

The emission data of the heating sources was collected very carefully and the traffic emissions were modeled using numerous results from actual traffic census data. The emission factors used for the calculation of the overall emissions for each source type and pollutant were checked with in-site monitoring measurements. With this procedures the overall accuracy of the emission data is estimated at ±5% for heating sources (SO_2 and NO_x) and at ±20% for NO_x and ±25% for SO_2 for emissions from traffic sources. This amounts to a total maximum estimated error in the emission data of 6.3% for SO_2 and, due to the larger contribution of traffic sources, of 14.3% for NO_x.

7.3.4 Urban set-up

The definition of the model surface is another key factor in the appropriate model set-up. When adapting continuous plume models to urban environments, there is no such thing as an averaged mean wind speed in the lowest, say, ten meters, i.e. between the building structures themselves. In order to avoid the use of a (relatively simple) Gaussian model for dispersion estimates *between* the roughness elements, a model surface corresponding to the zero displacement height (see Rotach 1994) rather than the physical surface $(z = 0)$ has been chosen. For the city of Zurich, the average building

height is $h = 12$ m (Rotach 1995); the thickness of the RS has been chosen to be $3h$. This corresponds with the approach adopted by Hanna and Chang (1993), where the depth of the mechanically well-mixed layer is set at three times the average obstacle height.

The zero displacement height, d, is set at $0.75h$ (Rotach 1994), as sketched in Figure 6. The height of the domestic and industrial area sources has been set to 5 m above the average building height, reflecting the fact that chimneys are situated at the very top of every building, and that in general stacks with emission rates above average are to be found on buildings with a height above average. The emission height of the traffic area sources corresponds to the lower model boundary. For the 33 largest sources, which are treated as individual point sources within this simulation, the emissions take place at the physical stack height. All concentrations have been predicted for a receptor height of $z' = 0\,\mathrm{m}$, where $z' = z - d$, i.e. at the lower model boundary.

No attempt has been made to develop vertical profiles of concentration within street canyons, in order to extrapolate any concentrations predicted at the $z' = 0\,\mathrm{m}$ level down to the physical ground level. In general, concentrations at street level are higher than at a height of several meters, i.e. $z' = 0\,\mathrm{m}$ (e.g. Lee and Park 1994; Zoumakis 1995). The measurements took place at 2 m above ground level, i.e. well below $z' = 0\,\mathrm{m}$ (for some of the continuously measuring stations, the receptor height is 5 m). But as the emission inventory does not resolve single street canyons, and since such influences depend on the wind direction and the surrounding buildings, such an extrapolation cannot be expected to improve the model accuracy. Instead, we will (in section 7.4) evaluate the predicted concentrations for the stations groups Q1 to Q3 separately. It is assumed that street canyon effects only occur at Q3 sites.

Special care has been taken to estimate the buoyant plume rise of the emissions. The buoyancy flux, $F_B = g\, F_V\, \Delta T / T_a$, is determined by the estimated maximum volume flux (as summarized in Table 4), F_V, caused by domestic heating. The maximum volume flux from Table 4 applies to daytime conditions during the coldest day of 1990 only: The actual volume flux is time dependent, where the same time series of scaling factors has been used as for the emission rate of the domestic area sources themselves (see preceding section). The temperature of the emission itself does in general not depend on

the ambient temperature; it is determined by the technical lay-out of the heating equipment. Therefore a constant level of exhaust gas temperature has been chosen.
The exhaust gases from mobile sources will experience a buoyancy induced rise as well. Here, we only address the over-all rise of traffic area source emissions, not of individual vehicles. Given the thermodynamical effectiveness of below 40% for gasoline engines, a considerable amount of heat is released through the tail pipe. But the exact proportion of energy being radiated as heat, emitted through the tail pipe, or being used for chemical reactions in the catalytic converters, is unknown. In general, the exhaust gas temperature does depend on the previous minutes of driving behavior of the vehicle. In congested (stop-and-go) traffic conditions, the catalytic converter is likely not to reach the required temperature level, causing the emission level to increase drastically as compared to fluent traffic conditions. Nevertheless the resulting buoyancy of traffic area sources has been scaled with the time series of traffic volume (see preceding section).

7.3.5 Background concentration

Even the "perfect" dispersion model and emission inventory should under-predict the observed concentrations by the amount of the natural, regional background. An estimate of this natural background is difficult to obtain in the case of the city of Zurich, because such locations, where one can be sure that there is no influence of local anthropogenic emissions, are to be found at high altitudes in the Swiss mountains only. Additionally, there is the impact of all the sources situated in the vicinity of the city, but which are not covered by the city's emission inventory. Hence, what is needed as "background" concentration is the sum of the natural background and of the (yearly averaged) concentration impact from all the sources that are in the agglomeration around the city (i.e. not part of the modeling domain). Therefore the "background" concentration cannot be a single constant level, but will be spatially varying, with lowest values in the center of the domain, increasing towards the boundaries of the emission inventory.
In order to obtain such a city background concentration map, the results from another study have been used where yearly averaged NO_2 concentrations have been computed for whole Switzerland (SAEFL 1997). For the present study, a special concentration map has been computed based on the emission inventory of the state of Zurich, where all those sources which are situated within the city itself have been removed. This yields

the complementary concentration map to the present work. Although the SAEFL (1997) dispersion model is simplified, and is not able to take into account the urban characteristics of the area, the results are considered to be accurate enough for use as a background concentration map.

Several steps are needed to transform the results into the required background concentration map. The underlying emission inventory in SAEFL (1997) is for NO_x, which is transformed into NO_2 with an exponential relationship which has been fitted to observations. The inverse function is thus applied to obtain the underlying NO_x concentrations needed for this study. The SAEFL (1997) concentrations are predicted as the sum of a regional (including the natural and non-Swiss contributions) and a national (anthropogenic) background, and a contribution from local sources. The background concentrations, which are based on a 1995 emission inventory, are transformed into values for 1990 by re-scaling the national component by the ratio of the 1990 to 1995 total NO_x emissions of Switzerland taken from SAEFL (1995).

SAEFL (1997) assumes an exponential decrease of the background concentration with increasing height above sea level. This causes very high background values for lower altitudes. This is partly caused by the fact that long-range (distances > 2 km) dispersion is not implemented in the SAEFL (1997) dispersion model. This causes a missing contribution to the local concentrations. By fitting the model predictions to observations, the exponential relationship has come to account for this in the SAEFL (1997) model. For the purpose of the present work, this exponential relationship has been replaced by a linear regression expression, which has itself been fitted to measurements of approximate background concentration.

The SO_2 background map has been derived from the NO_x background by a straight-forward procedure. For the four stations with hourly observed concentration, the NO_x-to-SO_2-ratio of the average of the 876 hours (i.e. 10% of the year) with the lowest observed concentrations has been computed (see Table 5). This ratio differs, depending on the quality of the measurement station. For the true urban background (Q1 station), this ratio is higher as compared to the site with some local influences (Q2), and much higher for data obtained from sites exposed to streets (Q3). For the present purpose of a background map, the NO_x background concentration has been divided by the ratio of

18.7 from the true urban background station. The resulting NO_x and SO_2 background maps are shown in Figure 7.

7.4 RESULTS

7.4.1 Overview

The OML has been used to predict SO_2 and NO_x concentrations at a uniform receptor height (located at the zero plane displacement height) at the positions of the 28 observational stations and at a regular grid covering the whole modeling domain with a spacing of 1000 m. The simulation has been run for the whole year 1990, with a principal time step of one hour.

Two different simulation runs have been conducted:

- 'non-urban' simulation: application of the OML model 'as it is', with the set-up as shown in Figure 6, roughness length $z_0 = 1$ m, area source plume rise settings as outlined in section 7.3.4, and the near-source concentration limit according to Eq. (6).
- 'urban' simulation: application of the 'OML-Urban' model, i.e. the OML with the modifications from section 7.2.3 (urban energy balance in meteorological pre-processor, Eqs. (1) to (5)) and section 7.2.4 (local scaling with friction velocity as a function of height). All other settings are identical to the 'non-urban' simulation run.

The major goal of the investigation is the correct prediction of the annual average concentration. New generation type Gaussian plume models are generally accepted to be suited for such predictions. However, a wide range of assumptions regarding source characteristics has inevitably to be made, as has been outlined in the previous sections. To minimize the risk that the correct annual average prediction (as it can be verified with respect to the 28 observational stations) actually arises from the sum of various severe over- and underpredictions, caused by inadequate parameterizations and/or source specifications, a multi-step validation procedure is undergone.

First, we will assess the effect of those parameters for which actual "urban" values have been chosen. Secondly, we will compare the hourly predicted concentration time series to the observed daily cycles of continuous (i.e., hourly) observations. Third, using

quantile-quantile plots it can be verified whether the distribution of predicted concentrations resembles the observed distribution. This is done for the 8760 hours of observations at the four continuously measuring stations. Finally, we will calculate the performance statistics of the predicted annual mean concentration at the positions of the 28 observational stations, separate for each receptor "quality group".

7.4.2 Pollutants considered

NO_2 is one of those pollutants which frequently exceeds the threshold value of the Swiss clean air act. The permitted yearly average is 30 μg m^{-3} for NO_2; the threshold of 80 μg NO_2 m^{-3} may be exceeded only once per year based on a 24-hour average, and the threshold of 100 μg NO_2 m^{-3} must not be exceeded during 95% of all 30-minute averages over the whole year. These limit values are considerably lower than in most other countries, including the United States. The chemical conversion of stack and tail pipe NO emissions to NO_2 takes place over distances of some hundred meters. Therefore, in this study, NO_x rather than NO_2 is modeled, which is a more robust quantity.

On the side of the emission inventory, the NO_x emissions consist of the sum of the two components NO and NO_2. On the side of the measurements from the air pollution monitoring stations, again the sum of NO and NO_2 is used for NO_x. The assumption that NO_x can be assumed as a tracer quantity holds to a high degree.

The other pollutant considered in the present study is sulfur dioxide (SO_2). Due to a general tendency of decreasing concentrations, the importance of this pollutant as a risk factor to human health is decreasing. The corresponding annual average threshold (30 μg m^{-3}) of the Swiss clean air act is not violated anymore in the city of Zurich at present. This is mainly due to the use of low-sulfur oil for domestic as well as commercial heating purposes. Also, the 100 μg m^{-3} threshold, which may be exceeded during only 1 day per year and during only 5% of all 30-minute averages as well, is not violated any more at present. SO_2 has been included in this study because unlike NO_x, which is emitted mainly by road traffic at street level, SO_2 originates for the larger part from residential and commercial non-mobile sources with different source characteristics.

7.4.3 Main effects of urban modification

A number of runs were performed with the OML using various configurations in connection to the points mentioned above, to find an optimal set-up for an urban dispersion simulation. Only when such a set-up is identified, it makes sense to introduce the roughness sublayer effects in order to (i) increase the physical significance of the dispersion simulations and (ii) see whether this additional change is likely to improve the quality of the simulation.

In this section, we investigate the effect of the most important ”urban” settings. The parameter with the largest influence on the ability to predict hourly concentrations is the roughness length z_0, because of the lower limit on the absolute value of Obukhov length, L (Eq. (5)). A histogram of the Obukhov length is displayed in Figure 8. More than 53% of all hours of the year are affected by this limit (note that the $100\,z_0$ limit is part of the standard OML meteorological pre-processor, and has not been changed for the present study).

The second-largest impact on the meteorological scaling parameters is caused by the increased lower limit to the friction velocity adopted in this study (section 7.2.3). In 18% of all hours of the year, the friction velocity equals this minimum value (Figure 9).

The simulation for the city of Zurich for the year 1990, of which the results are discussed in the next sections, has also been performed with a ‘semi-urban’ approach, i. e. by only introducing the RS turbulence but without the urban modifications to the energy balance as discussed in section 7.2.3 (affecting the albedo, the snow albedo, the ratio of sensible to latent heat flux, and the moisture availability). The combined effect of these urban energy balance settings alone is a decrease in NO_x annual averaged concentrations of 0.17%, and of 1.8% for SO_2. Since the major part of domestic emissions (which dominates the SO_2 concentrations) is emitted during winter conditions, the larger effect on SO_2 concentrations is likely to be caused in large part by the change in snow albedo.

7.4.4 Hourly predictions, reproduction of frequency distribution

Figure 10 shows an example of the hourly observed and predicted (both ‘non-urban’ and ‘urban’ approaches) NO_x concentrations. The daily cycle with concentration peaks induced by the road traffic peak hours can be clearly seen (the station depicted is a Q2

station with some influence from local traffic, but not located directly near a road) as well as the much lower concentration level on Sep. 16 (a Sunday).

Gaussian models with gridded emission inventories can not be expected to yield close hour-to-hour correspondences. This would need careful modeling of the actual flow field at each receptor site, and the use of a very fine emission inventory with individual source heights. But Figure 10 shows that there is neither a general underprediction nor overprediction during certain hours of the day: the night-time concentration level is well predicted, and the height of the concentration peaks during day-time always is of similar magnitude. This is to a large part due to the lower limit to the absolute value of the Obukhov length (Eq. 5). Without this limit, which would neglect the important role of mechanically induced turbulence by the buildings, a severe underprediction during night and corresponding overprediction during the day would result.

The differences between "urban" and "non-urban" approach are not very pronounced during night-time hours. During day-time conditions, however, the peak concentration generally is clearly higher for the "urban" approach.

Figure 11 depicts the so-called quantile-quantile plot for one out of the four stations with continuous measurements. For both the "urban" and "non-urban" set-up the graph is almost a straight line, indicating that the frequency distribution of predicted low and of high concentrations corresponds very well to observations. The "urban" simulation leads to a general increase of predicted concentrations of 35%.

7.4.5 Annual averages, statistical performance

A scatter plot with the annual averaged NO_x and SO_2 concentration is depicted in Figure 12. The different monitoring site groups Q1 to Q3 are marked with different symbols; additionally, large symbols denote stations with continuous measurements. For all stations, both the "urban" and "non-urban" simulation results are shown (filled and open symbols, respectively). In Table 6 the following statistical measures are compared for the two different simulations:

FB	the fractional bias: $FB = (\overline{C}_{\text{obs.}} - \overline{C}_{\text{pred.}}) \big/ (0.5(\overline{C}_{\text{obs.}} + \overline{C}_{\text{pred.}}))$
NMSE	the normalized mean square error: $NMSE = \overline{(C_{\text{obs.}} - C_{\text{pred.}})^2} \big/ (\overline{C}_{\text{obs.}} \overline{C}_{\text{pred.}})$
COR	the correlation coefficient: $COR = \overline{(C_{\text{obs.}} - \overline{C}_{\text{obs.}})(C_{\text{pred.}} - \overline{C}_{\text{pred.}})} \big/ (\sigma_{\text{obs.}} \sigma_{\text{pred.}})$
FAC2	percentage of simulations within a factor of two of the measurement

Here, $C_{obs.}$ is the observed concentration and $C_{pred.}$ the predicted one.

The performance of the OML-Urban model, with FAC2 = 100% for NO_x and SO_2 for Q1 and Q2 stations, is considered to be very satisfactory, showing that Gaussian plume models may be applied to urban environments, when some corrections are made, for the prediction of yearly averaged concentration. As expected (Section 7.3.2), the model performance is best for Q1 monitoring stations, second-best for Q2 data, whereas for Q3 locations, the local influence of major roads (not fully resolved by the gridded emission inventory) causes a slight underprediction of ground-level concentrations. All Q1 and Q2 data for both NO_x and SO_2 are within a factor of 2 from the observed values.

The bootstrap resampling method proposed by Hanna (1989) together with percentile-based resampled confidence intervals of 95% has been used to assess the presence of systematic errors. The NO_x predictions are almost bias-free, the FB value of 0.042 and 0.033 for Q1 and Q2 sites, respectively, not being significantly different from zero. Also, the FB value of 0.026 for Q1 stations for SO_2 does not differ significantly from zero, but it does for Q2 data. Figure 12 also confirms that whereas for NO_x, the 'urban' approach leads to an essentially bias-free prediction, for SO_2 the underprediction for the 'non-urban' approach turns into a slight overprediction when using the 'urban' set-up. Especially, the annual average concentration observed at the two continuously measuring stations being classified as Q1 or Q2, is very closely reproduced for NO_x. For SO_2 a small systematic overprediction of concentrations persists.

Table 7 gives the relationship between domestic/industrial and traffic area source emissions on the one hand, and the share of the respective source categories on the predicted ground-level (at the lower model boundary, i.e. z = 9 m) concentration on the other hand. The combined effect of the higher emission height and of the more pronounced buoyancy of the domestic/industrial emissions causes a decrease in the contribution to the concentration impact, as compared to the share in the emissions. For example, although over 38% of all NO_x emissions originate from non-mobile sources, the street-level concentrations (when the arithmetic mean over all station locations is computed) are influenced by the traffic emissions by more than 88% (without the background concentration).

7.5 SUMMARY AND CONCLUSIONS

To obtain a proper modification of operational (Gaussian) dispersion models for use within an urban environment, the concept of an "urban preprocessor" (Rotach 1997a) has been introduced. Its basic principle is to use similarity theory based on local fluxes for the parameterization of the turbulence structure within the urban roughness sublayer. The first validation step of this concept has been reported on elsewhere (Rotach and de Haan 1997) and was performed by use of a Lagrangian particle dispersion model for the simulation of a (sub)urban tracer experiment. A clear improvement of the predictability was the result. This indicates that the urban preprocessor is able to better take into account the rough character of the surface at the sites where this experiments took place. As a second validation step the performance of the operational Gaussian multi-source dispersion model OML for this experiment (Copenhagen) as well as for Lillestrøm showed a similar improvement of the correspondence between the simulated and the measured concentrations, when introducing the roughness sublayer (de Haan *et al.*1998). Therefore, the concept of the urban preprocessor can be used with operational Gaussian dispersion models to improve the model's prediction skills over urban surfaces.

The resulting OML-Urban model is used for the case study of the yearly average surface pollution concentration (NO_x and SO_2) in the city of Zurich in 1990, for which a very detailed emission inventory (100 m x 100 m resolution) is available. Some parameterizations within OML's meteorological pre-processor were changed in accordance with an urban energy budget. Data from air pollution monitoring stations were grouped according to the influence of nearby roads. The performance of OML-Urban is assessed for these different groups separately. The resulting prediction skill is very satisfactory, with a close reproduction of the frequency distribution of observed concentration, all predictions being within a factor of 2 of the observed values, and a small systematic error (bias). It is concluded that the method presented is suitable to allow the application of Gaussian plume models to urban environments for the prediction of yearly averaged concentrations.

Acknowledgements—The comments and suggestions of Dr S. R. Hanna and of Dr H. R. Olesen have been very helpful. Thanks go to Dr J. Heldstab and Dr T. Künzle for providing the background NO_x concentration map for the city of Zurich. The present work was partly financed by the Swiss Agency of Education and Sciences (BBW) through the TMR network (TRAPOS), and by the Swiss National Science Foundation through Grant No 21-46849.96.

REFERENCES

Berkowicz, R., and Prahm, L. P. (1982): Sensible heat flux estimated from routine meteorological data by the resistance method. *J. Appl. Meteor.*, **21**, 1845–1864

Briggs, G. A. (1973): Diffusion estimation for small emissions. 1973 Annual Report, Air Resources Atmos. Turb. and Diffusion Lab., Environmental Lab., Report ATDL-106, USDOC-NOAA

Briggs, G. A. (1984): Plume rise and buoyancy effects. Atmospheric Science and Power Production (ed. by Randerson D.), DOE/TIC 27601. Department of Commerce, Springfield, USA

Carruthers, D. J., Holroyd, R. J., Hunt, J. C. R., Weng, W.-S., Robins, A. G., Apsley, D. D., Smith, F. B., Thomson, D. J. and Hudson, B. (1992): UK Atmospheric Dispersion Modelling System. In: van Dop, H. and Kallos, G. (eds.), *Air Pollution Modelling and its Applications IX*, Plenum Press, New York

Feigenwinter, C.; Vogt, R. and Parlow, E. (1998): Vertical structure of selected turbulence characteristics above an urban canopy. Accepted for publication in *Theor. Appl. Clim.*

Gryning, S.-E., and Lyck, E. (1984): Atmospheric dispersion from elevated sources in an urban area: Comparisons between tracer experiments and model calculations. *J. Clim. Appl. Meteorol.*, **23**, 651–660

de Haan, P., Rotach, M. W, and Werfeli, M. (1998): Extension of an operational short-range dispersion model for applications in an urban environment. *Int. J. Vehicle Design*, **20**, 105–114

Häggkvist, K. (1997): Evaluation of dispersion models for an urban environment, an example from Stockholm, Sweden. *Inter. J. Environment Pollution*, **8**

Hanna, S. R. (1989): Confidence limits for air quality model evaluations, as estimated by bootstrap and jackknife resampling methods. *Atmospheric Env.*, **23**, 1385–1398

Hanna, S. R. and Chang, J. C. (1992): Applied dispersion modeling over urban areas. *Bound. Layer Meteor.*, **58**, 229–259

Hanna, S. R. and Chang, J. C. (1993): Hybrid Plume Dispersion Model (HPDM) improvements and testing at three field sites. *Atmospheric Env.*, **27A**, 1491–1508

Härkönen, J., Kukkonen, J., Valkonen, E., and Karppinen A. (1998): The influence of vehicle emission characteristics and meteorological conditions on urban NO_2 concentrations. *Int. J. Vehicle Design*, **20**, 125–130

Haugsbakk, I., and Tønnesen, D. A. (1989): Atmospheric dispersion experiments at Lillestrøm 1986–1987. Data Report NILU OR 41/89. Available from Norwegian Inst. for Air Research, PO Box 100, N-2007 Kjeller, Norway

Högström, U., Bergström, H., and Alexandersson, H. (1982): Turbulence characteristics in a near-neutrally stratified urban atmosphere. *Boundary-Layer Meteorol.*, **23**, 449–472

Holtslag, A. A. M., and van Ulden, A. P. (1983): A simple scheme for daytime estimates of the surface fluxes from routine weather data. *J. Clim. Appl. Meteor.*, **22**, 517–529

Lee, I. Y. and Park, H. M. (1994): Parametrization of the pollutant transport and dispersion in urban street canyons. *Atm. Environment*, **28**, 2324–2349

Monteith, J. L. (1981): Evaporation and surface temperature. *Quart. J. Roy. Meteorol. Soc.*, **87**, 159–170

Oikawa, S., and Meng, Y. (1995): Turbulence characteristics and organized motion in a suburban roughness sublayer. *Boundary-Layer Meteorol.*, **74**, 289–312

Oke, T. R. (1987): Boundary layer climates. 2nd edition. Methuen, London

Oke, T. R. (1988): The urban energy balance. *Progress in Physical Geography*, **12**, No. 4, 471–508

Oke, T. R., and Cleugh, H. A. (1987): Urban heat storage derived as energy balance residuals. *Boundary-Layer Meteorol.*, **39**, 233–245

Olesen, H. R., and Brown, N: The OML meteorological preprocessor; a software package for the preparation of meteorological data for dispersion models. MST Luft-A 122, 2nd ed. To be obtained from National Environmental Research Institute, DK-4000 Roskilde, Denmark

Olesen, H. R., Løfstrøm P., Berkowicz R. and Jensen A. B. (1992): An improved dispersion model for regulatory use: the OML model. In van Dop H. and Kallos G. (eds.), Air Pollution Modeling and its Applications IX, Plenum Press, New York

Olesen, H. R. (1995): The model validation exercise at Mol: Overview of results. *Int. J. Environment Pollution*, **5**, 761–784

Rafailidis, S. (1997): Influence of building areal density and roof shape on the wind characteristics above a town. *Boundary-Layer Meteorol.*, **85**, 255–271

Raupach, M. R., Antonia R. A. and Rajagopalan S. (1991): Rough-wall turbulent boundary layers. *Appl. Mech. Rev.*, **44**, 1–25

Rotach, M. W. (1993a): Turbulence close to a rough urban surface. Part I: Reynolds stress. *Boundary-Layer Meteorol.*, **65**, 1–28

Rotach, M. W. (1993b): Turbulence Close to a Rough Urban Surface Part II: Variances and Gradients. *Boundary-Layer Meteorol.*, **66**, 75–92

Rotach, M. W. (1994). Determination of the zero plane displacement in an urban environment. *Boundary-Layer Meteorol.*, **67**, 187–193

Rotach, M. W. (1995). Profiles of turbulence statistics in and above an urban street canyon. *Atm. Environment*, **29**, 1473–1486

Rotach, M. W., Gryning, S.-E. and Tassone, C. (1996): A two-dimensional stochastic Lagrangian dispersion model for daytime conditions. *Quart. J. Roy. Meteorol. Soc.,* **122**, 367–389

Rotach, M. W. (1997a): Towards meteorological preprocessing for dispersion models in an urban environment. *Inter. J. Environment Pollution*, **8**, 548–556

Rotach, M. W. (1997b): The turbulence structure in an urban roughness sublayer, in: Perkins, R. J. and Belcher, S. E. (Eds): Flow and dispersion through groups of obstacles, Clarendon Press, Oxford, 143–155

Rotach, M. W., and de Haan, P. (1997): On the urban aspect of the Copenhagen data set. *Inter. J. Environment Pollution*, **8**, 279–286

Roth, M., and Oke, T. R. (1993): Turbulent transfer relationships over an urban surface. I: Spectral characteristics. *Quart. J. Roy. Meteorol. Soc.*, **119**, 1071–1104

Roth, M. (1993): Turbulent transfer relationships over an urban surface. II: Integral statistics. *Quart. J. Roy. Meteorol. Soc.*, **119**, 1105–1120

SAEFL (1995): Anthropogenic emissions of air pollution in Switzerland from 1900 to 2010. (in German or French, with English abstract). Swiss Agency for Environment, Forests and Landscape, SRU No 256, Berne, Switzerland

SAEFL (1997): NO_2 concentration in Switzerland 1990 to 2010 (in German or French; with English abstract). Swiss Agency for Environment, Forests and Landscape, SRU No 289, Berne, Switzerland

Stull, R. B (1988): An introduction to boundary layer meteorology. Kluwer Academic Publishers, Dordrecht, the Netherlands

Werfeli, M. (1995): Modelling surface pollutant concentrations (SO2 and NOx) in the city of Zurich. *Inter. J. Environment Pollution*, **5**, 575–584

Zilitinkevich, S. (1972): Determining the height of the nocturnal boundary layer. *J. Appl. Meteorol*., **17**, 28–33

Zoumakis, N. M. (1995): A note on average vertical profiles of vehicular pollutant concentrations in urban street canyons. *Atm. Environment*, **29**, pp. 3719–3725

Table 1: Definition of concentration measurement station quality groups in urban areas.

Group	Description	Examples of locations
Q1	true urban background concentration	Park areas within city, residential areas with very low traffic
Q2	urban background concentration with local influences	Residential areas with non-major roads
Q3	street concentration station	Street canyon, near major roads

Table 2: Description of immediate and local environment of air pollution monitoring stations according to EU Council Directive 92/72/EC on Air Pollution by Ozone.

Immediate Environment (within a radius of 0 to 100 m)	
I1a, I1b, I1c, I1d	large street heavy/medium/local/no traffic
I2a, I2b, I2c, I2d	small street heavy/medium/local/no traffic
I3a, I3b, I3c, I3d	canyon street heavy/medium/local/no traffic
I4	footway
I5	front of building
I6	terrace, tower, belfry
I7	interior court, school, hospital
I8	trees
I9	large flat area
I91	channel
I92	meadow, field
I99	other
Local Environment (within a radius of 100 m to some km)	
LAa, LAb, LAc, LAd	urban commercial/industrial/residential/mixed
LBa, LBb, LBc	industrial heavy/medium/light concentration
LCa, LCb, LCc	road traffic heavy/medium/light
LD	commercial
LE	residential (isolated houses)
LF	harbor
LG	airport
LH	park, forest, natural field
LI	agricultural area
LJ	mountains, valleys
LK	sea side or lake side
LL	other

Table 3: Characteristics and classification of concentration measurement stations in the city of Zurich, 1990 field campaign. Station type "hourly conc." denotes continuos measurements, "annual av." stands for statisically derived annual mean values. For definition of environment description, see **Table 2**. DTV denotes daily traffic volume, "Pop." is population density per ha.

Station name	Type	x-coor-dinate [km]	y-coor-dinate [km]	Immediate environment [<100m]	Local environment [<1km]	DTV [veh./d]	Pop. [inh./ ha]	Noise level [dBA]	Group
Schwamendingen	hourly conc.	684.91	251.43	I7	LAc, LCa		65	55	Q1
Schwamendingen 2	annual av.	684.90	251.45	I7	LAc, LCa		65	55	Q1
Hard	annual av.	680.85	248.60	I7	LAd		91	59	Q1
Seefeld	annual av.	684.40	245.80	I7	LAc		91	60	Q1
Industriequartier	annual av.	682.05	248.80	I7	LAd		134	52	Q1
Oberstrass	annual av.	684.10	248.70	I7	LAc		64	57	Q1
Hirzenbach	annual av.	686.65	250.90	I7	LAc, LCa		84	55	Q1
Sihlfeld	annual av.	680.75	247.60	I8	LAc		n.a.	52	Q1
Enge	annual av.	682.65	245.35	I8, I9	LAc, LK		n.a.	57	Q1
Zoo	annual av.	685.90	248.55	I8, I9	LH		n.a.	47	Q1
Kaserne	hourly conc.	682.43	247.85	I2c, I7	LAd		n.a.	n.a.	Q2
Witikon	annual av.	687.05	245.65	I2c	LE, LH		34	58	Q2
Höngg	annual av.	680.10	250.95	I2c	LE, LH		41	57	Q2
Wollishofen	annual av.	682.20	244.10	I2c	LAc, LCa		47	53	Q2
Leimbach	annual av.	681.40	243.30	I2c	LE, LJ, LCa, LH		30	54	Q2
Altstetten	annual av.	678.55	248.85	I2c	LAc, LH		48	49	Q2
Affoltern	annual av.	680.90	252.45	I2c	LE, LH		37	60	Q2
Seebach	annual av.	683.30	253.35	I2c	LAc, LCa		41	55	Q2
Stampfenbach	hourly conc.	683.14	249.04	I1b, I5	LAd	10 000	84	72	Q3
Stampfenbach 2	annual av.	683.15	249.00	I1b, I5	LAd	10 000	84	72	Q3
Wiedikon	hourly conc.	681.95	247.25	I1a, I3a	LAd	33 000	126	72	Q3
Wiedikon 2	annual av.	681.95	247.25	I1a, I3a	LAd	33 000	126	72	Q3
Bellevue	annual av.	683.55	246.80	I1a	LAa, LK	60 000	38	74	Q3
Friesenberg	annual av.	680.35	246.70	I1a	LE	14 000	42	68	Q3
Wipkingen	annual av.	682.10	249.90	I1a, I3a	LAd	63 000	103	80	Q3
Schörli	annual av.	684.90	251.10	I1a, I3a	LAc, LH	83 000	65	75	Q3
Oerlikon	annual av.	683.40	251.40	I3a	LAd	18 000	62	70	Q3
Hirslanden	annual av.	685.00	246.10	I3b, I1b	LAc	15 000	74	72	Q3

Table 4: Assumptions for the estimation of buoyant rise of area source (heating and traffic) emissions. The max. buoyancy flux is multiplied with a monthly, daily and hourly varying time series to obtain the appropriate buoyancy flux for each season (heating) or time of day (traffic).

	domestic and commercial area sources	**traffic area sources**
max. volume flux per household	18 m^3 / h / household	
av. number of households per building	7.5	
max. volume flux per source	120 m^3 / h	2 m^3 / h
absolute temperature of emissions	333.2 K	313.2 K

Table 5: Determination of NO_x to SO_2 ratio to derive the SO_2 from the NO_x background map. For each of the four stations with continuous measurements, the 10% (i.e. 876 hours) of the hourly values with the lowest recorded concentration have been used.

Station	**station group**	**mean of lowest 10% hourly conc. values**		**Factor NO_x to SO_2**
		NO_x	**SO_2**	
Schwamendingen	Q1	22.1	1.2	18.7
Kaserne	Q2	20.8	1.7	12.1
Wiedikon	Q3	41.2	7.6	5.4
Stampfenbach	Q3	24.4	4.5	5.4

Table 6: Model prediction performance for 'urban' and 'non-urban' model set-up and meteorological preprocessor. For definition of FB, NMSE, COR, FAC2, see text.

	Approach	station group	NMSE	FB	COR	FAC2
Observations			0.000	0.000	1.000	100%
NO_x	'urban'	all	0.144	0.201	0.845	93%
		Q1	0.042	0.075	0.750	100%
		Q2	0.033	0.063	0.730	100%
		Q3	0.176	0.322	0.780	80%
	'non-urban'	all	0.355	0.465	0.870	82%
		Q1	0.229	0.395	0.616	90%
		Q2	0.145	0.338	0.728	100%
		Q3	0.372	0.548	0.884	60%
SO_2	'urban'	all	0.051	0.027	0.770	100%
		Q1	0.026	–0.062	0.776	100%
		Q2	0.078	0.035	0.592	100%
		Q3	0.050	0.082	0.656	100%
	'non-urban'	all	0.113	0.260	0.821	96%
		Q1	0.055	0.184	0.779	100%
		Q2	0.119	0.256	0.669	88%
		Q3	0.128	0.311	0.759	100%

Table 7: Share of different source categories in the total emission and corresponding contribution to predicted surface concentrations (arithmetic mean over all station locations, without the background concentration).

	Share in annual emission				Contribution to surface conc.			
	SO_2		NO_x		SO_2		NO_x	
	[t/a]	[%]	[t/a]	[%]	[µg/m³]	[%]	[µg/m³]	[%]
heating/industrial	1905	93.5%	1960	38.1%	14.2	81.0%	12.8	16.2%
traffic	132	6.5%	3189	61.9%	3.3	19.0%	66.6	83.8%
sum	*2037*	*100.0%*	*5149*	*100.0%*	17.5	100.0%	*79.5*	*100.0%*

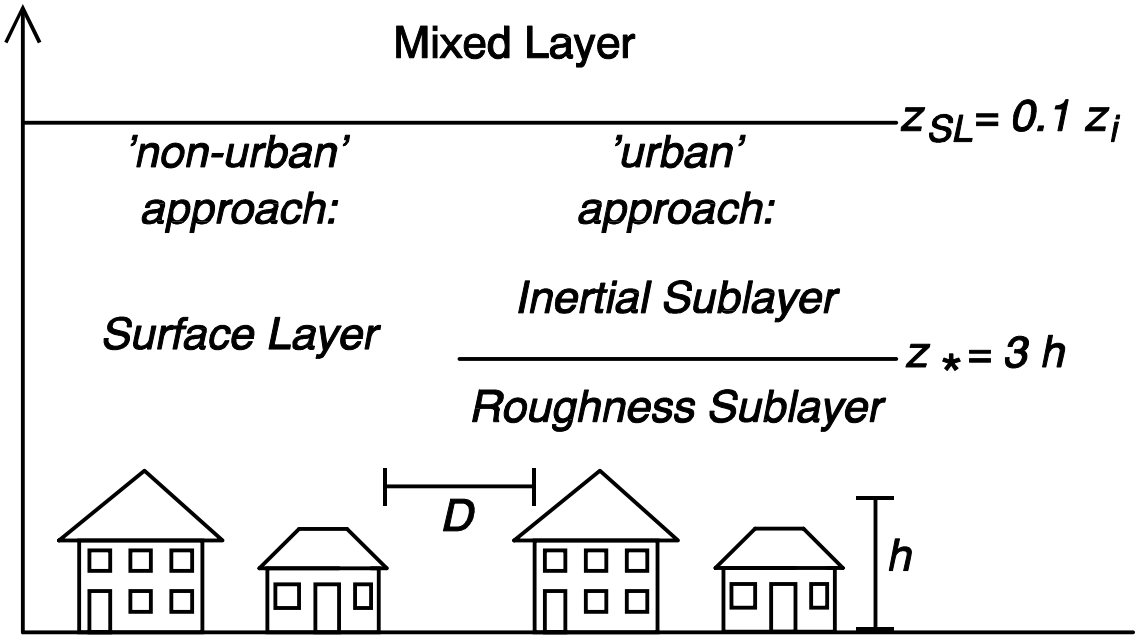

Figure 1 Conceptual sketch of the lowest layers within the boundary layer over an urban surface. The left hand side of the figure shows the situation as it is conventionally used in applied dispersion models ('non-urban' in the present terminology), while the right hand side depicts the actual situation with a roughness sublayer adjacent to the surface (referred to as 'urban' in the text). The height of the roughness sublayer is chosen as three times the average building height *h* for this study (see text for more details).

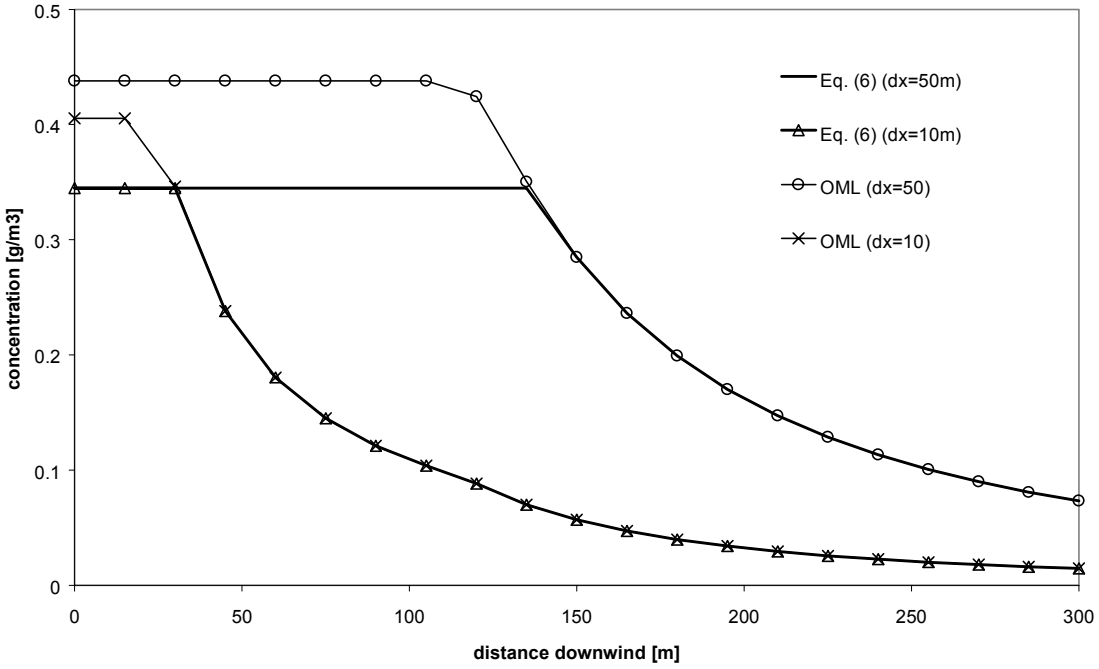

Figure 2: Effect of the upper limit on near-source concentration C for area sources. dx denotes the source size in down-wind direction. Comparison of the regular OML area source scheme (limiting $\sigma_z(x)$ by dx) and Eq. (6) (limiting C by the normalized emission rate). PGT dispersion coefficients and wind profile power law exponents taken from Hanna (1982, p. 289–293). Example for class C stability, urban conditions, roughness length 1 m, $U(z{=}10\text{ m}) = 4$ m/s, receptor height 2 m above ground, ground-based source with uniform emission rate 1 g/s/m^2. Lateral (cross-wind) size of the area source is 50 m for all cases.

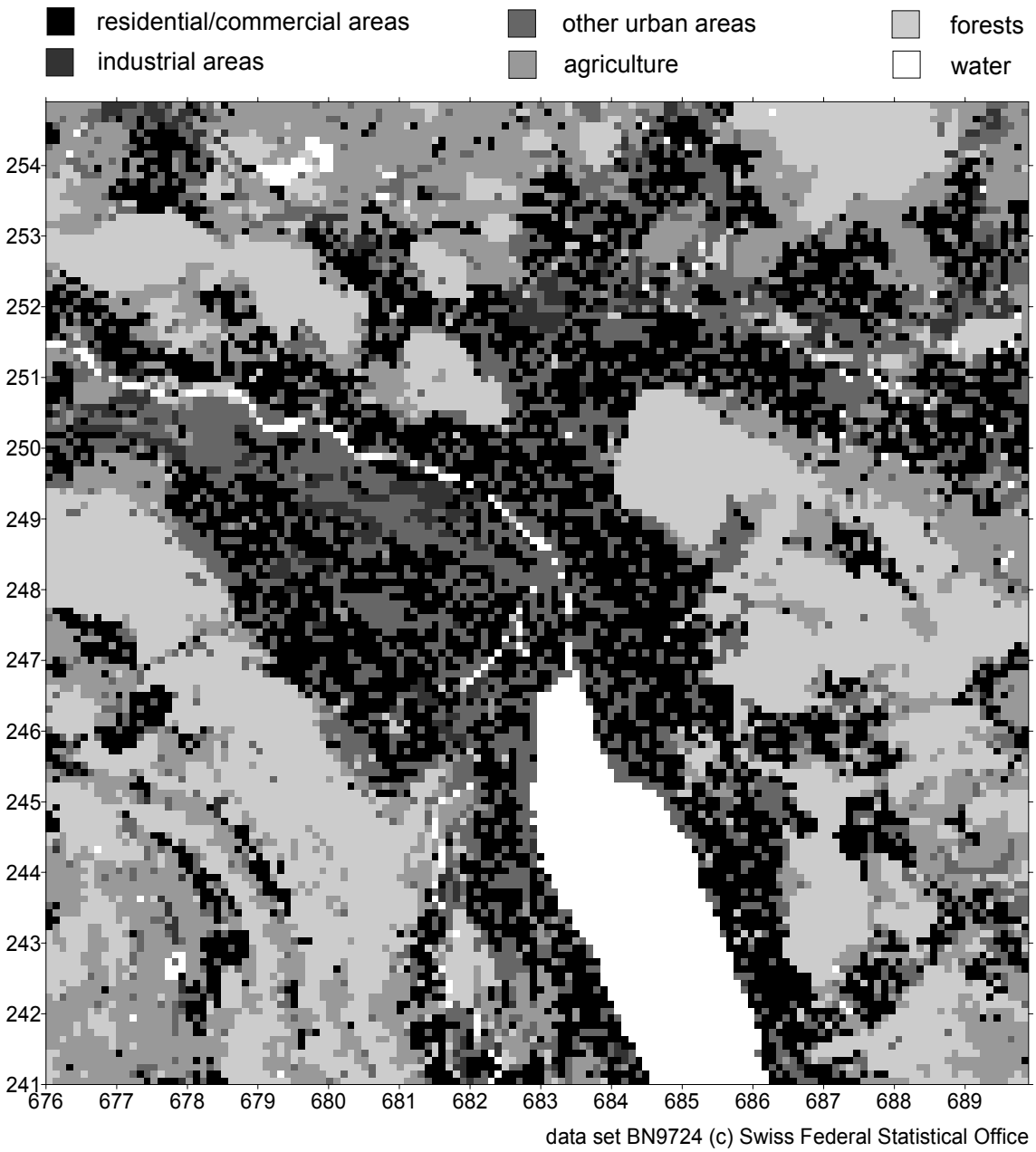

Figure 3 Land use (100 x 100 m^2 resolution; south-north and east-west axes use the Swiss coordinate system with 1 km spacing) of the city of Zurich and its surroundings, aggregated into six main categories. The city center is roughly situated at the transition of the Lake of Zurich (southern part of the figure) to the Limmat river.

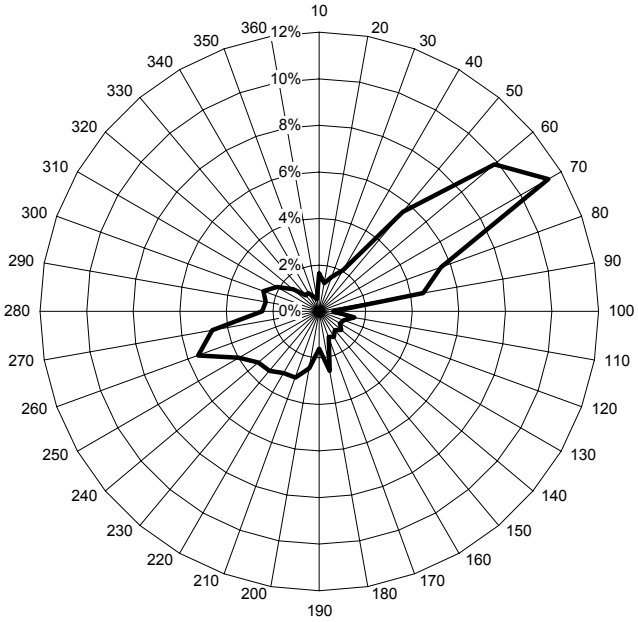

Figure 4 Wind rose of all hours of observed wind direction for 1990 at the meteorological station of the Swiss Meteorological Service in Zurich.

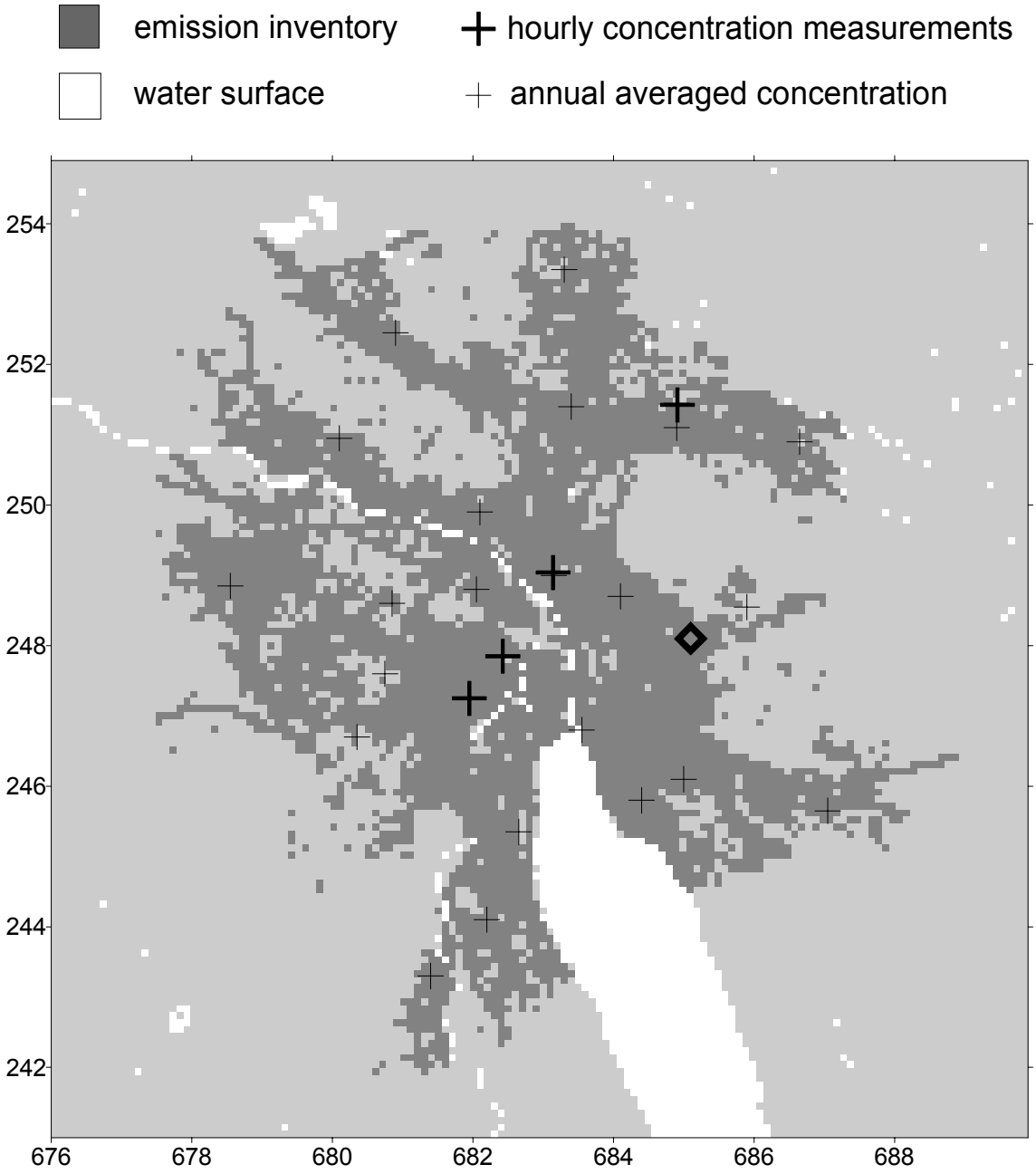

Figure 5 Location of air pollution monitoring stations and spatial extension of the emission inventory with 100 m x 100 m resolution (for 1990). The location of the national weather service meteorological station is denoted by '◆'.

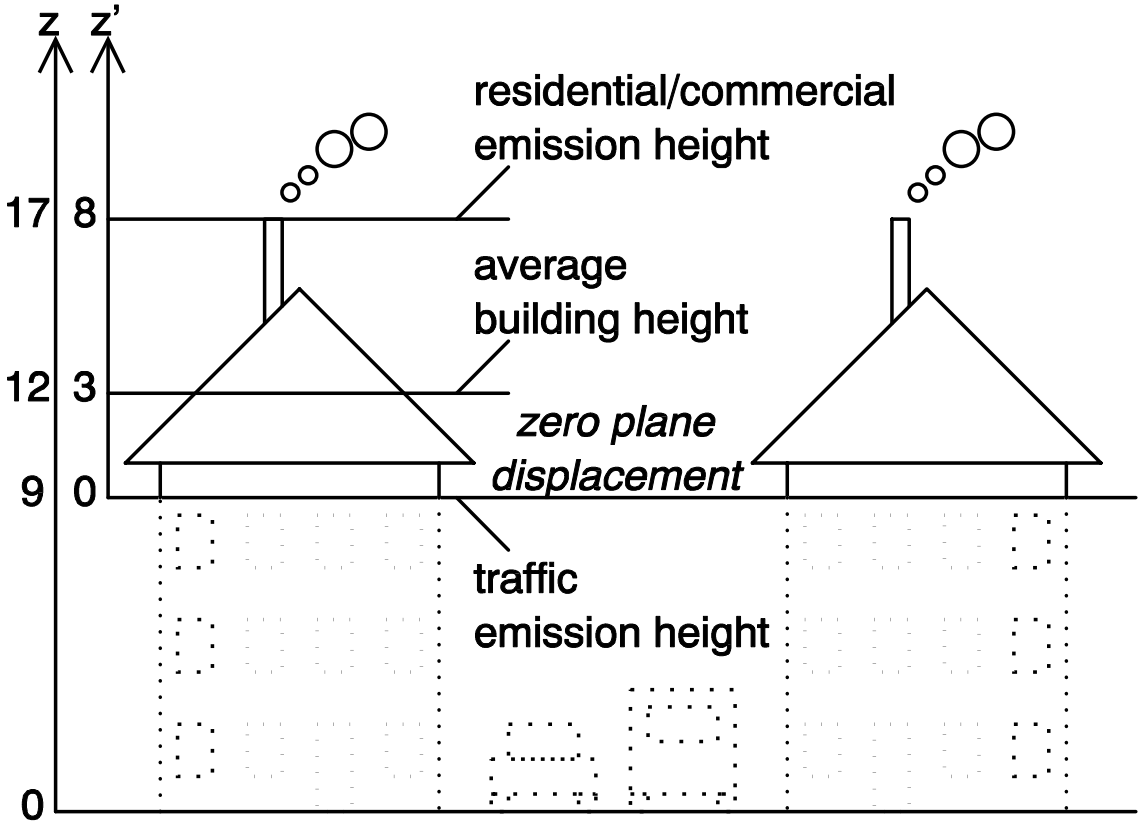

Figure 6: Set-up of the OML model for the simulation of the city of Zurich. The lower model boundary has been set to the zero plane displacement height, which is set to three quarters of the average building height. Traffic emissions are released at the bottom of the model domain. Receptor height for concentration prediction is $z' = 0$. For further explanations see text.

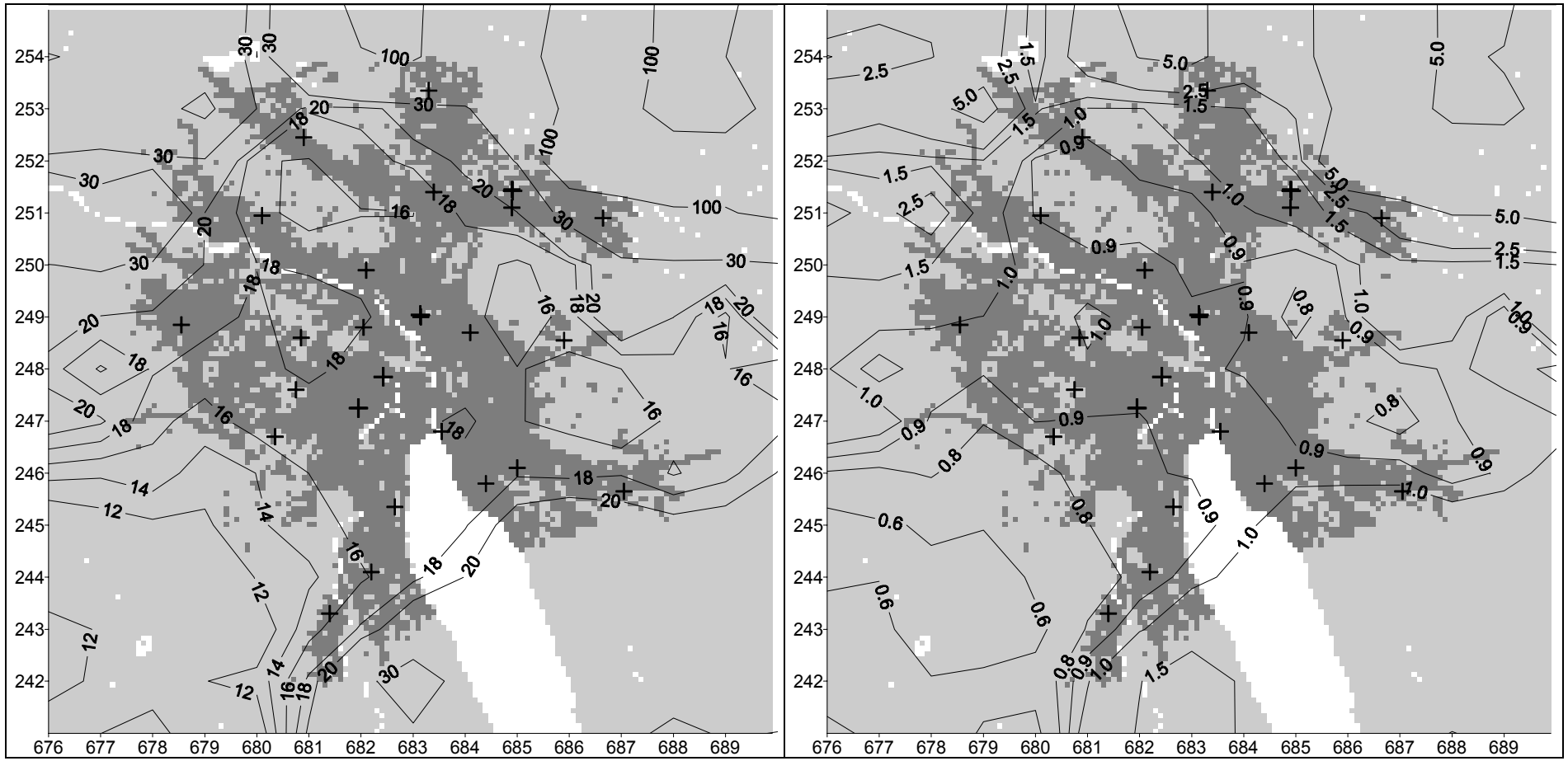

Figure 7: Background concentration maps (being the sum of the natural background concentration and the impact of all emission sources outside of the emission inventory domain) for NO_x (left panel) and SO_2 (right panel) for 1990. Annual averaged concentration in $\mu g\ m^{-3}$.

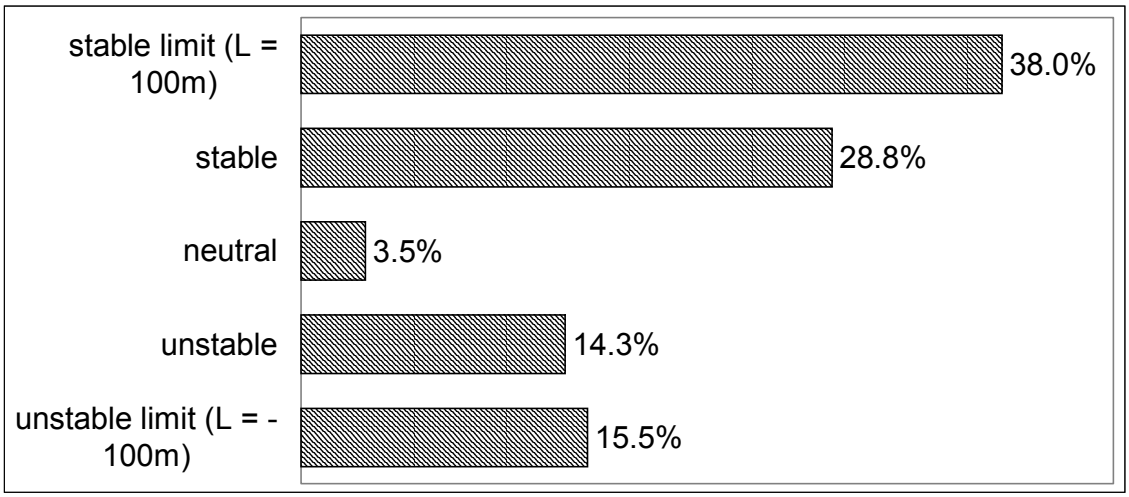

Figure 8: Effect of the lower limit on the absolute value of the Obukhov length of 100 times z_0, where z_0 = 1 m in this study.

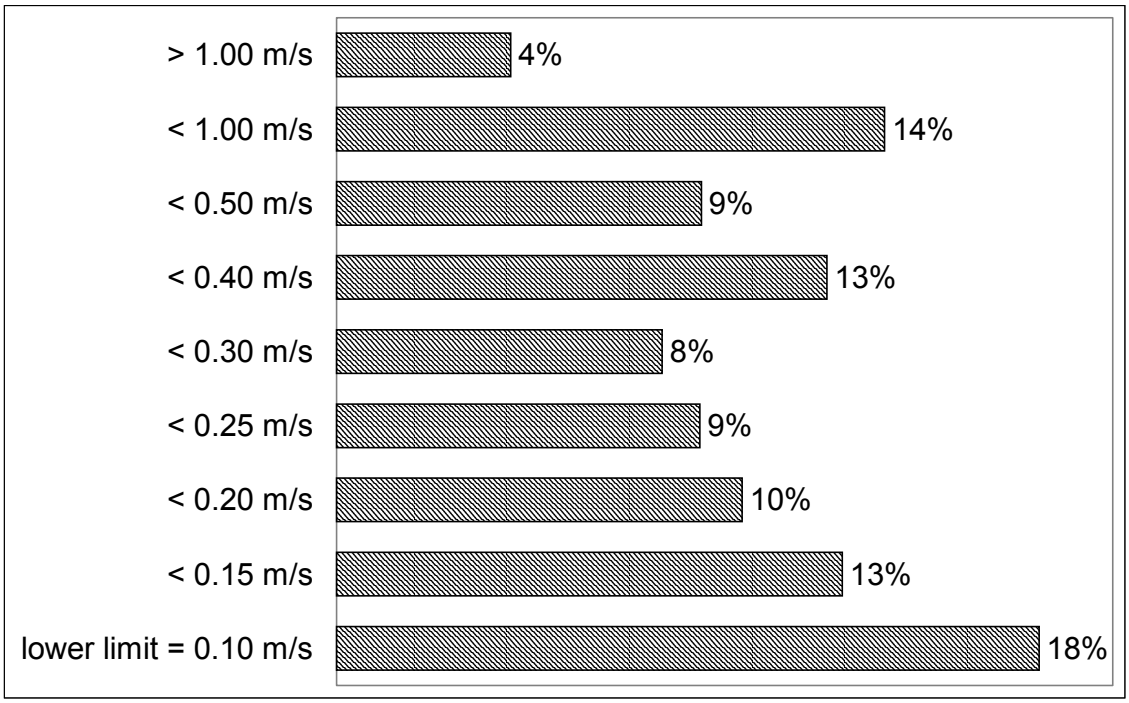

Figure 9: Classification of the roughness length u_*. The lowest limit in urban areas has been supposed to be 0.1 m s^{-1}.

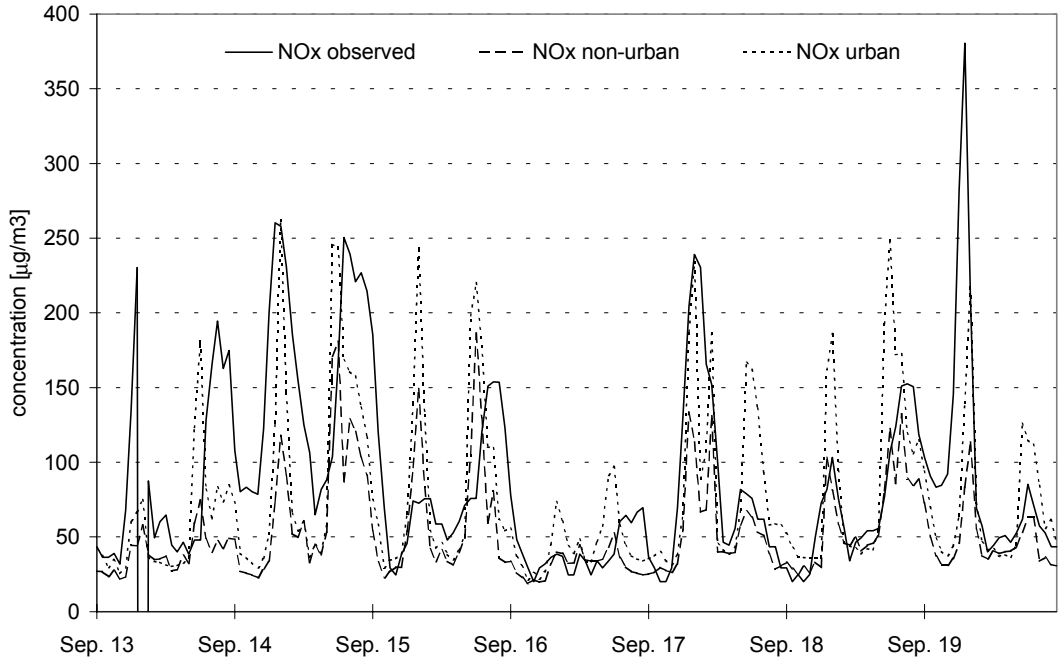

Figure 10: Example of hourly concentration data for NO_x for the location "Kaserne". The measured concentration (hourly averages) as well as OML model predictions with an 'urban' and a traditional 'non-urban' set-up are depicted.

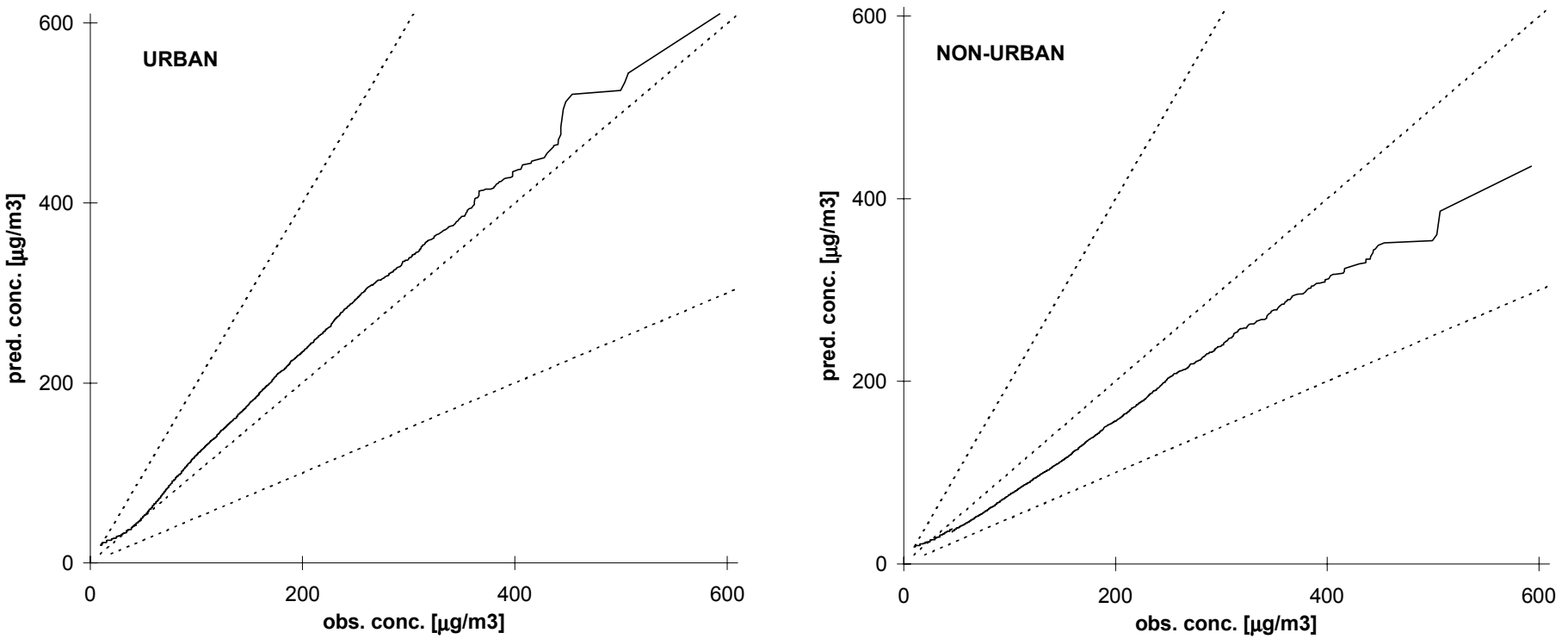

Figure 11: Quantile-quantile plot of hourly NO_x-concentrations at the location "Kaserne" for "urban" and "non-urban" model simulations. The upper and lower dashed lines indicate the range of predictions within a factor of two of observations.

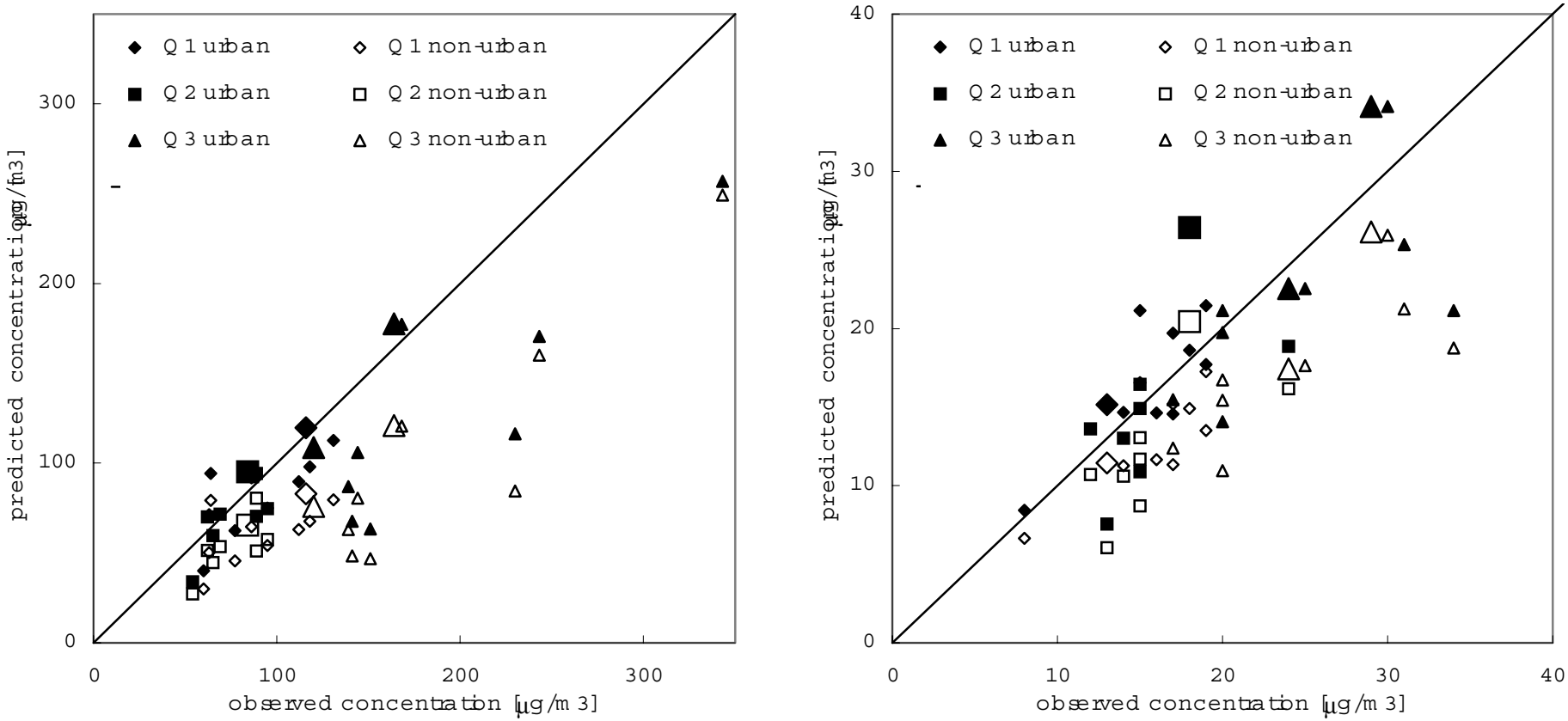

Figure 12: Scatter plot of yearly average concentration; left panel: NO_x; right panel: SO_2. Model predictions are depicted for "urban" and "non-urban" model simulations. Enlarged symbols mark those stations for which continuous (hourly) measurement data are available.

Curriculum Vitae

Peter Jan de Haan

Lentulusrain 26

CH-3007 Berne, Switzerland

Born November 16, 1969, in Enschede, the Netherlands

1982–1984	Utrechts Stedelijk Gymnasium (Linguistic high school)
1984–1989	Math.-Naturwiss. Gymnasium Basel (Science high school)
1989–1994	Studies on environmental physics at Swiss Federal Institute of Technology
1990–1993	Vice-president, president ETH Student Union; student representative in faculty and department board; 1993 non-voting member of ETH-Council
1995–1997	4 term course in statistics (Nachdiplomkurs Statistik)
1995–1999	Ph.D. studies in air pollution modeling at Department of Geography, Swiss Federal Institute of Technology
1998–	Position as consulting scientist and project manager, INFRAS Ltd., Berne